Oral Fungal Infection Impacts Epithelial Innate Immunity to Promote Local and Distal Squamous Cell Carcinoma Progression

Xin Li[1], Amit Kumar Singh[1], Na-Young Song[1,11], Jonathan H. Badger[2], Rodrigo Xavier das Neves[2], Chengfei Jiang[4], Feng Zhu[1], Zhonghe Sun[3], Gongping Shi[1], Jami Willette-Brown[1], Debra Tross[1], Peilin Zhang[5], Elise M.N. Ferré[6], Amir Seyedmousavi[7], King Chan[8], Xia Xu[8], Sayantan Banerjee[1], Timothy Gower[9], Thorkell Andresson[8], Yongmei Zhao[10], Bao Tran[10], Colm O'hUigin[2], Xiaolin Wu[3], Michail S. Lionakis[6], Giorgio Trinchieri[2], and Yinling Hu[1]

[1]Cancer Innovation Laboratory, Center for Cancer Research, National Cancer Institute, National Institutes of Health, Frederick, MD 21702, USA

[2]Laboratory of Integrative Cancer Immunology, Center for Cancer Research, National Cancer Institute, National Institutes of Health, Bethesda, MD 20892, USA

[3]Genomics Technology Laboratory, Cancer Research Technology Program, Frederick National Laboratory for Cancer Research, Leidos Biomedical Research Inc., Frederick, MD 21702, USA

[4]Cardiovascular Branch, National Heart, Lung, and Blood Institute, National Institutes of Health, Bethesda, MD 20892, USA

[5]PZM Diagnostics LLC, Charleston, WV 25314, USA

[6]Fungal Pathogenesis Section, Laboratory of Clinical Immunology and Microbiology, National Institute of Allergy and Infectious Diseases, Bethesda, MD 20892, USA

[7]Microbiology Service, Department of Laboratory Medicine, Clinical Center, National Institutes of Health, Bethesda, MD 20892, USA

[8]Protein Characterization Laboratory, Cancer Research Technology Program, Frederick National Laboratory for Cancer Research, Leidos Biomedical Research Inc., Frederick, MD 21702, USA

[9]Frederick National Laboratory for Cancer Research, Leidos Biomedical Research Inc., Frederick, MD 21702, USA

[10]Sequencing Facility, Cancer Research Technology Program, Frederick National Laboratory for Cancer Research, Leidos Biomedical Research Inc., Frederick, MD 21702, USA

[11]Present address: Department of Oral Biology, Yonsei University College of Dentistry, 50-1 Yonsei-ro, Seodaemun-gu, Seoul, 03722, Republic of Korea

Downloaded from aacrjournals.org/cancerres/article-pdf/doi/10.1158/0008-5472.CAN-26-0070/3828896/can-26-0070.pdf by National Institutes of Health user on 15 September 2026

X. Li, A.K. Singh, N. Song, and J.H. Badger contributed equally to this article.

Corresponding author: Yinling Hu, Laboratory of Cancer Immunometabolism, Center for Cancer Research, National Cancer Institute, National Institutes of Health, Frederick, MD 21701. Email: huy2@mail.nih.gov. Giorgio Trinchieri, Laboratory of Integrative Cancer Immunology, Center for Cancer Research, National Cancer Institute, National Institutes of Health, Bethesda, MD 20892. Email: trinchig@mail.nih.gov

Running title: Oral fungus and tumor interaction impairs innate immunity

Key words: Fungi, neutrophils, epithelial innate immunity, systemic inflammation, tumor-associated macrophages, STAT3, IL-1β, and EGFR, carcinogenesis

Conflict of Interest: The authors declare no conflict of interest.

Downloaded from aacrjournals.org/cancerres/article-pdf/doi/10.1158/0008-5472.CAN-26-0070/3828896/can-26-0070.pdf by National Institutes of Health user on 15 September 2026

ABSTRACT

Fungi have been detected within human tumors and shown to support tumor progression. A better understanding of how intratumoral fungi evade innate immunity, remodel the tumor microenvironment (TME), and promote tumorigenesis may provide insights into cancer pathogenesis and therapeutic strategies. Here, we showed that aggressive human head and neck squamous cell carcinomas (HNSCCs) harbor an elevated fungal burden, including the environmental fungus *Cladosporium cladosporioides*, and are infiltrated by *IL1B*-high neutrophils with impaired reactive oxygen species (ROS) production and phagocytosis, as well as *IL1B*-high macrophages. In a mouse model in which *Ikka* ablation drives tumorigenesis through EGFR and STAT3 activation, oral *C. cladosporioides* infection recapitulated key features of the human HNSCC TME, elevated serum IL-1β and IL-17A levels, and promoted both oral and skin SCC development. Oral fungal infection also increased the acidic metabolites uric acid and lactate in the TME. These metabolites enhanced *C. cladosporioides*-induced IL-1β production while reducing ROS production in neutrophils, thereby impairing fungal clearance. Mechanistically, *C. cladosporioides*, IL-1β, and IL-17A activated STAT3 and cyclin D1 signaling in SCC cells. Epithelial *Stat3* deletion abrogated both *Ikka* loss-driven and fungus-enhanced oral and skin carcinogenesis, reduced macrophage accumulation, restored normal oral neutrophil phenotypes, and cleared oral fungal infection. Furthermore, IL-1β induced by *C. cladosporioides* inoculation drove systemic inflammation that promoted skin SCC via an IL-1β/IL-1R feedback loop involving neutrophils and macrophages. Together, these findings identify a fungus-driven immunosuppressive circuit in which tumor-derived acidic metabolites impair antifungal immunity, thereby promoting both local and distal SCC progression.

Downloaded from aacrjournals.org/cancerres/article-pdf/doi/10.1158/0008-5472.CAN-26-0070/3828896/can-26-0070.pdf by National Institutes of Health user on 15 September 2026

SIGNIFICANCE: Fungal infections enhance IL-1β production and STAT3 signaling to promote infiltration of inflammatory neutrophils and macrophages that support squamous cell carcinoma progression, providing promising targets for cancer treatment and prevention.

Downloaded from aacrjournals.org/cancerres/article-pdf/doi/10.1158/0008-5472.CAN-26-0070/3828896/can-26-0070.pdf by National Institutes of Health user on 15 September 2026

INTRODUCTION

Pathogens and opportunistic microorganisms must overcome innate immune resistance mechanisms to cause disease. However, how interactions between pathogens and pattern recognition receptors (PRRs) dictate either the containment of pathogen spreading or disease progression remains unclear (1). Neutrophils provide the first line of defense against fungal pathogens by deploying fungicidal mechanisms, including the generation of reactive oxygen species (ROS) and granule protease-mediated phagocytosis (2-4). Intriguingly, diverse fungal taxa have been detected in human cancers (5-7).

To date, most studies have focused on fungus-induced inflammation in tumorigenesis and PRR activation in macrophages. Chronic *Cladosporium cladosporioides* infection in kinase-dead *Ikka* knockin mice promotes macrophage infiltration, T cell–mediated autoinflammation with blunted *Il17a* expression, and esophageal squamous cell carcinoma (ESCC) (8,9). Antifungal treatment prevents the development of fungus-promoted ESCC, pancreatic ductal adenocarcinoma (PDA), breast cancer, and lung adenocarcinoma (ADC) (5,10,11). In PDA, *Malassezia* translocates from the gut to the pancreas, binds mannose-binding lectin, and activates 3a/C3aR signaling (6), while *Alternaria alternata* activates Dectin-1 on PDA cells (12). Antibiotic-induced fungal expansion impairs radiotherapy in mammary cancer and melanoma via Dectin-1-mediated immunosuppressive macrophages (10). Similarly, *Aspergillus sydowii* recruits polymorphonuclear myeloid-derived suppressor cells (PMN-MDSCs) and promotes $Kras^{G12D}$-induced lung ADC via Dectin-1/CARD9 pathway in mice (13), although this PMN-MDSC population is not well characterized. However, how tumor-associated fungi evade immune surveillance and persist in the tumor microenvironment (TME) remains to be characterized.

Head and neck SCC (HNSCC), including oral SCC, is the sixth most common human cancer worldwide. The oral cavity provides a unique niche for commensal and environmental microbiota (5,14-16). HNSCCs arise from stratified or pseudostratified epithelial surfaces that are directly exposed to

Downloaded from aacrjournals.org/cancerres/article-pdf/doi/10.1158/0008-5472.CAN-26-0070/3828896/can-26-0070.pdf by National Institutes of Health user on 15 September 2026

environmental microbes, yet they infrequently harbor *RAS* mutations (cBioPortal). *C. cladosporioides* is a common environmental fungus associated with respiratory allergies and intrabronchial lesions in humans. Both *C. cladosporioides* and its metabolite, calphostin-C, which inhibits protein kinase C (PKC) and activates EGFR signaling, have been detected in human HNSCC, ESCC, breast cancer, glioblastoma, and lung cancers (7-9,17-19). Thus, defining how environmental fungi modulate epithelial oncogenic pathways and impair antitumor immunity may provide new insights into HNSCC pathogenesis and therapy.

Previously, we reported that mice with keratinocyte-specific *Ikka* ablation develop EGFR-dependent spontaneous skin SCC associated with increased STAT3 activity (20,21). STAT3 signaling regulates major immunoregulatory and inflammatory pathways (22,23). In this study, we targeted these pathways to engineer a novel oral SCC model that recapitulates key features of human HNSCC. We then used this model to investigate how oral *C. cladosporioides* infection influences local and distal epithelial immunity-associated carcinogenesis, and to evaluate the clinical relevance of these findings for improving the prognosis and treatment of human HNSCC.

Materials and Methods

Mouse strains and ethics statement

All mice used in this study were cared for in accordance with the guidelines of the Institutional Animal Care and Use Committee (IACUC) of the National Institutes of Health. All animal experiments (Protocols 17-051, 17-052, 20-051, 20-052, 23-051, and 23-052) were approved by IACUC. $Ikka^{f/f}$,(21) K15.Cre^{PR1} (stock #005249, The Jackson Laboratory, RRID:IMSR_JAX:005249) and $Stat3^{f/f}$ (stock #016923, The Jackson Laboratory, RRID:IMSR_JAX:016923) mice were on a C57BL/6 background. $Il1r1^{-/-}$ mice (B6.129S7-Il1r1tm1Imx/J) were purchased from the Jackson Laboratory (Stock#003245,

Downloaded from aacrjournals.org/cancerres/article-pdf/doi/10.1158/0008-5472.CAN-26-0070/3828896/can-26-0070.pdf by National Institutes of Health user on 15 September 2026

RRID:IMSR_JAX:003245). *Il1b*$^{-/-}$ mice were gifts from Dr. Yoichiro Iwakura, the University of Tokyo and Dr. Katrin Mayer-Barber, National Institutes of Health.

Cell culture

Human A431 epidermoid carcinoma cells (ATCC CRL-1555) and SCC-25 squamous cell carcinoma cells (ATCC CRL-1628) were obtained from the American Type Culture Collection (ATCC). Mouse B16F1 melanoma cells were obtained from the NIH cell repository. A431 and B16F1 cells were maintained in Dulbecco's modified Eagle's medium (DMEM) supplemented with 10% fetal bovine serum (FBS). SCC-25 cells were cultured in a 1:1 mixture of DMEM and Ham's F-12 medium supplemented with 10% FBS and 400 ng/mL hydrocortisone. Cells were maintained at 37°C in a humidified atmosphere containing 5% CO_2.

The identities of A431 and SCC-25 cells were verified by short tandem repeat (STR) profiling, and B16F1 cells were authenticated by mouse STR profiling. All cell lines were confirmed to be negative for mycoplasma contamination using a PCR-based mycoplasma detection assay before use in experiments. Early-passage cells were expanded and cryopreserved as multiple aliquots to establish working cell stocks. For all experiments, cells were used within 10 passages after thawing. Cultures exceeding 10 passages were discarded and replaced with freshly thawed cells from the cryopreserved stocks.

Gene ablation and mouse experiments

C57BL/6 *Ikka*$^{f/f}$ (wild-type, WT), *Ikka*$^{f/f}$;K15.Cre, and *Ikka*$^{f/f}$*Stat3*$^{f/f}$;K15.Cre mice were shaved at 6–8 weeks old. Then, 40 μg of RU486 (M8046, Sigma-Aldrich) in 200 μL of acetone was topically applied to the dorsal mouse skin and 200 μL of RU486 (200 μg/mL) in 50% DMSO was applied to the oral cavity for 10 consecutive days to generate *Ikka*$^{\Delta SOE}$ and *Ikka*$^{\Delta SOE}$*Stat3*$^{\Delta SOE}$ mice. After RU486 treatment, WT,

Downloaded from aacrjournals.org/cancerres/article-pdf/doi/10.1158/0008-5472.CAN-26-0070/3828896/can-26-0070.pdf by National Institutes of Health user on 15 September 2026

Ikka$^{\Delta SOE}$, and *Ikka*$^{\Delta SOE}$*Stat3*$^{\Delta SOE}$ mice were inoculated orally with 30 μL of 2 × 10^7 CFU *Cladosporium cladosporioides* or *Saccharomyces cerevisiae* (9). The inoculation was performed weekly for a total of 25 weeks. For the carcinogenesis experiment, mice were euthanized 13 months after the gene deletion, and the oral cavity and skin specimens were examined by histology, immunostaining, and various analyses. For EGFR inhibitor GW2974 (G0668, Sigma-Aldrich) treatment, experimental mice were orally infected with *C. cladosporioides* once per week for two weeks. Then, 0.3 μg GW2974 in 30 μL of PBS with 50% DMSO was dropped into the mouth of mice three times per week for four weeks. PBS with 50% DMSO in 30 μL was used as a control treatment. Oral swabs were collected after treatment with both *C. cladosporioides* and GW2974 for two months for examining fungal growth. For oral swabbing, 500 μL of sterile distilled water was added to a 1.5 mL tube. A cotton swab was soaked into the water, the extra water was squeezed off against the tube wall, and the swab was twirled slowly and thoroughly throughout the oral cavity of the mouse. The cotton swab was rinsed in the water in the 1.5 mL tube several times, and the extra water was squeezed out. All procedures, including swabbing and rinsing durations, were ultimately standardized at the same level (9).

For the subcutaneous B16F1 murine model, a 3 × 10^5 B16F1 (DCTD Tumor Repository, Sample ID# 0507501, RRID:CVCL 0158) cell suspension in 200 μL PBS was subcutaneously injected into the right flank of C57BL/6 mice at 8 weeks of age. Mice were divided into different groups with treatments. Tumor volume was recorded every day using a vernier caliper (tumor volume = ½ length × width^2). Once tumor volume reached approximately 40 mm^3 at day 8 post injection, mice were randomly allocated to different experimental groups and were inoculated orally with a fungal load of 2 × 10^7 CFU/ mouse in 30 μL PBS every other day. In the meantime, for neutralization of IL-1β, mice were injected intraperitoneally every other day with *InVivo*MAb anti-mouse/rat IL-1β antibody (200 μg per mouse, BE0246, BioX Cell, RRID:AB 2687727) or InVivoMAb polyclonal Armenian hamster IgG (200 μg per mouse, BE0091, BioX

Downloaded from aacrjournals.org/cancerres/article-pdf/doi/10.1158/0008-5472.CAN-26-0070/3828896/can-26-0070.pdf by National Institutes of Health user on 15 September 2026

Cell, RRID:AB 2687680). For macrophage depletion, mice were injected intraperitoneally every other day with 100 μL m-Clodrosome® liposomal clodronate or m-Encapsome® control liposome from a Mannosylated Macrophage depletion kit (5mg/mL, CLD-8914, Encapsula Nano Science) in 100 μL PBS. Each experiment was repeated three times. For the bone marrow (BM) transfer experiment, wild-type (WT) recipient mice were maintained on aqueous antibiotics by supplementing the water with amoxycillin for one week before BM transfer. After one week post transfer, 5×10^6 BM cells in 200 μL PBS through tail vein using 26G needle were injected into 900 cGy irradiated recipient WT mice. The red blood cells in the isolated BM cells from different mice with the same age and gender were removed. A 3×10^5 B16F1 cell suspension in 200 μL PBS was subcutaneously injected into the right flank of mice at day 20 post transfer. Half of these mice were orally inoculated with 30 μL 2×10^7 CFU live *C. cladosporioides* suspended in PBS at day 8 post injection. All tumor bearing mice were monitored regularly for reduced feeding, weight loss or dehydration. Tumor sizes were measured every day, and mice were sacrificed when the tumor volume reaches 2000 mm^3, as per IACUC limit.

Examination of pH values in water containing oral swabs from mice

Mice were inoculated orally with 30 μL of 2×10^7 CFU *Saccharomyces cerevisiae* (O2240200, obtained from Seyedmojtaba Seyedmousavi's laboratory) or *C. cladosporioides* weekly for eight weeks. Oral pH values were then measured. For each mouse, 500 μL of sterile distilled water was added to a 1.5 mL tube. A cotton swab was soaked into the water, the extra water was squeezed off against the tube wall, and the swab was twirled slowly and thoroughly throughout the oral cavity of the mouse. The cotton swab was rinsed in the water in the 1.5 mL tube several times, and the extra water was squeezed out. The pH of the water in each tube was measured using a small-tipped pH meter (H1981036, Hanna Instruments) and paper pH testing strips (ColorpHast pH Strip, 4.0 to 7.0).

Downloaded from aacrjournals.org/cancerres/article-pdf/doi/10.1158/0008-5472.CAN-26-0070/3828896/can-26-0070.pdf by National Institutes of Health user on 15 September 2026

Antibodies and human samples

Antibodies used for immunoblotting and immunostaining included STAT3 (sc-293151, RRID:AB_3717599) and cyclin D1 (sc-717, RRID:AB_631336) from Santa Cruz Biotechnology; α-tubulin (ab4074, RRID:AB_2288001), uric acid (ab53000, RRID:AB_883382), and HIF-1α (ab2185, RRID:AB_302883) from Abcam; NLRP3 (NBP2-12446, RRID:AB_2750946) from Novus Biologicals Scientific; p-STAT3 (CST-9145s, RRID:AB_2491009), and p-EGFR (CST-2234s, RRID:AB_331701) from Cell Signaling Technology; HIF-1α (16H4L13, RRID:AB_2741461) from Thermo Fisher Scientific; HIF-1α (700505, RRID:AB_2532327) from Invitrogen; and β-actin (A2228, RRID:AB_476697) from Sigma-Aldrich. Human HNSCC tissue arrays and sections (HN438b, HN241b, HN811b, HuCAT476, HuCAT536, T271b, and HuCAT526) were purchased from US Biomax. Human samples were approved (protocol: 09-H0172) by the National Institute of Allergy and Infectious Diseases Institutional Review Board and written informed consent was obtained from all patients prior to sample collection (24). Studies were conducted in accordance with one of the following recognized ethical guidelines: Declaration of Helsinki, International Ethical Guidelines for Biomedical Research Involving Human Subjects (CIOMS), Belmont Report, or U.S. Common Rule. The human SCC cell lines A431 and SCC-25 (CRL-1555 and CRL-1628, ATCC, RRID:CVCL_0037 and RRID:CVCL_1682) (25) were used in this study.

Single-cell RNA sequencing (scRNA-seq)

Freshly and carefully dissected buccal mucosal layers from experimental mice of C57BL/6 background at nine months of age. Totally one pooled wild-type (WT *Ikka*$^{f/f}$) (n=3), two independent pooled *Ikka*$^{\Delta SOE}$ (n=3 each) and one pooled *Ikka*$^{\Delta SOE}$*Stat3*$^{\Delta SOE}$ (n=3) samples were minced into small pieces and incubated in DMEM/F12 with antibiotics, 30 μg/mL DNaseI, and 3 mg/mL collagenase P for 30

Downloaded from aacrjournals.org/cancerres/article-pdf/doi/10.1158/0008-5472.CAN-26-0070/3828896/can-26-0070.pdf by National Institutes of Health user on 15 September 2026

minutes at 37 °C with intermittent shaking to dissociate cells. Cells were then filtered through a 70-μm filter into a new tube (26). Blood samples were collected from mice with or without fungi treatment (five mice per group), and red blood cells were removed by using ammonium-chloride-potassium (ACK) lysis buffer several times. The backs of the mice including one pooled WT (n=3) and one pooled *Ikka*$^{\Delta SOE}$ (n=4) samples with skin tumor lesion were shaved, and the dorsal skin was isolated and floated on HBSS + 0.04% BSA. The skin was then cut into smaller pieces (approximately 1 mm in width) and incubated in 0.2% collagenase at 37 °C for one hour. Partly digested skin was placed in a 70-μm cell strainer, smashed with a piston and rinsed three times with HBSS + 0.04% BSA. The flow-through was saved on ice, while the undigested tissue remaining in the cell strainer was incubated in 0.05% trypsin-EDTA for 15 minutes at 37 °C. Trypsin-digested tissue was smashed once more and then passed through a 70-μm cell strainer. The flow-through of the collagenase digestion (containing mainly stromal cells) and the flow-through of the trypsin digestion (containing mainly epidermal cells) were pooled, spun down, and filtered through a 70-μm cell strainer. Viability of the cell suspension was determined using trypan blue (27).

All samples were sent to the Sequencing Facility at the Center for Cancer Research, National Cancer Institute (https://ncifrederick.cancer.gov/services/accessioning/Services/LabServices/Area/10). 10× Genomics Single Cell Gene Expression libraries were sequenced. Primary analysis was performed with Cell Ranger 6.1.2 (RRID:SCR_017344) software under the default parameters. The Seurat v4.0.3 package (RRID:SCR_016341) for R was used to further analyze scRNA-seq data (28). Outliers to the 200–2500 read count (nFeature_RNA) were excluded to eliminate doublets and debris. After normalizing and scaling data, we performed a linear dimensional reduction by principal component analysis using the top 2,000 most viable genes (FindVariableFeatures). Based on an elbow plot, we selected principal appropriate components to calculate the shared nearest neighbor graph and clustered data using the Louvain algorithm (29) with a resolution of 0.5 using the function FindClusters (30). Clustered data were displayed using

Downloaded from aacrjournals.org/cancerres/article-pdf/doi/10.1158/0008-5472.CAN-26-0070/3828896/can-26-0070.pdf by National Institutes of Health user on 15 September 2026

uniform manifold approximation and projection (UMAP) dimensional reduction (RunUMAP function). Clusters were identified using the Seurat function FindAllMarkers for immune populations, and the SingleR package (31) was used to confirm each cluster. The DoHeatmap function was used to show marker genes in clusters of interest. The gene expression profile was presented using the Vlnplot function from the Seurat package. Differential gene expression between two groups was analyzed by DEsingle package (32).

For scoring of biological processes, the biological gene set signature was scored for individual cells using the "AddModuleScore" function from Seurat 4.1. The ROS production, Gelatinase, and Phagocytosis genes were used based on a reported method (33). The calculation was based on the average expression levels of each gene set signature subtracted by aggregated expression of control features set that are randomly selected. scRNA-seq data have been deposited in the NCBI Gene Expression Omnibus (accession number GSE223442 and GSE215966).

RNA-seq

Fungi (2×10^7 CFU) in 30 μL PBS were heated at 95 °C for 10 minutes and were used to treat cells. A431 or SCC25 cells were plated into a six-well plate at 5×10^5 cells per well. Cultured cells were collected after treatment with heat-killed *C. cladosporioides* or calphostin C. Bone marrow (BM) cells were flushed from femur/tibia pairs of 8–12-week-old WT C57BL/6 mice with PBS using a 25-gauge needle. Red blood cells were removed using ACK lysis buffer, and cells were washed with PBS. BM neutrophils were isolated with density gradient centrifugation using Histopaque 1119 (density, 1.119 g/mL) (11191, Sigma) and Histopaque 1077 (density, 1.077 g/mL) (10771, Sigma) (34) at 2000 rpm for 30 minutes. After being washed with PBS, neutrophils were seeded in 24-well plates at one million cells per well with 1 mL medium and treated with 10 μL heat-killed *C. cladosporioides* (approximately 6.7

Downloaded from aacrjournals.org/cancerres/article-pdf/doi/10.1158/0008-5472.CAN-26-0070/3828896/can-26-0070.pdf by National Institutes of Health user on 15 September 2026

293 $\times 10^6$) with or without lactic acid (2 mM) or uric acid (10 μM) overnight in RPMI-1640 medium with 10%
294 FBS and L-glutamine and 1× Penicillin-Streptomycin (Gibco, 15140122). Cells were collected and RNA
295 was extracted with RNeasy Mini Kit (74104, QIAGEN). Samples were pooled and sequenced on a
296 NextSeq at the Center for Cancer Research's Sequencing Facility (Frederick, MD21701) by using
297 Illumina TruSeq Stranded mRNA Library Prep and paired-end sequencing. Sequence data were analyzed
298 using R package DESeq2/3.1.0 (https://bioconductor.org/packages/release/bioc/html/DESeq2.html). For
299 Gene Set Enrichment Analysis (GSEA) of the RNA-seq data, the list of significant differentially expressed
300 genes (DEGs) (logFC > 0.4|, padj < 0.05) were ranked by fold change, and KEGG pathway enrichments
301 and other gene sets were analyzed by GSEA_4.0.3. The enriched pathways for fungus treated DEGs were
302 selected, and normalized enriched scores (NES) were plotted. Heatmaps were presented according to
303 related pathways. RNA-seq data were deposited in the NCBI Gene Expression Omnibus (GEO) (accession
304 number GSE192654 and GSE223080). Fgsea analysis and volcano plot were generated by R packages
305 based on RNA-seq data.
306
307 **Neutrophil extracellular trap visualization**
308 Bone marrow (BM) cells were flushed from femur/tibia pairs of 8–12-week-old WT C57BL/6 mice
309 with PBS using a 25-gauge needle. Red blood cells were removed using ACK lysis buffer, and cells were
310 washed with PBS. BM neutrophils were isolated by density gradient centrifugation using Histopaque
311 1119 (density, 1.119 g/mL) (11191, Sigma) and Histopaque 1077 (density, 1.077 g/mL) (10771, Sigma)
312 (34) at 2000 rpm for 30 minutes. After being washed with PBS, neutrophils were seeded in 24-well plates
313 at one million cells per well and treated with live *C. cladosporioides* (MOI to neutrophils is 10:1) with or
314 without lactic acid (2 mM) or uric acid (10 μM) for 2.5 hours in RPMI-1640 medium with 10% FBS and
315 L-glutamine and 1× Penicillin-Streptomycin (Gibco, 15140122). After incubation, supernatant culture

Downloaded from aacrjournals.org/cancerres/article-pdf/doi/10.1158/0008-5472.CAN-26-0070/3828896/can-26-0070.pdf by National Institutes of Health user on 15 September 2026

316 medium was collected and mixed well and 20 μL supernatant from each was added into 3 mL of YPD for
317 fungal culture overnight. Then cells were stained with 5 μM SYTOX™ Green Nucleic Acid Stain
318 (Invitrogen, S7020) in 1× HBSS (J67799.K2, Gibco). After staining, round coverslips in the wells were
319 picked out and put onto the slides, and a big drop of anti-fade mounting medium (H-1000-10, Vector Lab)
320 was dropped on the samples and the slides were sealed with a square coverslip and ready for observation
321 under fluorescence microscope. A SmartSpec 3000 spectrophotometer (Bio-Rad Laboratories) was used
322 to measure fungi density at OD_{600} on the next day.
323
324 **Fluorescence *in situ* hybridization (FISH) for fungal staining**
325 FISH was done on paraffin-embedded human HNSCC tissue array sections (HN241b and HN811b,
326 US Biomax) and human HNSCC tissue sections (HuCAT526, HuCAT536) and fungus-negative control
327 specimens (Fungus 4-Tissue Artificial TMA Aspergillus, Candida, Histoplasma and Negative control,
328 BSB-0335-CS, BioSB). To prevent tissue detachment during antigen retrieval, slides were baked for 60
329 minutes at 60 °C and then immediately were immersed in xylene two times for 10 minutes each time (fresh
330 xylene each time) and in 100% ethanol two times for 10 minutes each time (fresh ethanol each time), then
331 in 95% ethanol for 10 minutes, and finally in 70% ethanol for 3 hours at 4 °C. Slides were then rinsed in
332 RNase-free 2× SSC (AM9763, Invitrogen™) for 10 minutes, treated with proteinase K solution (10 μg/ml
333 in 2× SSC) for 10 minutes in 42 °C, and were then washed in 2× SSC for 5 minutes twice, followed by 2
334 rinses in wash buffer [2× SSC, 15% formamide (F9037, Sigma-Aldrich)] for 5 minutes each. For
335 Hybridization, D223 28S rRNA gene probe (5'-CCACCCACTTAGAGCTGC-3') labeled with Cy3 or
336 FAM fluorophore (Cy3 λex = 555 nm; λem = 569 nm; FAM: λex = 493 nm, λem = 517 nm) was used to
337 detect the fungal signals in the tissues. Slides were incubated with the 1 μM probe in hybridization buffer
338 [(2× SSC, 10% dextran sulfate (D8906, Sigma-Aldrich), 1 mg/mL salmon sperm DNA, 15% formamide,

Downloaded from aacrjournals.org/cancerres/article-pdf/doi/10.1158/0008-5472.CAN-26-0070/3828896/can-26-0070.pdf by National Institutes of Health user on 15 September 2026

0.02% BSA, 2mM vanadyl ribonucleoside (S1402S, New England Biolabs)] at 30 °C overnight in the humidified chamber of an incubator and then were washed in the wash buffer at 30 °C for 30 minutes. Samples were counterstained with VECTASHIELD® PLUS Antifade Mounting Medium with DAPI (#H-2000-10, Vector Laboratories). Slides were visualized under a confocal fluorescent microscope (Leica SP8 Laser Confocal Microscope).

Co-detection of RNAscope and immunofluorescent staining

Paraffin-embedded human HNSCC tissue sections (HN438b, HuCAT536 and HuCAT526, US Biomax), RNAscope with RNAscope® 2.5HD Detection kit (RED), and immunofluorescent staining were used for the co-detection. Slides were baked in a dry air oven at 60 °C for 60 minutes then incubated in xylene twice (5 minutes each time) and 100% ethanol twice (1 minute each time). After air drying, slides were incubated with RNAscope® hydrogen peroxide for 10 minutes at room temperature and washed with distilled water. Slides then were submerged into hot 1× co-detection target retrieval solution for 15 minutes at 98-102 °C and washed with distilled water and 1× PBS-T, and then moved up and down 3-5 times. Then 10 μg/mL Myeloperoxidase/MPO Antibody (#AF3667, R&D, RRID:AB_2250866) or Myeloperoxidase/MPO Antibody with 0.3 μg/mL Cladosporium Antibody (OX-CH1, DSHB Hybridoma, RRID:AB_2617415) diluted in co-detection antibody diluent was dropped on the slides and then the slides were placed in humidity tray and incubated at 4 °C overnight. Following antibody incubation, slides was washed by PBS-T twice and, submerged in 10% neutral buffered formalin (NBF) for 30 minutes in a fume hood, and then were washed by PBS-T. Slides were treated with 2-4 drops of RNAscope® protease plus and were incubated in the HybEZ^{TM} Oven at 40 °C for 30 minutes. After washing, slides were proceeded to RNAscope® protocol starting with IL-1β probe hybridization and ending with development of RED solution. Slides were washed by 1×wash buffer and incubated with co-detection blocker for 15 minutes at

Downloaded from aacrjournals.org/cancerres/article-pdf/doi/10.1158/0008-5472.CAN-26-0070/3828896/can-26-0070.pdf by National Institutes of Health user on 15 September 2026

40 °C. Second antibody of anti-goat IgG (H+L) Alexa Fluor™ 488 (#A-11055, Invitrogen, RRID:AB_2534102) or anti-goat IgG (H+L) Alexa Fluor™ 488 with anti-mouse IgG (H+L) Alexa Fluor™ 647 (A-21235, Invitrogen, RRID:AB_2535804) diluted in co-detection antibody diluent was added to the sections, which were then incubated for 60 minutes at room temperature. Slides were washed by PBS-T twice for 2 minutes, counterstained by VECTASHIELD® Antifade Mounting Medium with DAPI (#H-1200-10, Vector Laboratories), and finally sealed by a coverslip. Slides were visualized under a confocal fluorescent microscope (Leica SP8 Laser Confocal Microscope).

Immunoblotting

Cell lysates and protein extracts from tissues were applied to an acrylamide gel, and protein levels were measured by immunoblotting with specific antibodies. In brief, a lysate (10–50 μg) was dissolved in a protein gel loading buffer (Bio-Rad Laboratories), heated at 95 °C for 5 minutes, and resolved using 7–12% sodium dodecyl sulfate polyacrylamide gel electrophoresis (SDS-PAGE). Separated proteins were transferred to a polyvinylidene difluoride (PVDF) membrane (Immobilon-P, MilliporeSigma), blocked in 5% nonfat milk, and analyzed using the indicated primary and secondary antibodies. Proteins were detected using a chemiluminescence reagent (NEL104001EA, PerkinElmer). Human SCC A431 or SCC25 cells or murine cell line B16F1 were treated with heat-killed or live *C. Cladosporioides* or calphostin C (15383, Cayman Chemical) at a concentration of 10 nM, heat-killed *Saccharomyces cerevisiae*, heat-killed *Ramularia spp.* (P4211973, obtained from Seyedmojtaba Seyedmousavi's laboratory), IL-1β (10 ng/mL), IL-17A (10 ng/mL), and GW2974 (10 μM, G0668, Sigma-Aldrich) or osimertinib (AZD9291, 5 μM; Selleck Chemicals) at different time courses. Protein levels were examined by immunoblotting with antibodies against p-EGFR, EGFR, p-STAT3, STAT3, cyclin D1, HIF-1α, NOX2 or β-actin.

Downloaded from aacrjournals.org/cancerres/article-pdf/doi/10.1158/0008-5472.CAN-26-0070/3828896/can-26-0070.pdf by National Institutes of Health user on 15 September 2026

Neutrophils isolated from bone marrow were seeded in 24-well plates at one million cells per well and treated with heat-killed *C. cladosporioides* with or without lactic acid for three different time courses in RPMI-1640 medium with 10% FBS and L-glutamine and 1× Penicillin-Streptomycin (Gibco, 15140122). Cells were washed, centrifuged at 1000 *g* for 5 minutes, and resuspended in high-salt cell lysis buffer for 45 minutes on ice. Protein was quantified using Pierce BCA Protein Assay Kit (23225, Thermo Scientific).

RNA extraction and quantitative real-time polymerase chain reaction (qRT-PCR)

Total RNA was isolated from A431 cells and SCC25 cells using RNeasy Mini Kit (74104, QIAGEN). Complementary DNA (cDNA) was synthesized with a Tetro cDNA Synthesis Kit (BIO-65043, Bioline). For quantitative real-time polymerase chain reaction (qRT-PCR), genes of interest were examined with the PowerUp™ SYBR™ Green Master Mix (A25742, Applied Biosystems) and ABI Prism 7300 Detection System (4304437, Applied Biosystems) according to the manufacturer's instructions. PCR primers included human *STAT3* (*Forward*: CAGCAGCTTGACACACGGTA, *Reverse*: AAACACCAAAGTGGCATGTGA), *IL1B* (*Forward*: ATGATGGCTTATTACAGTGGCAA, *Reverse*: GTCGGAGATTCGTAGCTGGA), *CCND1* (*Forward*: GCTGCGAAGTGGAAACCATC, *Reverse*: CCTCCTTCTGCACACATTTGAA), *HIF1A* (*Forward*: GAACGTCGAAAAGAAAAGTCTCG, *Reverse*: CCTTATCAAGATGCGAACTCACA), *HK2* (*Forward*: TGCCACCAGACTAAACTAGACG, *Reverse*: CCCGTGCCCACAATGAGAC), *JUN* (*Forward*: TCCAAGTGCCGAAAAAGGAAG, *Reverse*: CGAGTTCTGAGCTTTCAAGGT), and *TRIB3* (*Forward*: AAGCGGTTGGAGTTGGATGAC, *Reverse*: CACGATCTGGAGCAGTAGGTG), all from Integrated DNA Technologies. Gene expression was normalized to expression level of the β-actin housekeeping gene, *ACTB* (*Forward*: CATGTACGTTGCTATCCAGGC, *Reverse*:

Downloaded from aacrjournals.org/cancerres/article-pdf/doi/10.1158/0008-5472.CAN-26-0070/3828896/can-26-0070.pdf by National Institutes of Health user on 15 September 2026

CTCCTTAATGTCACGCACGAT). Data were analyzed by the ΔΔCt method and were expressed as a fold-change in mRNA expression relative to control values.

For the Real-time PCR to detect *Cladosporium cladosporioides* in paraffin-embedded human cancer specimens, briefly, paraffin-embedded tissue sections of human cancer (HuCAT476, HuCAT471, HuCAT481, HuCAT526, HuCAT531, HuCAT536, HuCAT541) were collected and transferred to sterile Eppendorf tubes in biosafety level II hood and soaked in 1mL xylene/tube for 1 hour at room temperature, followed by three washes with 100% ethanol, 75% ethanol, and sterile 1× PBS, respectively. Tissue samples and human cell lines (A549, SCC25, A431) were then subjected to overnight digestion in tissue lysis buffer (100 mM Tris-HCL pH 8.0, 200 mM NaCl, 2mM EDTA, 0.2% SDS, 200 μg/mL proteinase K) at 0.3 mL/sample. After digestion, genomic DNAs were extracted using one volume of phenol:chloroform:isopropanol alcohol (77176, Sigma-Aldrich) at 25:24:1 according to the commercial manual. For Cladosporium real-time PCR, 300 ng/sample DNA was used and real-time PCR was performed using *Cladosporium cladosporioides* TaqMan PCR Detection Kits (TM33050, Norgen Biotek) with Specific Primer and Probe mix as well as *C. cladosporioides* positive DNA control in the kit and 100 ng/sample DNA was used as negative control by using PowerUp™ SYBR™ Green Master Mix with GAPDH primer of human genomic DNA (*Forward*: GTCAAGGCTGAGAACGGGAA, *Reverse*: AGCCACACCATCCTAGTTGC). Since there is no amplification of negative samples (no Ct value), relative quantification was measured by $2^{-\Delta Ct}$.

Immunohistochemical and immunofluorescent staining

The Histology and Tissue Core Facility at the Frederick National Laboratory for Cancer Research, as well as Histoserv (Germantown, MD, 20874), prepared paraffin sections of mouse organs and performed hematoxylin and eosin (H&E) staining and immunohistochemical (IHC) staining for p-STAT3, cyclin D1,

Downloaded from aacrjournals.org/cancerres/article-pdf/doi/10.1158/0008-5472.CAN-26-0070/3828896/can-26-0070.pdf by National Institutes of Health user on 15 September 2026

HIF-1α, F4/80 (macrophages), Foxp3 (regulatory T cells), keratin 5 and Ki-67. Slides were baked at 60 °C for 1 hour before experiment. Immunofluorescent staining of other antibodies was performed on paraffin sections of murine oral cavity, human HNSCC tissue sections and fungus-negative human lung tissue (same as before) as well normal tissues. In brief, slides were deparaffinized and rehydrated using the following protocol: Xylene for 10 minutes twice, 100% ethanol for 5 minutes, 95% ethanol for 5 minutes, 70% ethanol for 5 minutes and three washes in PBS for 2 minutes each. Then endogenous peroxidase quenching was performed by using Peroxide Blocking Reagent (927402, BioLegend) for 30 minutes, followed by Target Retrieval Solution (S236784-2, DAKO) for 10 minutes at 95 °C. Slides were left to cool at room temperature and then washed three times in PBS. Blocking was done with 1% BSA and 0.2% Triton in PBS for 60 minutes at room temperature. Slides were then incubated overnight at 4 ºC with primary antibodies against NLRP3 (NBP2-12446, RRID:AB_2750946), p-EGFR (CST-2234s, RRID:AB_331701) or uric acid (ab53000, RRID:AB_883382) or with anti-Cladosporium antibody (OX-CH1, DSHB Hybridoma, RRID:AB_2617415). Sections were then washed and stained with the fluorescence-conjugated secondary antibodies for one hour at room temperature. Finally, sections were mounted with VECTASHIELD® Antifade Mounting Medium with DAPI (#H-1200-10, Vector Laboratories). Immunofluorescent staining was visualized, and cells were photographed under a fluorescence microscope (Nikon Eclipse E800, Nikon Instruments) or a confocal fluorescent microscope (Leica SP8 laser confocal microscope). Numbers of macrophages and Treg cells were statistically analyzed by counting positive IHC-stained cells in the same numbers of views in each section from each group. Each group contained three to four mice. IHC staining intensity for p-STAT3, cyclin D1, and HIF-1α was determined by Image J software.

Bead-based flow cytometry for cytokines from serum

Downloaded from aacrjournals.org/cancerres/article-pdf/doi/10.1158/0008-5472.CAN-26-0070/3828896/can-26-0070.pdf by National Institutes of Health user on 15 September 2026

All blood samples were collected in nonheparinized tubes and allowed to clot at room temperature (RT) for one hour and then centrifuged at 1,000 *g* for 10 minutes at room temperature. Serum samples were absorbed from the coagulated blood, aliquoted, and stored at −80 °C. BioLegend LEGENDplex (Mouse Inflammation Panel Mix and Match panel, #740446) bead-based immunoassays were used to analyze 13 mouse cytokines, including IL-1α, IL-1β, IL-6, IL-10, IL-12p70, IL-17A, IL-23, IL-27, MCP-1, IFN-β, IFN-γ, TNF-α, and GM-CSF according to the manufacturer's instructions. In brief, 25 μL of each serum sample, diluted twofold with assay buffer, were added into 25 μL of mixed beads and an assay buffer solution in the wells. The plate was then covered with a plate sealer and placed on a plate shaker at 800 rpm for two hours at room temperature. After one wash with 1× washing buffer to remove unbound proteins, 25 μL of detection antibodies were added to each well. The plate was then covered with a plate sealer and shaken at 800 rpm for one hour at room temperature. Without washing the plate, 25 μL of SA-PE antibodies were added to each well. The plate was then covered with a plate sealer and shaken at 800 rpm for another 30 minutes at room temperature. After one wash with 1× washing buffer, samples were suspended with wash buffer and analyzed on a flow cytometer. Data were calculated and collected using the LEGENDplex data analysis software (BioLegend).

Flow cytometry

Freshly dissected oral buccal and skin samples, and bone marrow neutrophils were isolated as described above. Blood cells were collected from WT C57BL/6 mice (8–12 weeks old) in heparin tubes, and red blood cells were removed by several times with ACK lysis buffer. White blood cells were seeded in a 24-well plate and treated with 10 μL heat-killed *C. cladosporioides* (approximately 6.7×10^6 CFU) and lactic acid (2 mM) or uric acid (10 μM) overnight in RPMI-1640 medium with 10% FBS and L-glutamine. All cell samples were collected for flow cytometric analyses. For the ROS determination, cells

Downloaded from aacrjournals.org/cancerres/article-pdf/doi/10.1158/0008-5472.CAN-26-0070/3828896/can-26-0070.pdf by National Institutes of Health user on 15 September 2026

were stained with DHR123 (Dihydrorhodamine 123, Sigma-Aldrich D1054, 10 uM) in 100 μL PBS in a 37°C incubator for 10 minutes (protected from light). After staining, cells were blocked with rat serum in flow buffer (2 mM EDTA and 0.1% BSA in PBS) for 5 minutes, and then washed, and resuspended in PBS with LIVE/DEAD Fixable Violet Dead Cell Stain kit for 30 minutes at 4°C in dark. Then cells were stained with PE-eFluor™ 610-CD45 antibody (61-0451-82, Invitrogen, RRID:AB_2574555), PE-Ly-6G antibody (101207, BioLegend, RRID:AB_312790), APC-F4/80 antibody (17-4801-82, eBioscience, RRID:AB_2784648), PE- Cyanine7-CD11b antibody (101215, BioLegend, RRID:AB_312798) for 30 minutes at 4 °C after one time wash with PBS. For IL-1β staining, cells were blocked in the same way and stained with LIVE/DEAD™ Fixable Green Dead Cell Stain kit for 30 minutes at 4°C in dark. Then, Cells were stained with PE-eFluor 610-CD45 antibody (61-0451-82, Invitrogen, RRID:AB_2574555), APC anti-mouse CD326 (Ep-CAM) antibody (118213, BioLegend, RRID:AB_1134105) or APC-F4/80 antibody (17-4801-82, eBioscience, RRID:AB_2784648), Pacific Blue™ Ly-6G antibody (127612, BioLegend, RRID:AB_2251161), and PE-Cy7-CD11b antibody (101215, BioLegend, RRID:AB_312798) for 30 minutes at 4 °C, washed with PBS, and fixed in fixation buffer from staining buffer kit (00-5523-00, eBioscience) for 40 minutes. After washing with 1× permeabilization buffer, cell samples were stained with antibodies for biotin anti-mouse and rat IL-1β antibody (503505, BioLegend, RRID:AB_2295906) in 1× permeabilization buffer at room temperature for 30 minutes, washed, and stained with streptavidin PE conjugate antibody (12-4317-87, Invitrogen) for another 30 minutes at room temperature. Finally, cells were washed, resuspended in flow buffer, and analyzed with flow cytometry. For lymphocytes detection, cell samples were stained with LIVE/DEAD™ Fixable Violet Dead Cell Stain Kit (L34955, Invitrogen), and then with the appropriate antibodies including PE-Cyanine7-CD3e antibody (25-0031-82, eBioscience, RRID:AB_469572), PE-eFluor 610-CD45 antibody (61-0451-82, Invitrogen, RRID:AB_2574555), Brilliant Violet 785™ CD4 Antibody (100453, BioLegend, RRID:AB_2565843),

Downloaded from aacrjournals.org/cancerres/article-pdf/doi/10.1158/0008-5472.CAN-26-0070/3828896/can-26-0070.pdf by National Institutes of Health user on 15 September 2026

PerCP/Cyanine5.5 CD8a Antibody(100734, BioLegend, RRID:AB_2075238) at 4 °C for 30 minutes. Stained cells were washed with PBS and fixed in fixation buffer from the staining buffer kit (00-5523-00,

For reversed-phase ion-pairing LC-MS^2 assay for measuring glycolysis and intermediate metabolites, all reference standards compounds (TGP) were obtained from Sigma-Aldrich (St. Louis, MO). Stable isotope–labeled internal standards (SI-TGP) 13C_6-glucose-6-phosphate, and 13C_6-fructose-1,6-bisphosphate) were purchased from Medical Isotopes. All analytical standards have reported chemical and isotopic purity of ≥98% and were used without further purification. OmniSolv® LC-MS grade acetonitrile and methanol were obtained from EMD Millipore. Tributylamine (TBA), LC-MS grade acetic acid, and formic acid were purchased from Fisher Scientific. All chemicals and solvents used in this study were HPLC or reagent.

A431 and SCC25 cells were seeded into a six-well plate at 5×10^5 cells per well in triplicates and then treated with 30 μL heat-killed *C. cladosporioides* and 10 nM calphostin C. Cells were washed with PBS and then collected by scraping into PBS followed by centrifugation. Metabolites were extracted in 500 μl of chilled 80% methanol. Sample was vortexed vigorously for 30 s and centrifuged at 14,000*g* for 10 min. Fifty microlitre supernatant was transferred to an autosampler vial containing 50 μL 10 μM SI-TGP methanol solution. Sample was dried with the SpeedVac® vacuum concentrator (Thermo Fisher Scientific) and then reconstituted in 60 μL 3% (v/v) methanol in water. For glucose measurement, samples were derivatized with 3-nitrophenylhydrazine.

Ten microlitre sample was injected for reversed-phase ion-pairing LC-MS^2 analysis, performed on Thermo TSQ™ Quantiva triple quadrupole mass spectrometer (Thermo Scientific) coupled with a NexeraXR LC system (Shimadzu Scientific Instruments). Both the HPLC and mass spectrometer were controlled by Xcalibur™ software (Thermo Scientific). The chromatography was carried out on a 100-mm long × 2.1-mm i.d. Synergi Hydro-RP C18 column with 2.5 μm particles and 100Å pore size

Downloaded from aacrjournals.org/cancerres/article-pdf/doi/10.1158/0008-5472.CAN-26-0070/3828896/can-26-0070.pdf by National Institutes of Health user on 15 September 2026

(Phenomenex) kept at 40°C. The mobile phase, operating at a flow rate of 200 μL/min, consisted of 10 mM TBAA in water as solvent A and methanol as solvent B. For the analysis the linear gradient stayed at B/A solvent ratio 3:97 for 3 min and then the B/A solvent ratio was changed from 3:97 to 80:20 in 14 min. After washing with 98% B for 3 min, the column was re-equilibrated with a mobile phase composition B/A of 3:97 for 10 min before the next injection. The general MS settings were as follows: source: ESI; ion polarity: negative; spray voltage: 2500 V; sheath and auxiliary gas: nitrogen; sheath gas pressure: 40 arbitrary units; auxiliary gas pressure: five arbitrary units; ion transfer capillary temperature, 350°C; scan type: selected reaction monitoring; collision gas: argon; collision gas pressure: 2 mTorr. Quantitation of the selected metabolites was carried out using Xcalibur™ Quan Browser (Thermo Scientific). Calibration curves for each metabolite were constructed by plotting TGP/SI-TGP peak area ratios obtained from calibration standards and fitting the data using linear regression with $1/X$ weighting. The metabolite concentrations in the samples were then interpolated using this linear function.

For examination of lactate in cell culture supernatant, the collected culture medium from A431 cells with and without treatment (as described above) was stored at −80 °C to inactivate endogenous lactate dehydrogenase. The lactate level in 50 μL of cell culture supernatant from each sample was analyzed using a Lactate Colorimetric Assay Kit II (K627-100, BioVision). The experimental procedure followed the kit's instruction. Oral swab solution from the mouth of mice was also used to detect lactate levels with the same kit.

Analysis of scRNA-seq data of human normal and HNSCC Samples

Human scRNA-seq data were obtained from GEO database (GSE139324), including the tissue resident immune cell samples from 5 healthy donor tonsils and the tumor infiltrating immune cell samples from 26 HNSCCs. Additional Human scRNA-seq data were obtained from GSE164690, including $CD45^+$

Downloaded from aacrjournals.org/cancerres/article-pdf/doi/10.1158/0008-5472.CAN-26-0070/3828896/can-26-0070.pdf by National Institutes of Health user on 15 September 2026

cell samples from 18 treatment naïve HNSCC patients. The Seurat v4.0.3 package (28) for R was used to analyze scRNA-seq data as above. Tumor stage information was obtained from their table. A neutrophil cluster was a subset from the data identified by using markers, including S100A8 and others. *IL1B* and other gene expression between healthy donors and HNSCCs in neutrophils and macrophages were compared and visualized by ggplot with "stat_compare_means" function to show *P* value in the plots. Further, HNSCC samples were divided into two groups based on the median expression levels of *IL1B*. The gene expression with specific signature scores (such as, sets of differentially expressed genes), including ROS ("CYBA","CYBB","CYP1A1","CYP1A2","CYP1B1","DDAH1","DUOX1","DUOX2","GBF1","HSP90AA1","MPO","NCF1","NOS1","NOS2","NOS3","P2RX4","RORA","SLC7A2","SOD1","SOD2","SPR") and PHAGOCYTOSIS ("ABCA1","ADGRB1","AIF1","ARHGAP12","ARHGAP25","BECN1","BIN2","CDC42","CLCN3","ELMO1","FCER1G","FCGR1","FCGR3","GSN","GULP1","IGLL1","ITGAM","ITGB2","MARCO","MEGF10","MFGE8","MSR1","MYH9","RAC1","RAC3","RHOBTB1","RHOBTB2","SH3BP1","SIRPA","THBS1","TREM2","TREML4","VAMP7","XKR4","XKR6","XKR7","XKR8","XKR9") was compared to $IL1B^{low}$ or $IL1B^{high}$ neutrophils, respectively. 'FindAllMarkers' function was used to compare the differential gene expression between $IL1B^{low}$ and $IL1B^{high}$ neutrophils in HNSCC samples. Macrophage cluster was identified by using markers, including CSF1R and others. The TAM signature scores in macrophage were compared between HD and HNSCC or different stages of HNSCC ("CD163","CSF1R","TREM2","SPP1","GPNMB","LGALS3","VSIG4","CD14","FOLR2","APOE ").

Quantification and statistical analysis

Downloaded from aacrjournals.org/cancerres/article-pdf/doi/10.1158/0008-5472.CAN-26-0070/3828896/can-26-0070.pdf by National Institutes of Health user on 15 September 2026

Statistical parameters, including the exact *n* value that represents number of mice per group, dispersion and precision measures (mean ± SEM or SD), and statistical significance, are reported in the figures and figure legends. Data were judged to be statistically significant when $P < 0.05$ by the selected statistical analysis method: two-tailed Student's t-test for comparison between two groups, as well as Fisher's exact test, Chi-squared (χ^2) test, and the log-rank test. In figures, asterisks denote statistical significance as calculated by the selected statistical analysis method (*$P < 0.05$; **$P < 0.01$; ***$P < 0.001$; ****$P < 0.0001$). Statistical analysis was performed in GraphPad Prism 6.

Data Resources and Data and Materials Availability

The mRNA expression data in human HNSCCs were downloaded from TCGA using cBioPortal (https://www.cbioportal.org/). TCGA RNA-seq data in human HNSCC data sets for the correlation analyses were downloaded from the Broad GDAC Firehose (https://gdac.broadinstitute.org/). Human scRNAseq data were obtained from GEO at GSE139324 and GSE164690. The scRNA-seq data generated in this study have been deposited in the NCBI GEO under accession numbers GSE223442 and GSE215966. The RNA-seq data generated in this study were deposited in the NCBI GEO under accession numbers GSE192654 and GSE223080. All other raw data generated in this study are available upon request from the corresponding author.

RESULTS

Advanced human HNSCCs exhibit increased fungal burden and infiltration of *IL1B*-High neutrophils with reduced phagocytic and oxidative gene Signatures, along with *IL1B*-High TAM

Downloaded from aacrjournals.org/cancerres/article-pdf/doi/10.1158/0008-5472.CAN-26-0070/3828896/can-26-0070.pdf by National Institutes of Health user on 15 September 2026

The oral cavity is a primary entry site for environmental microbes, where innate immune resistance is essential for restraining their expansion; however, the impact of fungal interactions with innate immune cells on the TME and oral carcinogenesis remains largely uncharacterized. We first performed Periodic Acid-Schiff staining, which revealed fungal elements in human HNSCC sections (Supplementary Fig. S1A). Fluorescence in situ hybridization (FISH) using a pan-fungal probe confirmed higher fungal abundance in HNSCC and adjacent SCC tissues compared with healthy HN tissue controls (Fig. 1A and B; Supplementary Fig. S1B). Stronger signals were observed in stage III–IV than in stage I-II HNSCCs. We next analyzed DNA from paraffin-embedded sections of 20 stage II–IV HNSCC cases (16 larynx, 3 oral cavities, and 1 tongue) using internal transcribed spacer (ITS) rRNA gene sequencing, identifying multiple fungal taxa in each sample (Fig. 1C; Supplementary Fig. S1C). Most identified fungi were environmental species, with *Cladosporium spp*. and *C. cladosporioides* detected in 14 and 13 of 20 samples, respectively. PCR with species-specific primers further confirmed the presence of *C. cladosporioides* in tumor samples but not in pathogen-free human tumor cell lines used as negative controls (Supplementary Fig. S1D). Finally, immunofluorescence (IF) staining with a *Cladosporium*-specific antibody showed significantly higher fungal signals in HNSCCs compared with healthy HN tissues, fungi-free human lungs, and *Candida*- or *Aspergillus*-positive rat lungs (Fig. 1D; Supplementary Fig. S1E and S1F).

We analyzed $CD45^+$ infiltrating hematopoietic cells in tumor tissues from 26 HNSCC patients and in tonsils from 5 healthy donors (HD) using publicly available single-cell (sc)RNA-seq data (Fig. 1E; Supplementary Fig. S2A and S2B). Cluster 5, comprising neutrophils characterized by high expression of *S100A8*, *SOD2,* and *CSF3R,* showed high *IL1B* and *CYBB* expression (Fig. 1F; Supplementary Fig. S2C) (33,35,36). *IL1B* expression was higher in HNSCC-derived neutrophils than in HDs (Fig. 1F, right). Neutrophils were stratified into *IL1B*-High and *IL1B*-Low groups based on median expression

Downloaded from aacrjournals.org/cancerres/article-pdf/doi/10.1158/0008-5472.CAN-26-0070/3828896/can-26-0070.pdf by National Institutes of Health user on 15 September 2026

612 (Supplementary Fig. S2D). Compared with *IL1B*-Low cells, *IL1B*-High neutrophils from HNSCCs
613 exhibited reduced expression of *CYBB* and *CYBA* and reduced ROS and phagocytosis gene signatures, but
614 increased expression of inflammatory genes, including *NLRP3* (24), *NFE2L2*, *CD44*, and other encoding
615 multiple cytokines, chemokines, and inflammation regulators (Fig. 1G and H; Supplementary Fig. S2E).
616 In contrast, no significant differences in these signatures were observed between *IL1B*-High and *IL1B*-
617 Low neutrophils from HDs (Fig. 1G; Supplementary Fig. S2E, left). Similar patterns were confirmed in
618 an additional cohort of 18 human HNSCC samples (Supplementary Fig. S2F–S2H).

619 Concurrently, the tumor-associated macrophage (TAM) signature score (37) was significantly higher
620 in macrophage from HNSCC than in those from healthy HN controls (Fig. 1I; Supplementary Fig. S2I).
621 Neutrophils from advanced HNSCC (stage III and IV) exhibited higher *IL1B* but lower *CYBB* expression
622 and ROS and phagocytosis gene signatures compared with those from early-stage tumors (Fig. 1J).
623 Consistently, both the TAM signature score and *IL1B* expression were increased in advanced versus early-
624 stage HNSCCs, although *IL1B* expression in macrophages showed only a trend toward elevation relative
625 to healthy tissues (Fig. 1K; Supplementary Fig. S2J, right, and S2K), indicating that TAMs are enriched
626 in HNSCC and that *IL1B* expression in both neutrophils and TAMs increases with tumor progression.

627 RNAscope corroborated higher *IL1B* expression in HNSCCs compared with healthy HN controls
628 (Supplementary Fig. S3A). In the *IL1B*-rich regions of HNSCC, neutrophils and *IL1B* expression were
629 co-localized with fungal signals, as examined by spatial RNAscope, FISH, immunohistochemical (IHC),
630 and IF staining (Fig. 1L; Supplementary S3B–S3D). The HNSCC patients with *IL1B*-High neutrophil
631 signature showed shorter overall survival compared to patients with *IL1B*-Low signature (Fig. 1M, left).
632 The *IL1B* signature and *STAT3* expression were positively correlated in HNSCCs (Fig. 1M, right).
633

Downloaded from aacrjournals.org/cancerres/article-pdf/doi/10.1158/0008-5472.CAN-26-0070/3828896/can-26-0070.pdf by National Institutes of Health user on 15 September 2026

Chronic oral *C. cladosporioides* infection promotes epithelial *Ikka* deletion-initiated oral carcinogenesis and is associated with increased intratumor IL-1β$^+$ neutrophils and elevated serum IL-1β and IL-17A in a STAT3-dependent manner

We established an experimental HNSCC mouse model to evaluate the role of *C. cladosporioides* infection in tumorigenesis. Since ablation of *Ikka* with K15.Cre^{PR1} drives spontaneous skin SCC in *Ikka$^{f/f}$* mice, we deleted *Ikka* or *Ikka/Stat3* in K15-expressing skin and oral epithelial stem cells (ΔSOE) by topical RU486 administration to *Ikka$^{f/f}$*;K15.Cre^{PR1} and *Ikka$^{f/f}$Stat3$^{f/f}$*;K15.Cre^{PR1} mice (Fig. 2A) (21,38). Mice were then orally inoculated weekly with *C. cladosporioides* or vehicle control for four months. *Ikka$^{\Delta SOE}$* mice developed oral papilloma and SCC in situ, with increased incidence following fungal inoculation, whereas WT mice remained tumor-free regardless of exposure (Fig. 2B and C). Concurrent *Stat3* deletion abolished oral carcinogenesis in both inoculated and control *Ikka$^{\Delta SOE}$Stat3$^{\Delta SOE}$* mice (Fig. 2B and C), indicating that both *Ikka* loss-initiated and fungus-enhanced tumorigenesis are STAT3 dependent, and that STAT3 acts as a key downstream effector of IKKα loss in epithelial cells (20). Oral epithelial cells from *Ikka$^{\Delta SOE}$* mice exhibited increased phosphorylated (p)-STAT3, cyclin D1 (a STAT3's target) (39), K5, Ki67, and p-EGFR compared with WT and *Ikka$^{\Delta SOE}$Stat3$^{\Delta SOE}$* mice (Fig. 2D; Supplementary Fig. S4A–S4C). IF staining further showed that the early tumor lesion invading the oral mucosa in *Ikka$^{\Delta SOE}$* mice lacked IKKα expression and exhibited elevated p-STAT3, whereas adjacent tissues were positive for IKKα and negative for p-STAT3 (Supplementary Fig. S4D).

Consistent with the findings in mice, human HNSCCs exhibited higher expression of cyclin D1 and p-STAT3 than healthy controls (Supplementary Fig. S4E). In contrast, a greater proportion of HNSCCs showed reduced expression of *CHUK,* which encodes IKKα, than increased expression (Supplementary Fig. S4F, left). Patients with hemizygous *CHUK* deletion and gain/amplification of *CCND1*, which encodes cyclin D1, had poorer survival than those with diploid status for both genes (Fig. 2E). Elevated

Downloaded from aacrjournals.org/cancerres/article-pdf/doi/10.1158/0008-5472.CAN-26-0070/3828896/can-26-0070.pdf by National Institutes of Health user on 15 September 2026

EGFR or *STAT3* expression was also associated with poorer survival (Fig. 2F). Approximately 40% of HNSCCs overexpressed *EGFR*, and *EGFR* expression correlated with *STAT3* and *CCND1* levels (Supplementary Fig. S4F, right, and S2G). These findings indicate that human and mouse HNSCCs share similar molecular features.

Following *C. cladosporioides* infection, fungal colonization increased in the oral cavity of infected $Ikka^{\Delta SOE}$ mice, but not in fungus-infected WT or $Ikka^{\Delta SOE}Stat3^{\Delta SOE}$ mice, nor in uninfected WT, $Ikka^{\Delta SOE}$, or $Ikka^{\Delta SOE}Stat3^{\Delta SOE}$ mice (Fig. 2G; Supplementary Fig. S4H). These findings suggest that enhanced colonization requires epithelial STAT3 signaling and a permissive TME. This increased fungal burden also correlated with greater infiltration of neutrophils and macrophages than in the other groups (Supplementary Fig. S4I). *C. cladosporioides* infection also increased IL-1β$^+$ neutrophils, IL-17A$^+$CD4$^+$ cells, and IL-1β$^+$ EpCAM$^+$ oral buccal epithelial cells, while reducing ROS$^+$ neutrophils in $Ikka^{\Delta SOE}$ mice relative to WT and $Ikka^{\Delta SOE}Stat3^{\Delta SOE}$ mice (Fig. 2H; Supplementary Fig. S4J). Moreover, serum IL-1β and IL-17A levels were elevated in infected $Ikka^{\Delta SOE}$ mice compared with infected WT and $Ikka^{\Delta SOE}Stat3^{\Delta SOE}$ mice (Fig. 2I), indicating that oral fungal infection can exert a systemic effect *in vivo*.

Infection-induced tissue damage can lead to uric acid (UA) release, which activates inflammasomes and promotes IL-1β production (24,40). Oral *C. cladosporioides* inoculation increased levels of UA and NLRP3 in the oral tissues of $Ikka^{\Delta SOE}$ mice compared with uninfected $Ikka^{\Delta SOE}$ mice (Fig. 2J and K; Supplementary Fig. S4K). In contrast, *Stat3* ablation significantly reduced oral UA and NLRP3 levels in $Ikka^{\Delta SOE}Stat3^{\Delta SOE}$ mice, regardless of *C. cladosporioides* infection. Consistently, copy number gains of *NLRP3* were observed in 136 of 488 HNSCC samples, and *NLRP3* expression positively correlated with *IL1B* expression (Fig. 2L; Supplementary Fig. S4L). Collectively, these data suggest that human and mouse HNSCCs share similar TME features, including increased IL-1β^{High} and ROS^{Low} neutrophils and the presence of fungi.

Downloaded from aacrjournals.org/cancerres/article-pdf/doi/10.1158/0008-5472.CAN-26-0070/3828896/can-26-0070.pdf by National Institutes of Health user on 15 September 2026

To characterize neutrophil responses to oral *C. cladosporioides* infection, we performed scRNA-seq of buccal mucosa, skin, and blood from infected WT, *Ikka*$^{\Delta SOE}$, and *Ikka*$^{\Delta SOE}$*Stat3*$^{\Delta SOE}$ mice (Fig. 3A–C; Supplementary Fig. S5A and S5B). UMAP identified cluster 12 as a population of oral cells expressing neutrophil markers including *S100a8*, *Cxcr2*, and *Ly6g*. This cluster comprised two distinct subsets: one with high *Cybb* (encoding NOX2), and *Cd177* expression (41) but low *Il1b*, *Nlrp3*, and *Myd88* expression; and the other showing the opposite pattern with high *Il1b*, *Nlrp3*, and *Myd88* but low *Cybb* and *Cd177* (Fig. 3B and C). Based on *Il1b* expression, re-clustering of neutrophils identified five subsets (clusters 0 to 4), defined as 0-*Il1b*^{M}, 1-*Il1b*$^{HIGH-1}$, 2-*Il1b*$^{LOW-1}$, 3-*Il1b*$^{HIGH-2}$, and 4-*Il1b*$^{LOW-2}$ (Fig. 3D). Cluster 0 co-expressed *Il1b* and *Cybb* (Fig. 3D and E). In WT mice, most neutrophils belonged to cluster 0 or *Il1b*^{LOW} clusters (2 and 4) (Fig. 3E–G). In contrast, *Il1b*^{HIGH} clusters (1 and 3), enriched for CC and CXC chemokines, chemokine receptors, and inflammatory regulators including *Nlrp3* and *Nlrp2*, were predominantly expanded in *Ikka*$^{\Delta SOE}$ mice (Fig. 3E–G). Notably, *Stat3* deletion in *Ikka*$^{\Delta SOE}$ mice restored neutrophil cluster distributions to a pattern resembling that of WT mice (Fig. 3G).

Reactome pathway analysis revealed that oral neutrophils from infected *Ikka*$^{\Delta SOE}$ mice were enriched for IL-1β, inflammasome, p75NTR signaling, and innate immune response pathways, but showed reduced enrichment of phagocytosis, host defense, and ROS production pathways compared with neutrophils from infected WT mice (Fig. 3H). Consistent with these findings, oral neutrophils from *Ikka*$^{\Delta SOE}$ mice showed higher expression of genes linked to IL-1β signaling and myeloid activation, including *Nlrp3*, *Il1b*, *Myd88*, *Ccl6*, and *Atf3*, and lower levels of genes involved in host-defense functions, including *Capg*, *Ltf*, *Camp*, *Lcn2*, and *Cybb* (Fig. 3I). Thus, compared with those in WT and *Ikka*$^{\Delta SOE}$*Stat3*$^{\Delta SOE}$ mice, oral neutrophils in *Ikka*$^{\Delta SOE}$ mice exhibited increased *Il1b* expression but reduced ROS and phagocytosis gene signatures (Fig. 3J).

Downloaded from aacrjournals.org/cancerres/article-pdf/doi/10.1158/0008-5472.CAN-26-0070/3828896/can-26-0070.pdf by National Institutes of Health user on 15 September 2026

Because oral instillation exposes fungi directly to oral neutrophils, epithelial cells, and TME, we compared neutrophils from the buccal mucosa, blood, and skin across WT, *Ikka*$^{\Delta SOE}$, and *Ikka*$^{\Delta SOE}$*Stat3*$^{\Delta SOE}$ mice following *C. cladosporioides* infection (Fig. 3J). Skin neutrophils showed similar but less pronounced alterations compared with oral neutrophils, whereas blood neutrophils exhibited minimal changes (Fig. 3J; Supplementary Fig. S5C–S5E). In addition, the oral cavity of infected *Ikka*$^{\Delta SOE}$ mice showed an increased TAM signature score, including genes *Cd163*, *Csf1r*, *Trem2*, *Lgals3*, *Folr2*, *Gpnmb*, *Spp1*, *Cd14*, *Ctss*, and *Ccl6* (Fig. 3K; Supplementary Fig. S5E). Oral macrophage infiltration was also higher in *Ikka*$^{\Delta SOE}$ mice than in WT and *Ikka*$^{\Delta SOE}$*Stat3*$^{\Delta SOE}$ mice (Supplementary Fig. S4I). *Il1b* expression in oral macrophages was also higher in *Ikka*$^{\Delta SOE}$ mice than in *Ikka*$^{\Delta SOE}$*Stat3*$^{\Delta SOE}$ mice, although it did not differ significantly between WT and *Ikka*$^{\Delta SOE}$ mice (Supplementary Fig. S5F). Collectively, these results suggest that oral neutrophils and macrophages contribute to the elevated serum IL-1β levels observed in fungus-infected *Ikka*$^{\Delta SOE}$ mice.

C. cladosporioides induces STAT3-dependent secretion of acidic metabolites by epithelial tumor cells and in the oral cavity of *Ikka*$^{\Delta SOE}$ mice

The increased oral fungal colonization in *Ikka*$^{\Delta SOE}$ mice requires epithelial cell STAT3 activity, suggesting involvement of downstream STAT3 targets. STAT3 regulates expression of HIF-1α (42) and of HK2, a target of HIF-1α required for glycolysis (43). Infection can elevate glucose metabolism (44,45), leading to the production of glycolytic metabolites such as lactate that promote tumor progression (46). We analyzed by RNA-seq the transcriptome of human SCC A431 cells exposed or not to *C. cladosporioides.* Fungal exposure upregulated genes involved in glucose transmembrane transport, including *TRIB3*, *CAPN10*, *IRS1*, *FGF19*, and *IL1B,* as well as HIF-1α targets related to glycolysis, such as *HK2*, *ENO2*, *JUN*, *EP300*, and *CREB1* (Fig. 4A, left and right) (47,48). *C. cladosporioides* treatment

Downloaded from aacrjournals.org/cancerres/article-pdf/doi/10.1158/0008-5472.CAN-26-0070/3828896/can-26-0070.pdf by National Institutes of Health user on 15 September 2026

increased lactate levels in the supernatant of A431 cell cultures compared to untreated controls (Fig. 4B). Silencing *HIF1A* reduced *C. cladosporioides*–induced lactate levels (Supplementary Fig. S6A). In vitro, fungal cell viability was not required for induction of glycolysis because exposure to heat-killed *C. cladosporioides* elevated the levels of glucose, lactate, and six intermediate metabolites in A431 and SCC25 cells in a STAT3-dependent manner (Fig. 4C–E; Supplementary Fig. S6B). Treatment with calphostin-C, a *C. cladosporioides* metabolite, also increased glucose and lactate levels in A431 cells (Supplementary Fig. S6C).

C. cladosporioides inoculation induced lactate production in the oral cavity of $Ikka^{\Delta SOE}$ mice but not in WT or $Ikka^{\Delta SOE}Stat3^{\Delta SOE}$ mice. Notably, lactate production was observed only in $Ikka^{\Delta SOE}$ mice inoculated with *C. cladosporioides*, and not with *S. cerevisiae* (Fig. 4F). Lactate and lactic acid (LA) are inter-exchangeable forms of the same metabolite (49-51). Consistent with this, *C. cladosporioides*, not *S. cerevisiae*, reduced oral pH in $Ikka^{\Delta SOE}$ mice, but not in WT and $Ikka^{\Delta SOE}Stat3^{\Delta SOE}$ mice (Fig. 4G; Supplementary Fig. S6D). Thus, *C. cladosporioides* infection induces secretion of acidic metabolites (LA and UA) in the oral cavity of $Ikka^{\Delta SOE}$ mice via a STAT3-dependent pathway.

STAT3 expression positively correlated with *HIF1A* expression in 523 human HNSCC samples, and both genes also correlated with *HK2*, *JUN*, *EP300*, and *CREB1* expression (Fig. 4H). In addition, *HIF1A*, *TRIB3,* and *IL1B* expression was higher in 519 human HNSCCs than in 44 healthy controls (Supplementary Fig. S6E). HNSCC patients whose tumors expressed high levels of both *STAT3* and *HIF1A* had poorer survival than those with lower expression of these genes (Supplementary Fig. S6F). HIF-1α IHC staining was stronger in human HNSCC sections than in healthy human oral epithelium and was also increased in oral lesions of *C. cladosporioides*–inoculated $Ikka^{\Delta SOE}$ mice compared to fungus-inoculated $Ikka^{\Delta SOE}Stat3^{\Delta SOE}$ and WT mice (Supplementary Fig. S6G and S6H). Together, these findings

Downloaded from aacrjournals.org/cancerres/article-pdf/doi/10.1158/0008-5472.CAN-26-0070/3828896/can-26-0070.pdf by National Institutes of Health user on 15 September 2026

support a shared phenotype between HNSCC patients and the mouse model, characterized by enhanced glucose metabolic pathway that promotes lactate secretion.

Acidic metabolites inhibit *C. cladosporioides*–induced ROS production and fungitoxicity, but promote IL-1β expression in neutrophils

In response to oral *C. cladosporioides* infection, fungal colonization, increased infiltration of neutrophils with aberrant signatures, and elevated levels of UA and LA, were observed in $Ikka^{\Delta SOE}$ mice, but not in WT and $Ikka^{\Delta SOE}Stat3^{\Delta SOE}$ mice. Therefore, we tested whether UA and LA influence neutrophil activity following fungal stimulation. *C. cladosporioides* treatment increased ROS and IL-1β production in neutrophils isolated from the bone marrow (BM) and blood of WT mice (Fig. 5A; Supplementary Fig. S7A). Consistently, fungal treatment of BM neutrophils elevated NOX2 levels, whereas LA repressed fungus-induced NOX2 expression (Supplementary Fig. S7B). Treatment of neutrophils with LA or UA suppressed fungus-induced ROS production but enhanced IL-1β expression (Fig. 5A), indicating that while *C. cladosporioides* induces ROS, LA or UA attenuates this response while promoting IL-1β expression.

To elucidate the pathways through which *C. cladosporioides*, UA, and LA regulate neutrophil activity, we treated BM neutrophils with the fungus and acidic metabolites. RNA-seq analysis revealed that *C. cladosporioides*, but not LA or UA, stimulated ROS-producing pathways and *Il1b* expression (Fig. 5B; Supplementary Fig. S7C). However, treatment of neutrophils with UA or LA inhibited fungus-induced expression of genes involved in ROS production and phagocytosis, while modestly enhancing the expression of *Il1b, Nlrp3,* and related inflammatory pathways, as shown by GO pathway and heatmap analyses (Fig. 5C–F). We confirmed that LA or UA suppressed fungus-induced expression of genes encoding two key receptors involved in phagocytosis: CD302, a C-type lectin receptor, and TLR2 (Fig.

Downloaded from aacrjournals.org/cancerres/article-pdf/doi/10.1158/0008-5472.CAN-26-0070/3828896/can-26-0070.pdf by National Institutes of Health user on 15 September 2026

5D, right) (52,53). Neutrophils kill pathogens in part through the formation of neutrophil extracellular traps (NETs) (54). To examine the effect of these metabolites on NETs formation, BM neutrophils were treated with live *C. cladosporioides* alone or in combination with UA or LA. Both UA or LA significantly inhibited *C. cladosporioides*-induced NETs formation (Fig. 5G and H, left; Supplementary Fig. S7D). To assess neutrophil-mediated fungitoxicity, an equal volume of each culture supernatant was added to YPD medium. Supernatants from neutrophils treated with *C. cladosporioides* alone markedly inhibited fungal growth, whereas this fungicidal effect was absent in supernatants from co-cultures treated with *C. cladosporioides* and either LA or UA (Fig. 5H, left, middle, and right). These results suggest that the metabolites suppress the fungicidal activity of neutrophils, mimicking the oral microenvironment observed in *C. cladosporioides*–infected $Ikka^{\Delta SOE}$ mice (Fig. 5I).

IL-1β and *C. cladosporioides* activate STAT3 in SCC cells

As increased fungal colonization was associated with enhanced oral tumor progression in *C. cladosporioides*-infected $Ikka^{\Delta SOE}$ mice, we investigated whether *C. cladosporioides* induces the expression of oncogenic molecules in tumor cells using RNA-seq analysis. Many genes with pro-tumorigenic activity were among the top 20 upregulated genes by the fungus (Supplementary Fig. S8A, left). Gene set enrichment and volcano plot analyses showed that fungal stimulation significantly activated multiple pathways, including IL-1β/STAT3/cyclin D1 and STAT3/HIF-1α/HK2 signaling (Fig. 6A and B; Supplementary Fig. S8A, right).

Because *C. cladosporioides* infection in $Ikka^{\Delta SOE}$ mice results in epithelial STAT3-dependent oral fungal expansion and in an increase of IL-1β in oral neutrophils and of IL-1β and IL-17A in the serum, we next investigated how these cytokines and *C. cladosporioides* influence STAT3 activity on tumor cells. Treatment with IL-1β, IL-17A, and heat-killed or live *C. cladosporioides* strains isolated from either mice

Downloaded from aacrjournals.org/cancerres/article-pdf/doi/10.1158/0008-5472.CAN-26-0070/3828896/can-26-0070.pdf by National Institutes of Health user on 15 September 2026

or humans induced p-STAT3, cyclin D1, and HIF-1α in human SCC cell lines A431 and SCC25, although with varying efficiency (Fig. 6C and D; Supplementary Fig. S8B–S8E, left). In contrast, heat-killed *S. cerevisiae* or *Ramularia spp.* isolated from human sputum failed to elicit these effects in A431 cells (Fig. 6D; Supplementary Fig. S8E, right). RT-PCR confirmed that *C. cladosporioides* induced *STAT3* expression and stimulated STAT3-dependent *IL1B* and *CCND1* expression in A431 and SCC25 cells (Fig. 6E; Supplementary Fig. S8F).

Fungus-induced endocytosis has been reported to activate EGFR on epithelial cells (55). Calphostin-C, a metabolite produced by *C. cladosporioides* that activates EGFR (19,56), was also found to stimulate STAT3 activity and induce cyclin D1 expression (Fig. 6F). STAT3 can be a downstream target of EGFR signaling (20,57). Previously, we showed that the EGFR inhibitor GW2974 diminishes skin SCC development driven by *Ikka* ablation in keratinocytes (21). To determine whether EGFR is required for calphostin-C- or *C. cladosporioides*–induced STAT3 activation, we treated A431 and SCC25 cells with the EGFR inhibitors GW2974 and AZD9291 (58), respectively, for 3 hours before exposure to *C. cladosporioides*. These inhibitors effectively blocked *C. cladosporioides*–induced p-EGFR and p-STAT3 levels (Fig. 6F; Supplementary Fig. S8G and S8H). Consistently, GW2974 also blocked calphostin-C–induced EGFR and STAT3 activation in A431 cells (Fig. 6F; Supplementary Fig. S8I). Increased p-EGFR staining was observed in oral cells of *C. cladosporioides*–infected $Ikka^{\Delta SOE}$ mice compared to WT mice (Supplementary Fig. S4C). Moreover, oral administration of GW2974 significantly reduced fungal colonization in the oral cavity of oral *C. cladosporioides*–infected $Ikka^{\Delta SOE}$ mice relative to vehicle controls (Fig. 6G), demonstrating that EGFR inhibition recapitulates the effect of *Stat3* depletion *in vivo* and *in vitro* on fungal growth.

In addition, both *C. cladosporioides* and calphostin-C promoted cell cycle progression (Supplementary Fig. S8J). However, the gene expression profile induced by *C. cladosporioides* was substantially broader

Downloaded from aacrjournals.org/cancerres/article-pdf/doi/10.1158/0008-5472.CAN-26-0070/3828896/can-26-0070.pdf by National Institutes of Health user on 15 September 2026

than that induced by calphostin-C, suggesting that calphostin-C contributes only partially to the activity of *C. cladosporioides*. Overall, these findings indicate that microenvironmental IL-1β and IL-17A and *C. cladosporioides* can activate epithelial cell STAT3 signaling and its downstream targets (Fig. 6H).

Oral *C. cladosporioides* infection enhances distal tumor growth by inducing systemic IL-1β

Oral *C. cladosporioides* inoculation also significantly enhanced *Ikka*-deletion-initiated, STAT3-dependent skin carcinogenesis (Fig. 7A; Supplementary Fig. S9A). The expression of p-STAT3, cyclin D1, and p-EGFR, as well as STAT3-dependent proliferation, were increased in $K5^+$ keratinocytes of skin tumors from $Ikka^{\Delta SOE}$ mice compared to normal skin from WT mice (Fig. 7B; Supplementary Fig. S9B and S9C). Compared to WT cells, K5- and K15-positive keratinocytes in $Ikka^{\Delta SOE}$ mice exhibited elevated expression of numerous genes that may contribute to skin carcinogenesis, as analyzed by scRNA-seq (Supplementary Fig. S9D, S9E, and S5A). These genes included markers associated with keratinocyte hyperproliferation, growth factor and MAPK pathway activation, stem cell identity, host defense responses, inflammatory pathways, and glucose metabolism (Supplementary Fig. S9E).

Lung tumors in *Ikka*-deficient mice present an immunosuppressive TME with increased ROS^+ macrophages and $Foxp3^+$ regulatory T (Treg) cells (20,21,59). Similarly, IHC staining revealed increased numbers of p-$STAT3^+$ epidermal keratinocytes, macrophages, and Treg cells in the skin of $Ikka^{\Delta SOE}$ mice compared to WT and $Ikka^{\Delta SOE}Stat3^{\Delta SOE}$ mice. Oral *C. cladosporioides* inoculation in $Ikka^{\Delta SOE}$ mice further enhanced these skin cell populations (Fig. 7C; Supplementary Fig. S9F). Notably, no increased fungal growth was observed in the skin of any of the six mouse groups, regardless of oral fungal inoculation (Supplementary Fig. S9G), and no increase in IL-$17A^+CD4^+$ T cells was detected in the skin of orally infected $Ikka^{\Delta SOE}$ mice. Thus, oral fungal infection may induce systemic mediators that contribute to distal tumorigenesis.

Downloaded from aacrjournals.org/cancerres/article-pdf/doi/10.1158/0008-5472.CAN-26-0070/3828896/can-26-0070.pdf by National Institutes of Health user on 15 September 2026

839 Because oral fungal infection significantly increased infiltrating macrophages in the skin of *Ikka*$^{\Delta SOE}$
840 mice compared to uninfected *Ikka*$^{\Delta SOE}$ mice, we analyzed, using scRNA-seq, the skin macrophages
841 expressing *Csf1r*, *Lyz2*, and *Itgam,* as well as the skin neutrophils expressing *Csf3r* and *S100a8* (Fig. 7D).
842 In UMAP plots, the macrophage cluster was much larger than the neutrophil population, suggesting that
843 macrophages are the predominant immune population contributing to the pro-cancer TME. UMAP
844 analysis revealed that *Il1b* and *Nlrp3* expression in macrophages were highly similar (Fig. 7D). The
845 expression of *Il1b*, *Nlrp3*, *Cybb*, *Cyba*, *Cxcl16*, and *Ccl3* as well as TAM genes (*Csf1r*, *Trem2*, *Spp1*,
846 *Apoe*, *Lgals3*, *Pla2g7*, and *Tgfbi*), was markedly upregulated in skin macrophages from *Ikka*$^{\Delta SOE}$ mice
847 compared to those from WT mice (Fig. 7E; Supplementary Fig. S9H). Based on *Il1b* expression, skin
848 macrophages were classified into two subsets: *Cybb*$^{+}$*Il1b*$^{+}$ and *Cybb*$^{+}$*Il1b*$^{-}$ (Fig. 7F). *Cybb*$^{+}$*Il1b*$^{+}$
849 macrophages displayed an inflammatory phenotype characterized by high expression of genes encoding
850 inflammatory regulators (*Il1a*, *Tnf*, *Cd274*, *Tnfrsf1b*, *Cxcl2*, and *Ccl4*) and multiple cytokine and
851 chemokine receptors, along with reduced expression of genes encoding C-type lectin PRRs, such as
852 CD209f, CD209g, and CD209d (Fig. 7F) (60). *Cybb*$^{+}$*Il1b*$^{-}$ macrophages highly expressed genes encoding
853 complement components (61), C-type lectin PRRs (62), and regulators of phagocytosis, including *Cd163*,
854 *Mrc1*, *C4b*, *Cd209s*, and *Cd36* (Fig. 7F) (63-66). The proportion of inflammatory *Cybb*$^{+}$*Il1b*$^{+}$ macrophage
855 was increased in the skin of *Ikka*$^{\Delta SOE}$ mice compared to WT mice (Fig. 7G, left).

856 Additionally, skin macrophages from *Ikka*$^{\Delta SOE}$ mice exhibited increased expression of genes involved
857 in inflammatory responses, IL-1 cytokine production pathways, NADH regeneration, ROS metabolism,
858 and innate immune response, while showing decreased expression of *Cd209* and complement component
859 genes, along with reduced phagosome activity, C-type lectin receptor signaling, and cellular responses to
860 pathogens compared to WT mice (Fig. 7G, right). Furthermore, oral *C. cladosporioides* infection elevated
861 IL-1β and ROS levels in skin macrophages from infected *Ikka*$^{\Delta SOE}$ mice compared to uninfected *Ikka*$^{\Delta SOE}$

Downloaded from aacrjournals.org/cancerres/article-pdf/doi/10.1158/0008-5472.CAN-26-0070/3828896/can-26-0070.pdf by National Institutes of Health user on 15 September 2026

mice (Fig. 7H). These findings suggest that the expansion of inflammatory IL-1β–expressing macrophages is associated with skin tumor progression induced by oral fungal infection.

IL-1β, a key cytokine that promotes a pro-inflammatory TME, stimulates expression of its own gene in both macrophages and neutrophils (67,68). Treatment of BM and blood neutrophils from WT mice with *C. cladosporioides* stimulated IL-1β expression and ROS production (Fig. 5A; Supplementary Fig. S7A). We hypothesized that systemic IL-1β levels induced by oral *C. cladosporioides* inoculation may contribute to skin tumor progression. To test this, we established a skin tumor model to dissect the roles of oral *C. cladosporioides,* IL-1β, oral neutrophils, and skin macrophages. We selected B16F, a skin melanoma cell line capable of forming tumors within a short timeframe. The B16F melanoma model was also well suited for this study because it has previously been used to investigate fungal contributions to tumorigenesis (10). Consistent with the relevance of this model, patients with skin cutaneous melanomas expressing low levels of *CHUK* exhibited worse survival than those with high *CHUK* expression (Supplementary Fig. S9I). In addition, IL-1β treatment induced p-STAT3 and HIF1A expression in B16F1 melanoma cells (Fig. 7I), while *STAT3* and *IL1B* macrophage signatures were highly correlated in human skin cutaneous melanomas (Fig. 7J). We therefore subcutaneously injected B16F1 cells into C57BL/6 WT mice (Fig. 7K). As the intratumoral neutrophil population in these skin tumors was markedly smaller than the macrophage population (Supplementary Fig. S9J, left), we focused on tumor-associated macrophages. Because WT mice rapidly clear oral fungal infections, repeated oral inoculations were necessary to maintain sustained interactions between fungi and neutrophils in the oral cavity. After tumors developed by day 8 following injection, oral *C. cladosporioides* inoculation every two days significantly promoted B16F1 tumor growth, which was associated with increased oral IL-1β$^+$ neutrophils, elevated serum IL-1β levels, and a higher number of IL-1β$^+$ macrophages within tumors compared to uninfected mice (Fig. 7L–P; Supplementary Fig. S9J, right). Treatment of orally fungus-infected mice with an anti-IL-1β antibody

Downloaded from aacrjournals.org/cancerres/article-pdf/doi/10.1158/0008-5472.CAN-26-0070/3828896/can-26-0070.pdf by National Institutes of Health user on 15 September 2026

markedly reduced tumor volume and weight, accompanied by decreased numbers of oral IL-1β$^+$ neutrophils, tumor-associated IL-1β$^+$ macrophages, and serum IL-1β levels compared to IgG-treated controls (Fig. 7L–P; Supplementary Fig. S9J). To confirm the role of fungal infection, we administered the antifungal drug Amphotericin B concurrently with oral fungal inoculation. This treatment inhibited subcutaneous tumor growth compared to mice receiving fungal inoculation alone (Fig. 7Q). Additionally, depletion of macrophages in orally fungus–infected mice using clodronate liposomes markedly reduced tumor-associated macrophages and blocked oral fungus-enhanced tumor growth compared to liposomes controls (Fig. 7R; Supplementary Fig. S9K). To confirm the roles of IL-1β and IL-1R in BM–derived cells, we generated chimeric mice transplanted with *Il1b*$^{-/-}$ or *Il1r1*$^{-/-}$ BM and injected B16F1 cells into these mice. These chimeras exhibited reduced oral-fungus-enhanced tumorigenesis, decreased numbers of intratumoral IL-1β$^+$ macrophage, and suppressed serum IL-1β levels compared to chimeric mice with WT BM (Supplementary Fig. S9L and S9M).

Collectively, this grafted tumor model shows that systemic IL-1β induced by oral *C. cladosporioides* infection promotes distal skin tumor growth through the cooperative actions of oral neutrophils and skin macrophages (Fig. 7S). These findings indicate that oral *C. cladosporioides* infection reshapes epithelial innate immunity to promote both local and distal tumor growth.

DISCUSSION

Accumulating evidence from both human studies and experimental animal models supports the presence of fungi within the TME and their role in carcinogenesis. In this study, we demonstrate that persistent oral infection with *C. cladosporioides* compromises local and distal epithelial innate resistance to pathogens and enhances tumor growth in a somatic mutation–driven spontaneous SCC mouse model. This model recapitulates key features of human HNSCC, including aberrant innate immune responses,

Downloaded from aacrjournals.org/cancerres/article-pdf/doi/10.1158/0008-5472.CAN-26-0070/3828896/can-26-0070.pdf by National Institutes of Health user on 15 September 2026

908 fungal colonization, activation of IL-1β, STAT3, and EGFR signaling, and IKKα loss-induced oncogenic
909 pathway. We show that fungal infection-induced acidic metabolites derived from tumor cells impair
910 neutrophil phagocytotic activity, facilitating fungal persistence and colonization. In turn, the fungi and
911 fungus-induced cytokines released by immune and epithelial cells stimulate tumor cell growth. These
912 findings establish a mechanistic framework linking fungal activity to the development of an
913 immunosuppressive TME.

914 The TME associated with HNSCC progression in both humans and mice is characterized by increased
915 fungal burden, elevated infiltration of inflammatory *IL1B*–expressing neutrophils with impaired gene
916 signature of ROS production and phagocytic activity, and accumulation of TAMs. *C. cladosporioides*, a
917 fungal species detected in most in human HNSCCs, enhances *Ikka* deletion–induced oral SCC
918 development in mice and increases oral fungal colonization through an EGFR–STAT3 pathway that
919 promotes both tumor growth and fungal expansion. In vivo and in vitro studies demonstrate that *C.*
920 *cladosporioides* stimulates epithelial-cell STAT3/Cyclin D1 signaling to promote cell cycle progression,
921 and STAT3/HIF-1α/glycolysis signaling that leads to the production of the acidic metabolite lactate (LA).
922 In addition, oral *cladosporioides* infection in $Ikka^{\Delta SOE}$ mice induces, in a STAT3-dependent manner, the
923 release of uric acid (UA), which increases NLRP3 expression (40) at oral malignant lesions. Together, the
924 acidic metabolites LA and UA impair the phagocytic and fungicidal activities of neutrophils induced by
925 *C. cladosporioides,* shifting them from protective, phagocytic neutrophils into inflammatory IL-1β–
926 expressing neutrophils and thereby worsening oral inflammation. These dysfunctional neutrophils fail to
927 provide effective immune surveillance, allowing fungal expansion and establishing a synergistic loop
928 among fungi, tumor cells, neutrophils, and TAMs that further amplifies oncogenic signaling.

929 Notably, oral fungal burden recruited neutrophils and macrophages. *C. cladosporioides* stimulated
930 *Il1b* expression in neutrophils and treatment with an anti-IL-1β antibody reduces the fungus-infection-

Downloaded from aacrjournals.org/cancerres/article-pdf/doi/10.1158/0008-5472.CAN-26-0070/3828896/can-26-0070.pdf by National Institutes of Health user on 15 September 2026

enhanced accumulation of both IL-1β$^+$ neutrophils in the oral cavity and IL-1β$^+$ TAMs in cutaneous tumors. These findings are consistent with the observation in human HNSCC, where increased *IL1B* expression in both neutrophils and TAMs is associated with advanced tumors. In line with our mouse studies, IL-1β has been reported to upregulate its own expression in human neutrophils and macrophages via an IL-1β/IL-1R-dependent positive feedback loop (67,68). Together, these findings suggest that elevated IL-1β in the TME promotes macrophage recruitment and *IL1B* expression. *IL1B*-high neutrophils in advanced HNSCC exhibit reduced phagocytic capacity and diminished ROS signatures. Furthermore, recruited TAMs show increased expression of genes such as *SPP1*, *GPNMB*, *TREM2*, *FOLR2*, *APOE*, *VSIG4*, and *CD14*, which promote cell growth, angiogenesis, and metastasis, as well as phagocytic activity that clears debris within the TME (69). Whether macrophages compensate for impaired neutrophil function remains to be determined. The interactions between neutrophils and macrophages in infection-associated carcinogenesis warrant further investigation.

Moreover, our data show that the extent of reduction in tumor-associated IL-1β$^+$ macrophages correlates with the degree of tumor growth inhibition when clodronate-liposomes treatment is compared with anti-IL-1β antibody treatment. Recent studies have shown that targeting specific TAM populations can suppress tumorigenesis (37,69). Given the nonspecific nature of clodronate-liposomes treatment and its potential adverse effects, targeting IL-1β$^+$ macrophages may represent a more precise therapeutic strategy for cancer.

Although oral *C. cladosporioides* infection does not lead to fungal dissemination to the skin in mice, elevated serum IL-1β levels were identified as a potential promoter of skin tumorigenesis. The skin TME associated with enhanced skin carcinogenesis exhibited increased levels of IL-1β, NLRP3, ROS, IL-1β$^+$ TAMs, and inflammation activators. While WT mice rapidly clear oral fungi, *C. cladosporioides* still induces IL-1β expression in WT neutrophils. Using a fast-growing skin tumor mouse model, we

Downloaded from aacrjournals.org/cancerres/article-pdf/doi/10.1158/0008-5472.CAN-26-0070/3828896/can-26-0070.pdf by National Institutes of Health user on 15 September 2026

demonstrate that repeated oral inoculation with *C. cladosporioides* promotes skin tumor growth through a systemic IL-1β axis involving oral neutrophils, circulating IL-1β, and TAMs. Blockade of IL-1β in any of these IL-1β$^+$ compartments is sufficient to suppress tumor progression, establishing IL-1β as a central systemic driver linking oral fungal exposure to distal tumor growth.

Studies have identified inborn errors in *CHUK* in patients with autoimmune diseases, which are associated with increased susceptibility to fungal infections (70-72). Patients with autoimmune diseases caused by mutations in the autoimmune regulator gene (*AIRE*) or in genes that regulate *AIRE* expression, as well as those with gain-of-function mutations in *STAT1*, are highly susceptible to fungal infections and exhibit an increased risk of developing oral and esophageal SCC, as well as gastrointestinal carcinomas (9,71,73,74), suggesting that increased susceptibility to fungal infection is closely associated with SCC pathogenesis. Here, we show that *Ikka* deletion-mediated SCC and fungus-enhanced SCC progression converge on the EGFR and STAT3 pathways, and that increased *IL1B* expression depends on STAT3 in human SCC cells and in the TME of animal models. Consistent with these findings, patients with HNSCC who exhibited similar molecular patterns have poorer survival.

Further studies are needed to determine whether increased fungal infection alters the compositions of oral and gut microbiota, thereby affecting the TME and carcinogenesis. In this study, the scRNA-seq analysis was restricted to neutrophils and TAMs, and future studies will explore broader immune and epithelial remodeling driven by local fungal interactions and systemic inflammation.

Authors' contributions

N-Y.S., J.W., F.Z., and Y.H. initiated the project. X.L., A.K.S., J.H.B., and R.D.N. further revealed the mechanism. X.L., N-Y.S., A.K.S., J.WB., D.T., F.Z., G.S., S.B., and T.G. performed various animal, biological, molecular, and histological analyses. X.L., J.H.B., R.D.N., C.J., C.O., K.C., X.X., T.A., Y.Z.,

Downloaded from aacrjournals.org/cancerres/article-pdf/doi/10.1158/0008-5472.CAN-26-0070/3828896/can-26-0070.pdf by National Institutes of Health user on 15 September 2026

Z.S., B.T., and X.W. performed RNA sequencing, single-cell RNA sequencing and mass spectrometry as well as analysis. M.S.L., E.M.N.F., S.S., and P.Z. provided human samples and histology examination. Y.H. and G.T. provided conceptualization and wrote the manuscript.

Acknowledgments

This research was supported by the Intramural Research Program of the National Institutes of Health (NIH): Center for Cancer Research, National Cancer Institute (ZIA BC011212 and ZIA BC011391 to Y.H.; ZIA BC 010793, ZIA BC 011152 and ZIA BC 011153 to G.T.); by the National Institute of Allergy and Infectious Diseases (ZIA AI001175-1 to M.S.L.); by the National Research Foundation of Korea (RS-2026-25475913 to N.-Y.S.); and by the National Cancer Institute under Contract No. 75N91025F00016 (Z.S., K.C., X.X., T.G., T.A., Y.Z., B.T., X.W.). The contributions of the NIH authors were made as part of their official duties as NIH federal employees, are in compliance with agency policy requirements, and are considered Works of the United States Government. However, the findings and conclusions presented in this paper are those of the authors and do not necessarily reflect the views of the NIH or the U.S. Department of Health and Human Services.

The authors declare no use of AI-assisted technologies and writing processes.

Competing interests

The authors declare no competing interests.

Note

Supplemental data for this article are available at Cancer Research Online.

Downloaded from aacrjournals.org/cancerres/article-pdf/doi/10.1158/0008-5472.CAN-26-0070/3828896/can-26-0070.pdf by National Institutes of Health user on 15 September 2026

References

1. Li D, Wu M. Pattern recognition receptors in health and diseases. Signal Transduct Target Ther 2021;6:291.
2. Jaillon S, Ponzetta A, Di Mitri D, Santoni A, Bonecchi R, Mantovani A. Neutrophil diversity and plasticity in tumour progression and therapy. Nat Rev Cancer 2020;20:485–503.
3. Masucci MT, Minopoli M, Carriero MV. Tumor Associated Neutrophils. Their Role in Tumorigenesis, Metastasis, Prognosis and Therapy. Front Oncol 2019;9:1146.
4. Desai JV, Lionakis MS. The role of neutrophils in host defense against invasive fungal infections. Curr Clin Microbiol Rep 2018;5:181–9.
5. Zhu F, Hu Y. Integrity of IKK/NF-kappaB Shields Thymic Stroma That Suppresses Susceptibility to Autoimmunity, Fungal Infection, and Carcinogenesis. Bioessays 2018;40(4):e1700131.
6. Aykut B, Pushalkar S, Chen R, Li Q, Abengozar R, Kim JI*, et al.* The fungal mycobiome promotes pancreatic oncogenesis via activation of MBL. Nature 2019;574:264–7.
7. Narunsky-Haziza L, Sepich-Poore GD, Livyatan I, Asraf O, Martino C, Nejman D*, et al.* Pan-cancer analyses reveal cancer-type-specific fungal ecologies and bacteriome interactions. Cell 2022;185:3789–806 e17.
8. Yew SM, Chan CL, Ngeow YF, Toh YF, Na SL, Lee KW*, et al.* Insight into different environmental niches adaptation and allergenicity from the Cladosporium sphaerospermum genome, a common human allergy-eliciting Dothideomycetes. Sci Rep 2016;6:27008.
9. Zhu F, Willette-Brown J, Song NY, Lomada D, Song Y, Xue L*, et al.* Autoreactive T Cells and Chronic Fungal Infection Drive Esophageal Carcinogenesis. Cell Host Microbe 2017;21:478–93 e7.
10. Shiao SL, Kershaw KM, Limon JJ, You S, Yoon J, Ko EY*, et al.* Commensal bacteria and fungi differentially regulate tumor responses to radiation therapy. Cancer Cell 2021;39:1202–13 e6.
11. Rahal Z, Kadara H. Beyond bacteria: How the intratumor mycobiome modulates lung adenocarcinoma progression. Cancer Cell 2023;41:1846–8.
12. Alam A, Levanduski E, Denz P, Villavicencio HS, Bhatta M, Alhorebi L*, et al.* Fungal mycobiome drives IL-33 secretion and type 2 immunity in pancreatic cancer. Cancer Cell 2022;40:153–67 e11.
13. Liu NN, Yi CX, Wei LQ, Zhou JA, Jiang T, Hu CC*, et al.* The intratumor mycobiome promotes lung cancer progression via myeloid-derived suppressor cells. Cancer Cell 2023 doi 10.1016/j.ccell.2023.08.012.
14. Underhill DM, Iliev ID. The mycobiota: interactions between commensal fungi and the host immune system. Nat Rev Immunol 2014;14:405–16.
15. Grotz KA, Genitsariotis S, Vehling D, Al-Nawas B. Long-term oral Candida colonization, mucositis and salivary function after head and neck radiotherapy. Support Care Cancer 2003;11:717–21.
16. Bagg J, Sweeney MP, Lewis MA, Jackson MS, Coleman D, Al MA*, et al.* High prevalence of non-albicans yeasts and detection of anti-fungal resistance in the oral flora of patients with advanced cancer. Palliat Med 2003;17(6):477–81 doi 10.1191/0269216303pm793oa.
17. Perera M, Al-Hebshi NN, Perera I, Ipe D, Ulett GC, Speicher DJ*, et al.* A dysbiotic mycobiome dominated by Candida albicans is identified within oral squamous-cell carcinomas. J Oral Microbiol 2017;9:1385369.

Downloaded from aacrjournals.org/cancerres/article-pdf/doi/10.1158/0008-5472.CAN-26-0070/3828896/can-26-0070.pdf by National Institutes of Health user on 15 September 2026

18. Shay E, Sangwan N, Padmanabhan R, Lundy S, Burkey B, Eng C. Bacteriome and mycobiome and bacteriome-mycobiome interactions in head and neck squamous cell carcinoma. Oncotarget 2020;11:2375–86.
19. Gamou S, Shimizu N. Calphostin-C stimulates epidermal growth factor receptor phosphorylation and internalization via light-dependent mechanism. J Cell Physiol 1994;158:151–9.
20. Liu B, Willette-Brown J, Liu S, Chen X, Fischer SM, Hu Y. IKKalpha represses a network of inflammation and proliferation pathways and elevates c-Myc antagonists and differentiation in a dose-dependent manner in the skin. Cell death and differentiation 2011;18:1854–64.
21. Liu B, Xia X, Zhu F, Park E, Carbajal S, Kiguchi K, *et al.* IKKalpha is required to maintain skin homeostasis and prevent skin cancer. Cancer Cell 2008;14:212–25.
22. Grivennikov SI, Karin M. Dangerous liaisons: STAT3 and NF-kappaB collaboration and crosstalk in cancer. Cytokine Growth Factor Rev 2010;21:11–9.
23. Stark GR, Darnell JE, Jr. The JAK-STAT pathway at twenty. Immunity 2012;36:503–14.
24. Zhu F, Willette-Brown J, Zhang J, Ferre EMN, Sun Z, Wu X, *et al.* NLRP3 Inhibition Ameliorates Severe Cutaneous Autoimmune Manifestations in a Mouse Model of Autoimmune Polyendocrinopathy-Candidiasis-Ectodermal Dystrophy-Like Disease. J Invest Dermatol 2020 doi 10.1016/j.jid.2020.10.016.
25. Xia X, Liu S, Xiao Z, Zhu F, Song NY, Zhou M, *et al.* An IKKalpha-Nucleophosmin Axis Utilizes Inflammatory Signaling to Promote Genome Integrity. Cell reports 2013;5:1243–55.
26. Jones KB, Furukawa S, Marangoni P, Ma H, Pinkard H, D'Urso R, *et al.* Quantitative Clonal Analysis and Single-Cell Transcriptomics Reveal Division Kinetics, Hierarchy, and Fate of Oral Epithelial Progenitor Cells. Cell Stem Cell 2019;24:183–92 e8.
27. Joost S, Annusver K, Jacob T, Sun X, Dalessandri T, Sivan U, *et al.* The Molecular Anatomy of Mouse Skin during Hair Growth and Rest. Cell Stem Cell 2020;26:441–57 e7.
28. Hao Y, Hao S, Andersen-Nissen E, Mauck WM, 3rd, Zheng S, Butler A, *et al.* Integrated analysis of multimodal single-cell data. Cell 2021;184:3573–87 e29.
29. Vincent D Blondel, Jean-Loup Guillaume RL, Lefebvre E. Fast unfolding of communities in large networks. Journal of Statistical Mechanics: Theory and Experiment 2008;P100008.
30. McDavid A, Finak G, Chattopadyay PK, Dominguez M, Lamoreaux L, Ma SS, *et al.* Data exploration, quality control and testing in single-cell qPCR-based gene expression experiments. Bioinformatics 2013;29:461–7.
31. Aran D, Looney AP, Liu L, Wu E, Fong V, Hsu A, *et al.* Reference-based analysis of lung single-cell sequencing reveals a transitional profibrotic macrophage. Nat Immunol 2019;20:163–72.
32. Miao Z, Deng K, Wang X, Zhang X. DEsingle for detecting three types of differential expression in single-cell RNA-seq data. Bioinformatics 2018;34:3223–4.
33. Xie X, Shi Q, Wu P, Zhang X, Kambara H, Su J, *et al.* Single-cell transcriptome profiling reveals neutrophil heterogeneity in homeostasis and infection. Nat Immunol 2020;21:1119–33.
34. Swamydas M, Lionakis MS. Isolation, purification and labeling of mouse bone marrow neutrophils for functional studies and adoptive transfer experiments. J Vis Exp 2013:e50586 doi 10.3791/50586.
35. Cillo AR, Kurten CHL, Tabib T, Qi Z, Onkar S, Wang T, *et al.* Immune Landscape of Viral- and Carcinogen-Driven Head and Neck Cancer. Immunity 2020;52:183–99 e9.
36. Williams DW, Greenwell-Wild T, Brenchley L, Dutzan N, Overmiller A, Sawaya AP, *et al.* Human oral mucosa cell atlas reveals a stromal-neutrophil axis regulating tissue immunity. Cell 2021;184:4090–104 e15.

Downloaded from aacrjournals.org/cancerres/article-pdf/doi/10.1158/0008-5472.CAN-26-0070/3828896/can-26-0070.pdf by National Institutes of Health user on 15 September 2026

37. Mateus-Tique J, Lakshmi A, Singh B, Iyer R, Sanchez-Paulete AR, Falcomata C*, et al.* Armored macrophage-targeted CAR-T cells reset and reprogram the tumor microenvironment and control metastatic cancer growth. Cancer Cell 2026;44:534–50 e11.
38. Blanpain C, Horsley V, Fuchs E. Epithelial stem cells: turning over new leaves. Cell 2007;128:445–58.
39. Kim DJ, Angel JM, Sano S, DiGiovanni J. Constitutive activation and targeted disruption of signal transducer and activator of transcription 3 (Stat3) in mouse epidermis reveal its critical role in UVB-induced skin carcinogenesis. Oncogene 2009;28:950–60.
40. Braga TT, Forni MF, Correa-Costa M, Ramos RN, Barbuto JA, Branco P*, et al.* Soluble Uric Acid Activates the NLRP3 Inflammasome. Sci Rep 2017;7:39884 doi 10.1038/srep39884.
41. Levy Y, Wiedemann A, Hejblum BP, Durand M, Lefebvre C, Surenaud M*, et al.* CD177, a specific marker of neutrophil activation, is associated with coronavirus disease 2019 severity and death. iScience 2021;24:102711 doi 10.1016/j.isci.2021.102711.
42. Niu G, Briggs J, Deng J, Ma Y, Lee H, Kortylewski M*, et al.* Signal transducer and activator of transcription 3 is required for hypoxia-inducible factor-1alpha RNA expression in both tumor cells and tumor-associated myeloid cells. Mol Cancer Res 2008;6:1099–105.
43. Chen R, Li J, Zhou X, Liu J, Huang G. Fructose-1,6-Bisphosphatase 1 Reduces (18)F FDG Uptake in Hepatocellular Carcinoma. Radiology 2017;284:844–53.
44. Bochicchio GV, Bochicchio KM, Joshi M, Ilahi O, Scalea TM. Acute glucose elevation is highly predictive of infection and outcome in critically injured trauma patients. Ann Surg 2010;252:597–602.
45. McGuinness OP. Defective glucose homeostasis during infection. Annu Rev Nutr 2005;25:9–35.
46. Yu L, Chen X, Wang L, Chen S. The sweet trap in tumors: aerobic glycolysis and potential targets for therapy. Oncotarget 2016;7:38908–26.
47. Valle-Mendiola A, Soto-Cruz I. Energy Metabolism in Cancer: The Roles of STAT3 and STAT5 in the Regulation of Metabolism-Related Genes. Cancers (Basel) 2020;12 doi 10.3390/cancers12010124.
48. Nagao A, Kobayashi M, Koyasu S, Chow CCT, Harada H. HIF-1-Dependent Reprogramming of Glucose Metabolic Pathway of Cancer Cells and Its Therapeutic Significance. Int J Mol Sci 2019;20 doi 10.3390/ijms20020238.
49. Choi SY, Collins CC, Gout PW, Wang Y. Cancer-generated lactic acid: a regulatory, immunosuppressive metabolite? J Pathol 2013;230:350–5.
50. de la Cruz-Lopez KG, Castro-Munoz LJ, Reyes-Hernandez DO, Garcia-Carranca A, Manzo-Merino J. Lactate in the Regulation of Tumor Microenvironment and Therapeutic Approaches. Front Oncol 2019;9:1143.
51. Rostamian H, Khakpoor-Koosheh M, Jafarzadeh L, Masoumi E, Fallah-Mehrjardi K, Tavassolifar MJ*, et al.* Restricting tumor lactic acid metabolism using dichloroacetate improves T cell functions. BMC Cancer 2022;22:39.
52. Levitz SM. Interactions of Toll-like receptors with fungi. Microbes Infect 2004;6:1351–5.
53. Peng J, Li J, Liang J, Li W, Yang Y, Yang Y*, et al.* A C-type lectin-like receptor CD302 in yellow drum (Nibea albiflora) functioning in antibacterial activity and innate immune signaling. Int J Biol Macromol 2023;247:125734.
54. Poli V, Zanoni I. Neutrophil intrinsic and extrinsic regulation of NETosis in health and disease. Trends Microbiol 2022 doi 10.1016/j.tim.2022.10.002.

Downloaded from aacrjournals.org/cancerres/article-pdf/doi/10.1158/0008-5472.CAN-26-0070/3828896/can-26-0070.pdf by National Institutes of Health user on 15 September 2026

55. Zhu W, Phan QT, Boontheung P, Solis NV, Loo JA, Filler SG. EGFR and HER2 receptor kinase signaling mediate epithelial cell invasion by Candida albicans during oropharyngeal infection. Proc Natl Acad Sci U S A 2012;109:14194–9.
56. Kobayashi E, Nakano H, Morimoto M, Tamaoki T. Calphostin C (UCN-1028C), a novel microbial compound, is a highly potent and specific inhibitor of protein kinase C. Biochem Biophys Res Commun 1989;159:548–53.
57. Levy DE, Darnell JE, Jr. Stats: transcriptional control and biological impact. Nat Rev Mol Cell Biol 2002;3:651–62.
58. Cross DA, Ashton SE, Ghiorghiu S, Eberlein C, Nebhan CA, Spitzler PJ*, et al.* AZD9291, an irreversible EGFR TKI, overcomes T790M-mediated resistance to EGFR inhibitors in lung cancer. Cancer Discov 2014;4:1046–61.
59. Song NY, Li X, Ma B, Willette-Brown J, Zhu F, Jiang C*, et al.* IKKalpha-deficient lung adenocarcinomas generate an immunosuppressive microenvironment by overproducing Treg-inducing cytokines. Proc Natl Acad Sci U S A 2022;119.
60. Jiang S, Sun L. Tongue Sole CD209: A Pattern-Recognition Receptor that Binds a Broad Range of Microbes and Promotes Phagocytosis. Int J Mol Sci 2017;18 doi 10.3390/ijms18091848.
61. Gavin C, Meinke S, Heldring N, Heck KA, Achour A, Iacobaeus E*, et al.* The Complement System Is Essential for the Phagocytosis of Mesenchymal Stromal Cells by Monocytes. Front Immunol 2019;10:2249 doi 10.3389/fimmu.2019.02249.
62. Mnich ME, van Dalen R, van Sorge NM. C-Type Lectin Receptors in Host Defense Against Bacterial Pathogens. Front Cell Infect Microbiol 2020;10:309 doi 10.3389/fcimb.2020.00309.
63. Pennathur S, Pasichnyk K, Bahrami NM, Zeng L, Febbraio M, Yamaguchi I*, et al.* The macrophage phagocytic receptor CD36 promotes fibrogenic pathways on removal of apoptotic cells during chronic kidney injury. Am J Pathol 2015;185:2232–45.
64. N AG, Quintana JA, Garcia-Silva S, Mazariegos M, Gonzalez de la Aleja A, Nicolas-Avila JA*, et al.* Phagocytosis imprints heterogeneity in tissue-resident macrophages. J Exp Med 2017;214:1281–96.
65. Kneidl J, Loffler B, Erat MC, Kalinka J, Peters G, Roth J*, et al.* Soluble CD163 promotes recognition, phagocytosis and killing of Staphylococcus aureus via binding of specific fibronectin peptides. Cell Microbiol 2012;14:914–36.
66. Healy LM, Jang JH, Won SY, Lin YH, Touil H, Aljarallah S*, et al.* MerTK-mediated regulation of myelin phagocytosis by macrophages generated from patients with MS. Neurol Neuroimmunol Neuroinflamm 2017;4:e402.
67. Toda Y, Tsukada J, Misago M, Kominato Y, Auron PE, Tanaka Y. Autocrine induction of the human pro-IL-1beta gene promoter by IL-1beta in monocytes. J Immunol 2002;168:1984–91.
68. Sims JE, Smith DE. The IL-1 family: regulators of immunity. Nat Rev Immunol 2010;10:89–102.
69. Sun X, Park MD, Merad M, Brown BD. Macrophages: Targets for next-generation cancer immunotherapy. Cancer Cell 2026;44:498–518.
70. Cadieux-Dion M, Safina NP, Engleman K, Saunders C, Repnikova E, Raje N*, et al.* Novel heterozygous pathogenic variants in CHUK in a patient with AEC-like phenotype, immune deficiencies and 1q21.1 microdeletion syndrome: a case report. BMC Med Genet 2018;19:41.
71. Bainter W, Lougaris V, Wallace JG, Badran Y, Hoyos-Bachiloglu R, Peters Z*, et al.* Combined immunodeficiency with autoimmunity caused by a homozygous missense mutation in inhibitor of nuclear factor ?B kinase alpha (IKKα) Sci Immunol 2021;6:eabf6723.

Downloaded from aacrjournals.org/cancerres/article-pdf/doi/10.1158/0008-5472.CAN-26-0070/3828896/can-26-0070.pdf by National Institutes of Health user on 15 September 2026

72. Cildir G, Aba U, Pehlivan D, Tvorogov D, Warnock NI, Ipsir C*, et al.* Defective kinase activity of IKKalpha leads to combined immunodeficiency and disruption of immune tolerance in humans. Nat Commun 2024;15:9944.
73. Toubiana J, Okada S, Hiller J, Oleastro M, Lagos Gomez M, Aldave Becerra JC*, et al.* Heterozygous STAT1 gain-of-function mutations underlie an unexpectedly broad clinical phenotype. Blood 2016;127:3154–64.
74. Rautemaa R, Hietanen J, Niissalo S, Pirinen S, Perheentupa J. Oral and oesophageal squamous cell carcinoma--a complication or component of autoimmune polyendocrinopathy-candidiasis-ectodermal dystrophy (APECED, APS-I). Oral oncology 2007;43:607–13.

Figure legends

Figure 1. Advanced human HNSCCs show increased fungal burden, *IL1B*^{High}*CYBB*^{Low} neutrophils, and TAM.

A, FISH with a pan-fungal probe showing fungal signals in human healthy controls (HC), tumor adjacent tissues (Adj), and HNSCCs (left, right).

B, FISH confocal images with fungal probe (green) and DAPI (blue) in healthy tissue (left) and HNSCC with an enlarged image (middle) from right section. Scale bar=100 μm.

C, Sequencing analyses (left) of fungal genus in DNA from paraffin sections of 20 human HNSCCs with fungal names (right).

D, Immunofluorescent (IF) staining with anti-*Cladosporium* antibody (green) in healthy tissue and HNSCC. DAPI, blue. Scale bar=25 μm.

E–F, scRNA-seq analysis of CD45$^+$ cells from 5 human healthy donor tonsils (HD) and 26 HNSCCs with t-distributed stochastic neighbor embedding (tSNE) (GSE139324). Cluster 5*, neutrophils and macrophages (**E**). *S100A8* and *IL1B* expression in CD45$^+$ cells and violin plot showing *IL1B* expression in neutrophils in HD and HNSCCs (**F**).

G, Expression of indicated genes or signature scores in *IL1B*-high and *IL1B*-Low neutrophils (n=24 HD, n=2279 HNSCC cells).

H, Heatmap showing gene expression in *IL1B*-High and *IL1B*-Low neutrophils from HNSCC. Fold change≥2.

I, GSEA analysis of tumor-associated macrophage (TAM) signature. Genes listed on right. NES, Normalized Enrichment Score.

J, Violin plots showing indicated gene expression or signature scores correlated with neutrophils from stage I–IV HNSCCs (GSE139324).

Downloaded from aacrjournals.org/cancerres/article-pdf/doi/10.1158/0008-5472.CAN-26-0070/3828896/can-26-0070.pdf by National Institutes of Health user on 15 September 2026

K, Violin plot showing TAM signature scores (left) and *IL1B* expression (right) in macrophages correlated with stage 1-IV HNSCCs (see Figure 1I, GSE139324).

L, Co-staining of confocal spatial images with IF-MPO, RNAscope-IL1B, IF-*Cladosporium*, and DAPI in HNSCCs (see Figure S9B). Scale bar=15 μm.

M, Left: Kaplan-Meier curve displaying survival of HNSCC patients from TCGA stratified by expression of *IL1B*-High and *IL1B*-Low neutrophil signature (*IL1B*, *NLRP3*, *CXCL8*, *AREG*, *CSF3R*, *SOD2*, FCGR3B, and *TIMP1*), normalized by *CSF3R* with quartile. Right: Spearman's correlation of *STAT3* and neutrophil *IL1B* signature (*IL1B*, CSF3R, SOD2, FCGR3B) in 519 human HNSCCs (GEPIA2).

Data represent mean ± SEM. **P*<0.05; ***P*<0.01; ****P*<0.001; *****P*<0.0001; ns, not significant; as determined by Wilcoxon test (**F**, **G**, **J**, **K**) and Student's t-test (**A**).

Figure 2. Chronic oral *C. cladosporioides* infection increases STAT3-dependent oral carcinogenesis, fungal expansion, IL-1β$^+$ neutrophil numbers, and serum IL-1β/IL-17A levels.

A–B, Scheme for oral-fungal-infection-associated carcinogenesis. M, month (**A**). Incidence of oral epithelial malignancy in mice with and without *C. cladosporioides* (*Cladosp*) inoculation. Mouse numbers shown on top of each column (**B**).

C, Hematoxylin and eosin (H&E) staining for WT oral epithelium and SCC in *Ikka*$^{\Delta SOE}$ mice at endpoints of experiments. Scale bar=50 μm.

D, Immunohistochemical (IHC) staining for p-STAT3 and cyclin D1 (brown) in oral epithelium of mice at endpoints of experiments. Scale bar=40 μm.

E–F, Survival of HNSCC patients carrying *CHUK* hemizygous deletion/*CCND1* gain and amplification compared to patients with diploid *CHUK*/*CCND1* expression (**E**, cBioPortal, *Nature,* 2015); survival of HNSCC patients expressing high *EGFR* (left) or *STAT3* (right) levels compared to those expressing low levels of these genes (**F**, cBioPortal, TCGA, HNSCC).

G, Fungal colonies from mouth of nine-month-old mice with and without oral fungal inoculation.

H, Flow cytometry showing IL-1β$^+$- and ROS$^+$-neutrophil and IL-17A$^+$ CD4$^+$ T cell numbers from mouth of fungus–infected mice.

I, Serum IL-1β and IL-17A levels in nine-month-old mice, analyzed by bead-based flow cytometry.

J, Oral uric acid levels in mice at endpoints with and without oral *Cladosp* inoculation, analyzed with IF staining.

Downloaded from aacrjournals.org/cancerres/article-pdf/doi/10.1158/0008-5472.CAN-26-0070/3828896/can-26-0070.pdf by National Institutes of Health user on 15 September 2026

K, IF stained-NLRP3 in oral tissues of mice at endpoints. Epi, epidermis between two white dashes indicated by arrows; ns, nonspecific staining indicated by arrow. Scale bar=50 μm.

L, Correlation of *NLRP3* and *IL1B* expression in 523 human HNSCCs (cBioPortal, PanCancer Atlas).

Data represent mean ± SEM. **P*<0.05; ***P*<0.01; ****P*<0.001; *****P*<0.0001; ns, not significant; as determined by Fisher's exact test (**B**), log-rank test (**E**, **F**), and Student's t-test (**G**, **H**, **I**, **K**).

Figure 3. Oral *C. cladosporioides* infection induces oral neutrophils with High-*Il1b* and Low-ROS/phagocytosis signatures.

A–C, UMAP plot from scRNA-seq showing cell clusters in oral buccal tissues of three fungus-infected mice at nine months of age (**A**). Neutrophil markers in $CD45^+$ cells (**B**) and neutrophil cluster with multi-markers (**C**). Macro, macrophages; Neutro, neutrophils.

D, Heatmap representing five neutrophil clusters based on *Il1b* levels.

E, Five neutrophil cluster distributions in UMAP format.

F, Gene expression in $Il1b^{LOW}$ and $Il1b^{HIGH}$ neutrophils.

G, Distributions of five neutrophil clusters in oral cavities of mice with oral fungal infection.

H, Differentially expressed genes in pathways related to neutrophil activities in $Ikka^{\Delta SOE}$ versus WT mice.

I, Violin plots showing expression of indicated genes in neutrophils. Dotted lines indicate median values.

J, Violin plots of indicated signature scores and gene expression in neutrophil clusters. Middle lines indicate median values. * and #, gene expression in $Ikka^{\Delta SOE}$ mice and WT mice.

K, GSEA analysis of TAM signature. Genes listed at bottom.

Data represent mean ± SEM. **P*<0.05; ***P*<0.01; *****P*<0.0001; ns, not significant; as determined by Student's t-test **(I)** and Wilcoxon test (**J**).

Figure 4. *C. cladosporioides* infection increases acidic metabolite levels in oral cavity of $Ikka^{\Delta SOE}$ mice.

A, Heatmaps for HIF1A-associated glucose metabolism (left) and glucose transmembrane transport signaling (right) in A431 cells treated with or without heat-killed *Cladosp* for 5 hours, analyzed by RNA-seq.

B, Lactate levels in culture supernatants of A431 cells treated with or without heat-killed *Cladosp.*

C–D, RT-PCR for indicated gene expression in A431 (**C**) and SCC25 (**D**) cells treated with or without heat-killed *Cladosp* and *STAT3* siRNA (si-STAT3). si-Ctrl, control siRNA.

Downloaded from aacrjournals.org/cancerres/article-pdf/doi/10.1158/0008-5472.CAN-26-0070/3828896/can-26-0070.pdf by National Institutes of Health user on 15 September 2026

E, Glucose, intermediated metabolites, and lactate levels in A431 (left) and SCC25 cells (right) following heat-killed *Cladosp* or DMSO (control, Ctrl) stimulation for 24 hours (n=3/group).

F, Lactate levels in oral cavities of mice with oral fungal infection for two months.

G, pH values in oral swabs of infected mice.

H, Correlation of *HIF1A* (left) or *STAT3* (right) expression with indicated gene expression in human HNSCCs (TCGA and PanCancer Atlas, 523 samples).

Data represent mean ± SEM. **P*<0.05; ***P*<0.01; ****P*<0.001; *****P*<0.0001; ns, not significant; as determined by Student's t-test (**B**, **C**, **D**, **E**, **F**, **G**), two-tailed t-test (**H**).

Figure 5. Acidic metabolites inhibit *C. cladosporioides*–induced fungitoxicity but enhance IL-1β expression in neutrophils.

A, Flow cytometry showing ROS (left) and IL-1β levels (middle), with representative images (right) in blood neutrophils of WT mice treated with heat-killed *Cladosp* (10 μL), lactic acid (lactate), or uric acid overnight.

B, Volcano plot of RNA-seq for *Cladosp*–treated bone marrow (BM) neutrophils versus control. Increased gene expression on right.

C, Gene Ontology (GO) pathways shown in BM neutrophil controls, treatment with heat-killed *Cladosp* versus neutrophils treated with *Cladosp* and lactic acid (LA) or uric acid (UA) overnight, analyzed by gene set enrichment analysis (GSEA).

D, Left: Heatmaps for phagocytosis signaling in control BM neutrophils; *Cladosp* treatment; *Cladosp* treatment plus UA or LA overnight. Right: CPM (counts per million) levels of *Tlr2* and *Cd302* in neutrophils treated with *Cladosp* or *Cladosp* + LA or UA.

E–F, Heatmap for IL-1β (**E**) and ROS (**F**) pathway in BM neutrophils (Control), treated with heat-killed *Cladosp*, and treated with *Cladosp* with UA or LA overnight.

G, Images of SYTOX-Green-stained BM neutrophils for neutrophil extracellular traps (NETs) after cultured with live fungi for 16 hours. Scale bar=8 μm.

H, Left: NETs in neutrophil culture with *Cladosp* plus UA or LA. Middle: survived fungi (CFU) after culturing neutrophils and fungi plus UA or LA. Right: Images of cultures.

I, A model showing UA and LA generation pathways in an epithelial STAT3-dependent manner (left) and effects of *Cladosp*, LA, and UA on neutrophil fungitoxicity (right).

Downloaded from aacrjournals.org/cancerres/article-pdf/doi/10.1158/0008-5472.CAN-26-0070/3828896/can-26-0070.pdf by National Institutes of Health user on 15 September 2026

Data represent mean ± SEM. *P<0.05; **P<0.01; ***P<0.001; ****P<0.0001; ns, not significant; as determined by Student's t-test (**A**, **D**-right, **H**).

Figure 6. *C. cladosporioides*, calphostin-C, IL-1β, and IL-17A increase STAT3 activity in SCC cells.

A, GSEA from RNA-seq showing pathways in *C. cladosporioides*–treated A431 cells versus control cells. Bars, normalized enrichment scores.

B, Volcano plot of RNA-seq showing differential gene expression in *C. cladosporioides*–treated A431 cells versus controls.

C–D, Immunoblots showing p-STAT3, STAT3, and cyclin D1 levels in A431 and SCC25 cells treated with IL-1β (10 ng/mL) or IL-17A (10 ng/mL) (**C**), or with heat-killed *C. cladosporioides* and *S. cerevisiae* (**D**). kDa, protein sizes; β-actin, protein loading controls; Ctrl, vehicle control; m, minute; hr, hour.

E, RT-PCR showing *STAT3, IL1B*, and *CCND1* expression in A431 cells treated with *STAT3* siRNA (si-STAT3), si-control (Si-Ctrl), or heat-killed *Cladosp*.

F, Immunoblots showing indicated protein levels in A431 cells treated with fungi, calphostin-C (10 nM), or GW2974 (10 μM).

G, Fungal growth in YPD (left) and colony images (right) for oral swabs of oral fungus–infected $Ikka^{\Delta SOE}$ mice treated with GW2974 or vehicle control.

H, A model for *C. cladosporioides*- and IL-1β-led pathways in epithelial tumor cells.

Data represent mean ± SEM. **P<0.01; ***P<0.001; as determined by Student's t-test (**E**, **G**).

Figure 7. IL-1β induced by oral fungal infection promotes distal tumor growth.

A, Incidence of skin carcinomas in mice with and without oral *Cladosp* inoculation. Mouse numbers on top of each column.

B, IHC stained p-STAT3 and cyclin D1 in skin and SCCs of mice at endpoints. Scale bar=50 μm.

C, IHC-stained p-$STAT3^{+}$-epithelial cells and macrophages in epidermis of nine-month-old mice with and without oral fungal inoculation.

D, UMAP plots with markers for skin macrophages and neutrophils of oral fungus infected-mice. neutro, neutrophil; macro, macrophage.

E, Violin plots from scRNA-seq showing *I1b, Nlrp3,* and *Cybb* levels in skin macrophages. Middle lines indicate median values in plots.

Downloaded from aacrjournals.org/cancerres/article-pdf/doi/10.1158/0008-5472.CAN-26-0070/3828896/can-26-0070.pdf by National Institutes of Health user on 15 September 2026

F, Heatmap showing transcriptomics in *Cybb*$^{+}$*Il1b*$^{+}$ and *Cybb*$^{+}$*Il1b*$^{-}$ skin macrophages from oral fungus-infected mice.

G, Left: Distributions of *Cybb*$^{+}$*Il1b*$^{+}$ and *Cybb*$^{+}$*Il1b*$^{-}$ skin macrophages. Right: GO analyses of various pathways in skin macrophages of *Ikka*$^{\Delta SOE}$ versus WT mice. Blue and red bars, downregulated and upregulated pathways.

H, ROS levels in skin macrophages and IL-1β^{+} macrophages (%) of oral fungus-infected and uninfected *Ikka*$^{\Delta SOE}$ mice.

I, Immunoblot showing indicated protein levels in B16F1 cells treated with IL-1β (10 ng/mL). Ctrl, vehicle control; m, minute; hr, hour; β-actin, protein loading controls.

J, Spearman's correlation of *STAT3* and *IL1B* macrophage signature (*IL1B*, *CSF1R*, *CD68*) in 461 human skin cutaneous melanomas (SKCM, GEPIA2).

K, A scheme for effects of IL-1β induced by oral fungi on skin tumor growth derived from subcutaneous cell injection.

L–P, Effects of oral *Cladosp*-infection on B16F1 cell-induced tumor growth (n=5/group, L), tumor weight (g, gram, M), IL-1β^{+} oral neutrophils (N), intratumoral IL-1β^{+}-macrophages (O), and serum IL-1β levels (P) in WT mice treated with anti-IL-1β antibody (Ab) or IgG.

Q, Effects of Amphotericin B on oral *Cladosp*-promoted skin tumor growth (n=5/group).

R, Effects of macrophage depletion on oral *Cladosp*-promoted tumor growth (left, n=5/group). Ctrl, control; Lips, liposomes as negative controls; Clodronate-Lips, clodronate-coated liposomes.

S, A model for effects of oral *Cladosp* infection-induced systemic IL-1β on skin tumor growth. BM, bone marrow; +, add; -, deletion; AmpB, Amphotericin B; arrows, promotion; crosslines, inhibition.

Data represent mean ± SEM. **P*<0.05; ***P*<0.01; ****P*<0.001; *****P*<0.0001; ns, not significant; as determined by Fisher's exact test (**A**), Student's t-test (**C**, **E**, **H**, **M–P**), and Wilcoxon test (**G**, **L**, **Q**, **R**).

Downloaded from aacrjournals.org/cancerres/article-pdf/doi/10.1158/0008-5472.CAN-26-0070/3828896/can-26-0070.pdf by National Institutes of Health user on 15 September 2026

Figure 1

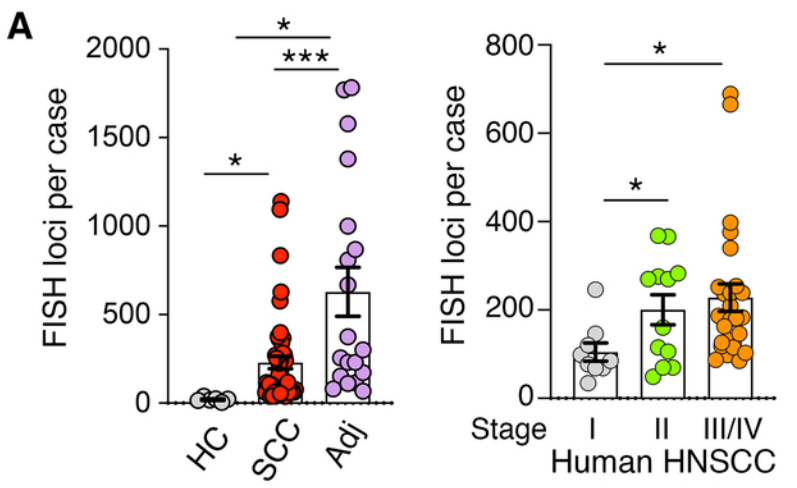

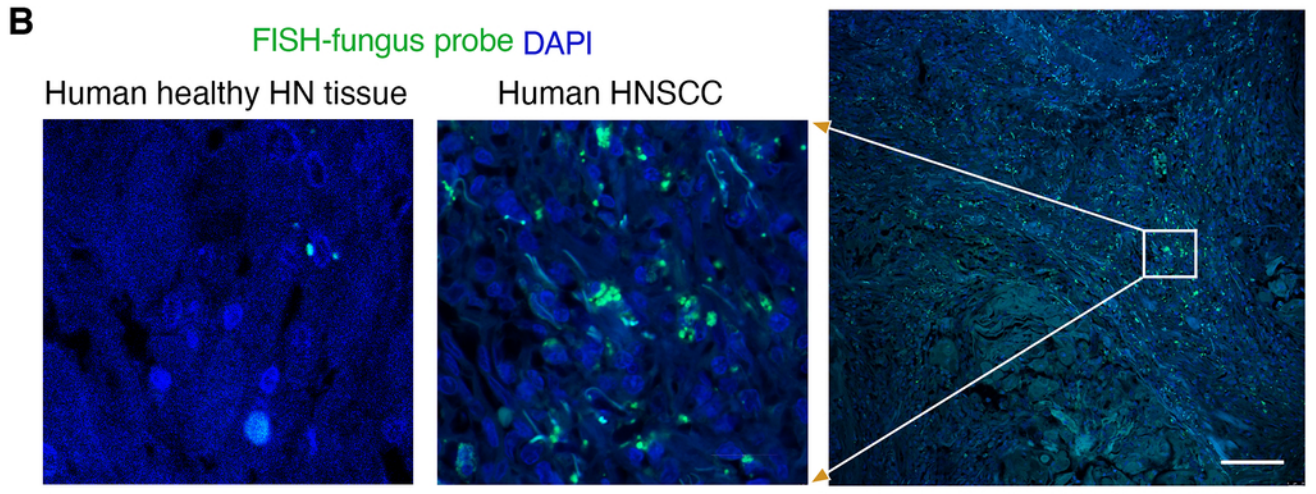

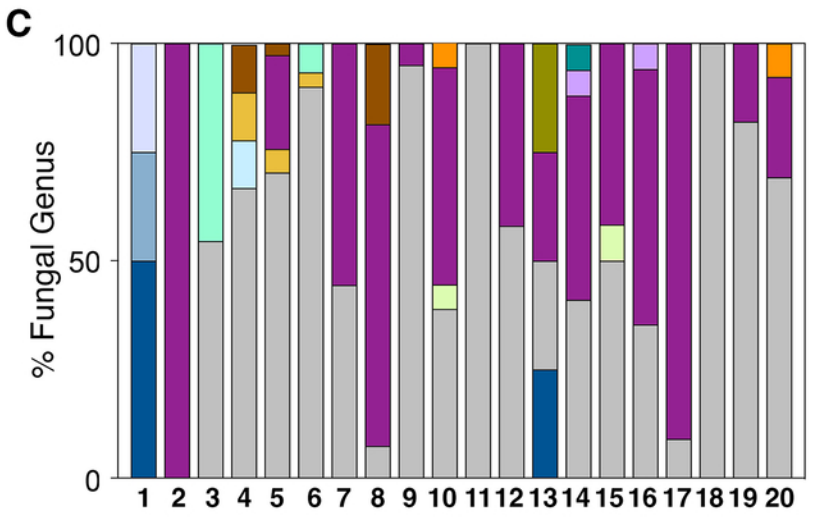

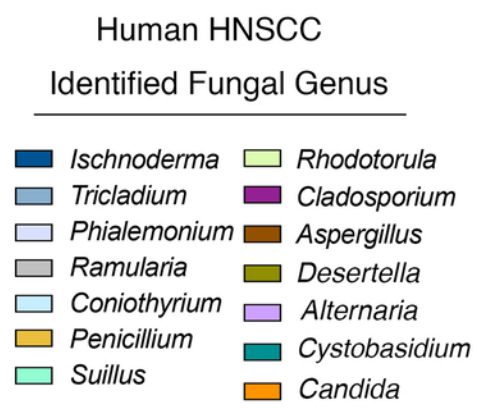

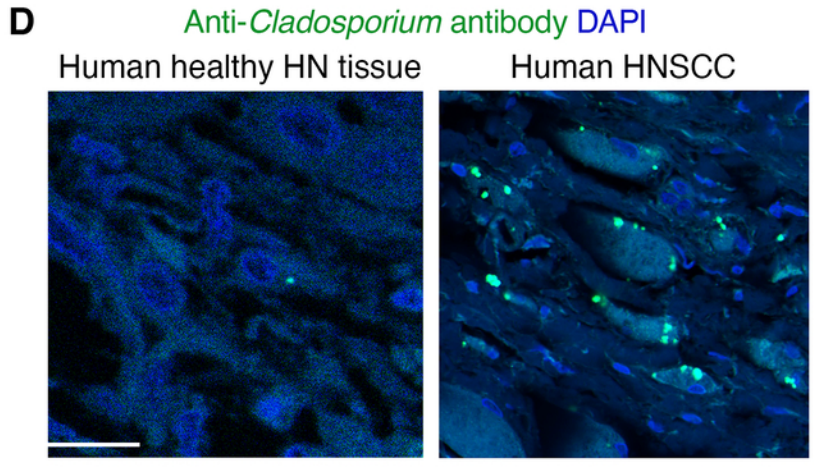

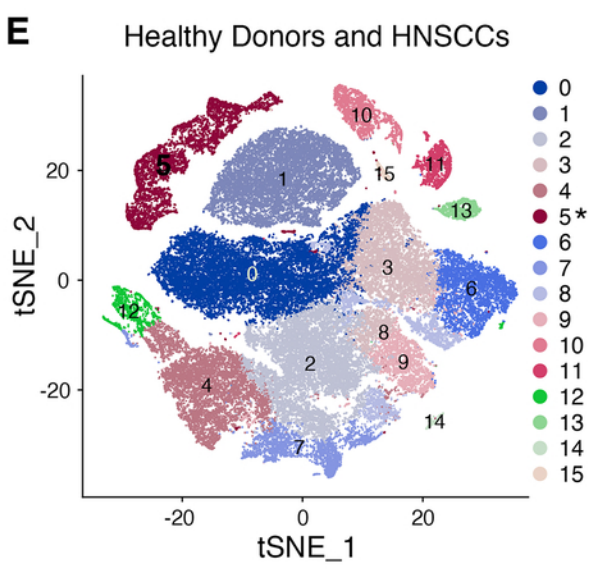

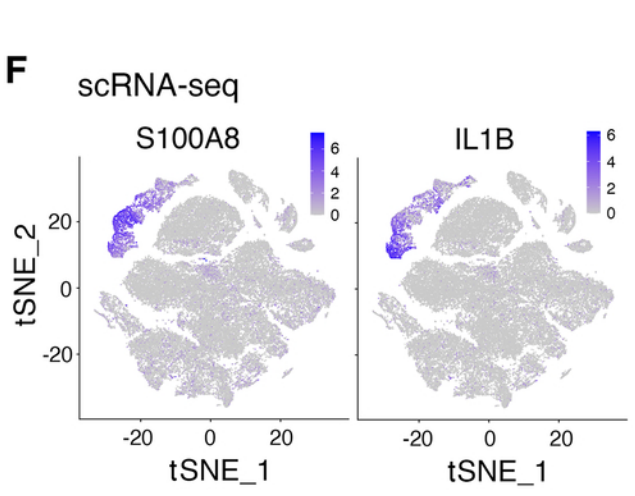

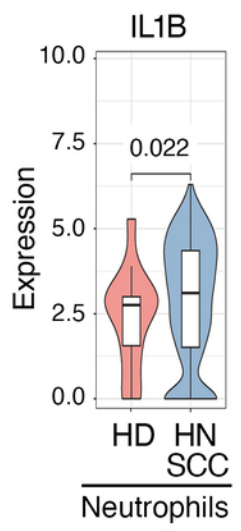

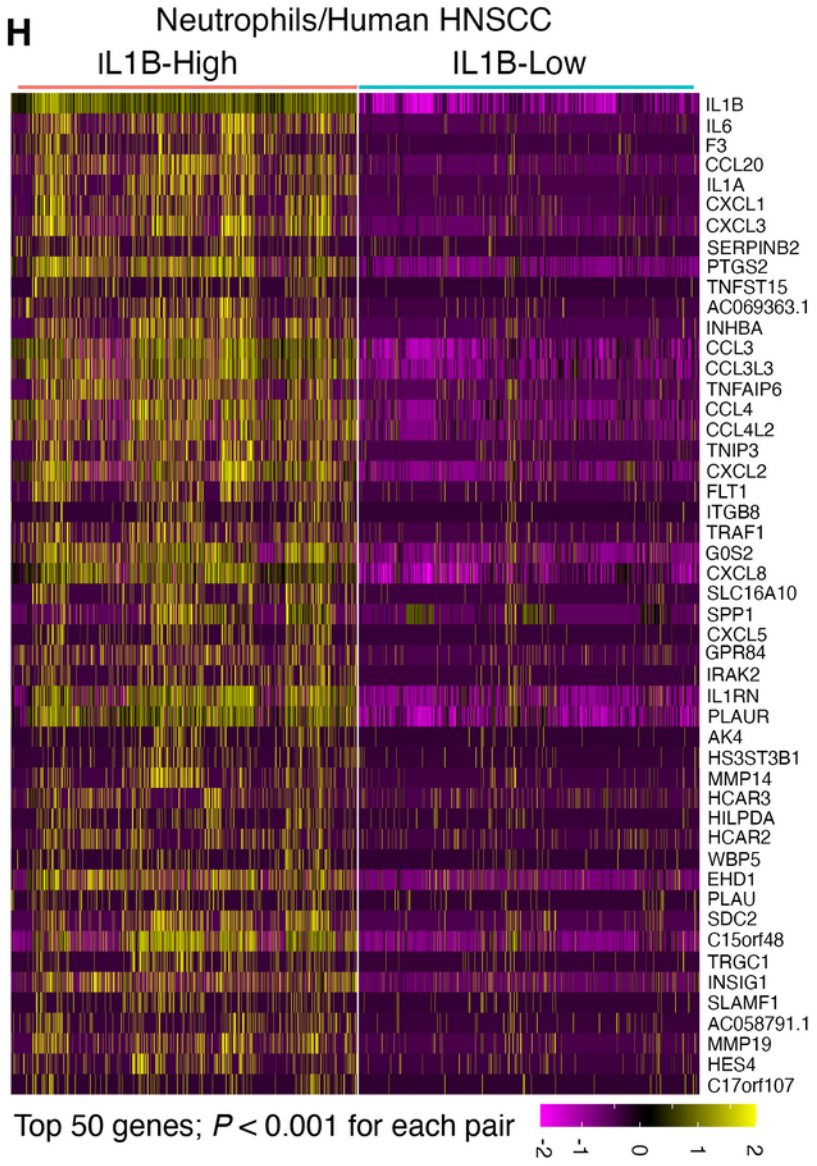

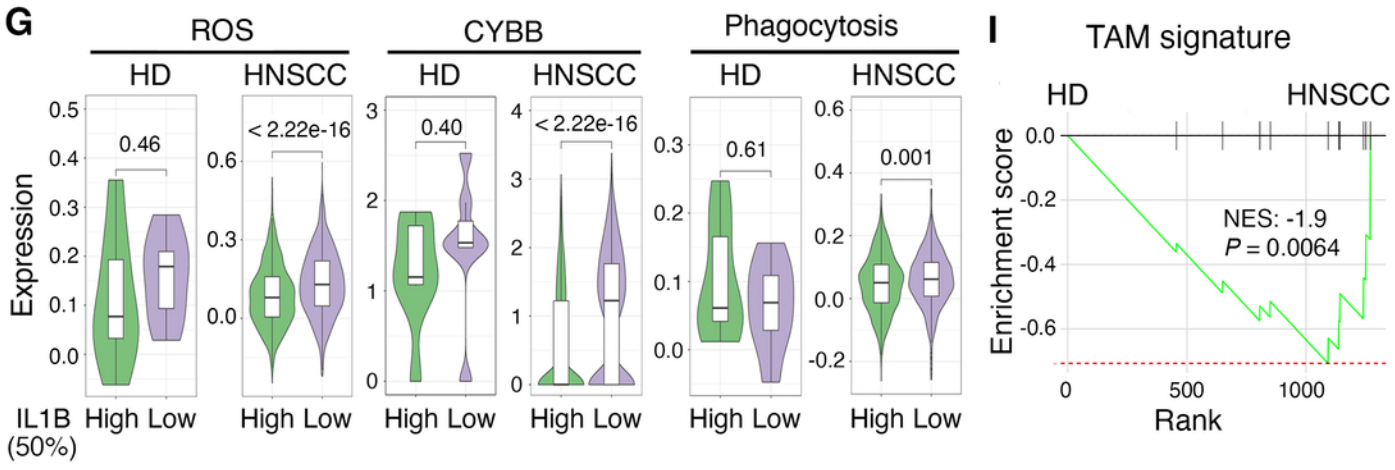

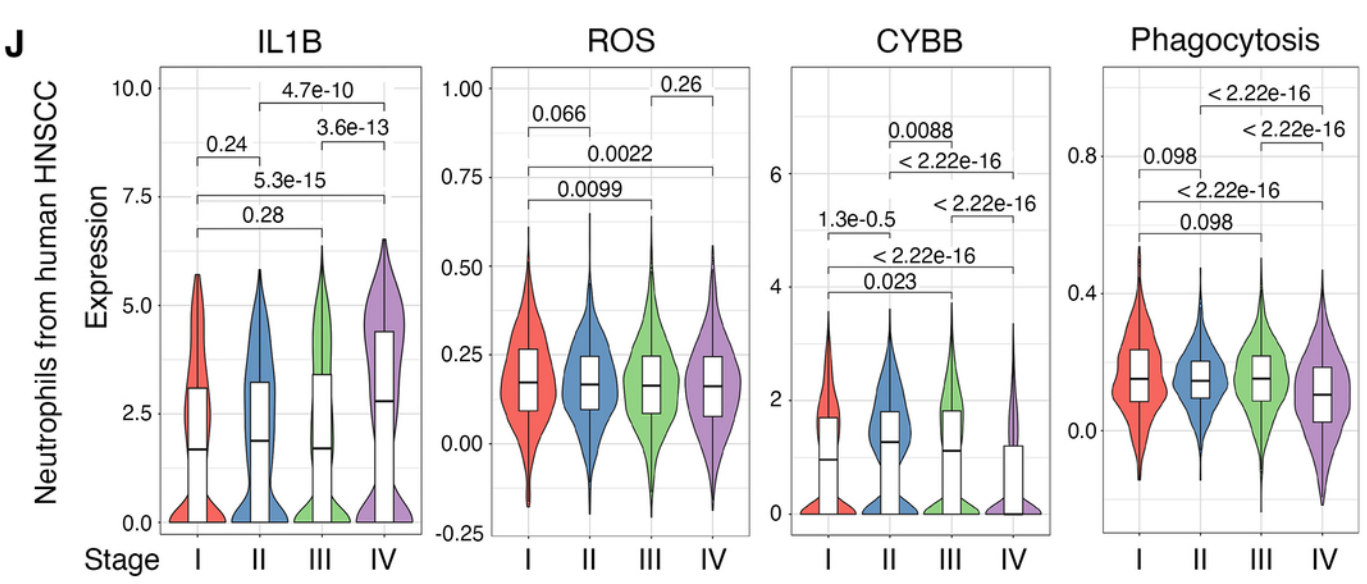

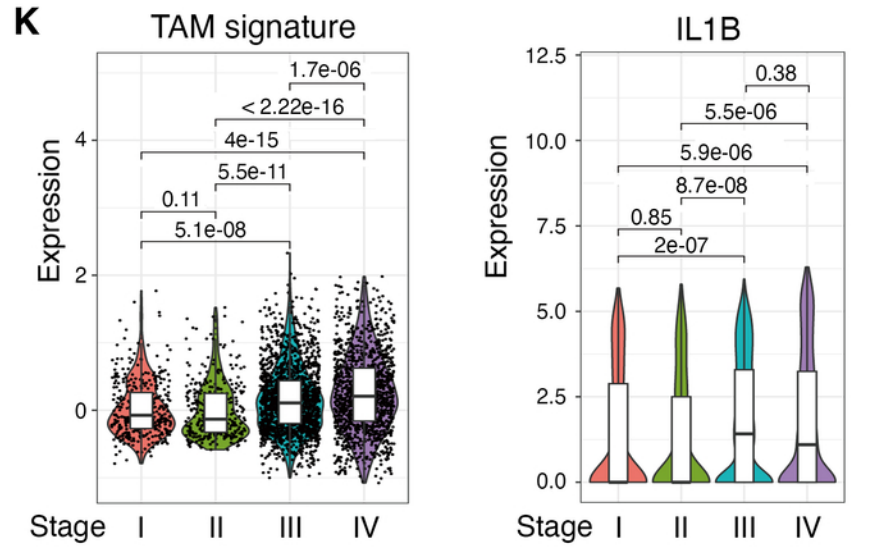

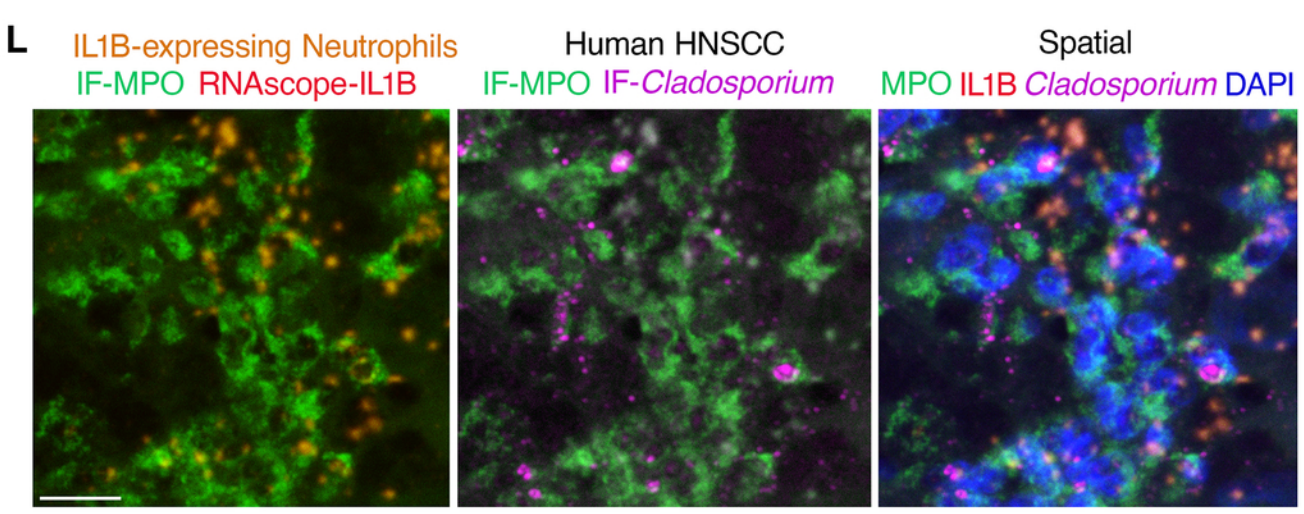

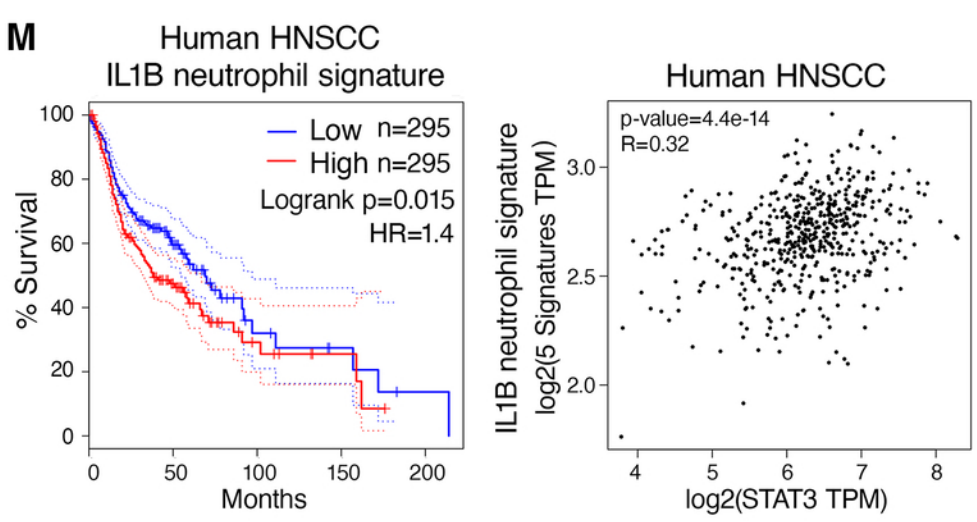

Downloaded from aacrjournals.org/cancerres/article-pdf/doi/10.1158/0008-5472.CAN-26-0070/3828896/can-26-0070.pdf by National Institutes of Health user on 15 September 2026

Figure 2

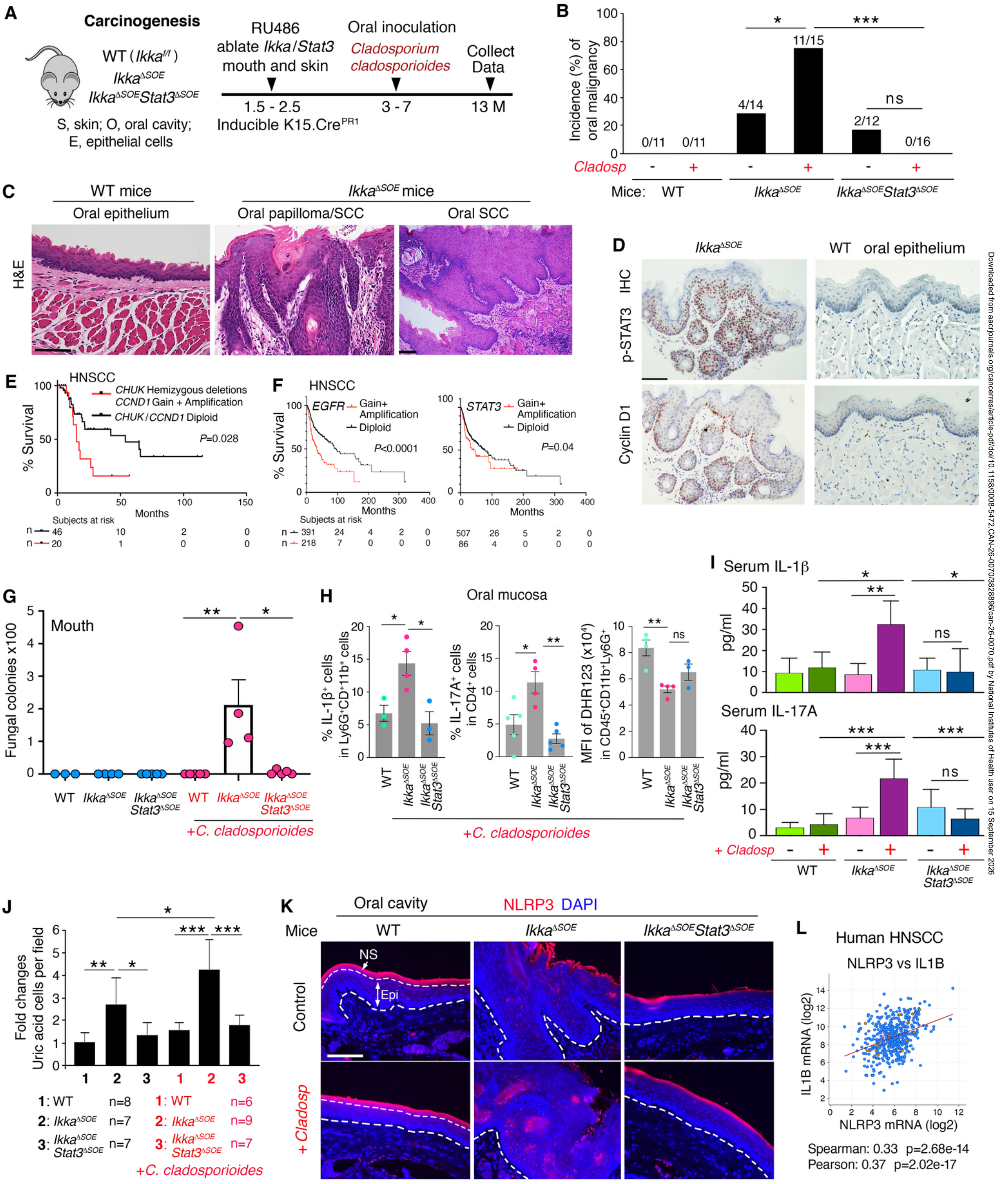

Downloaded from aacrjournals.org/cancerres/article-pdf/doi/10.1158/0008-5472.CAN-26-0070/3828896/can-26-0070.pdf by National Institutes of Health user on 15 September 2026

Figure 3

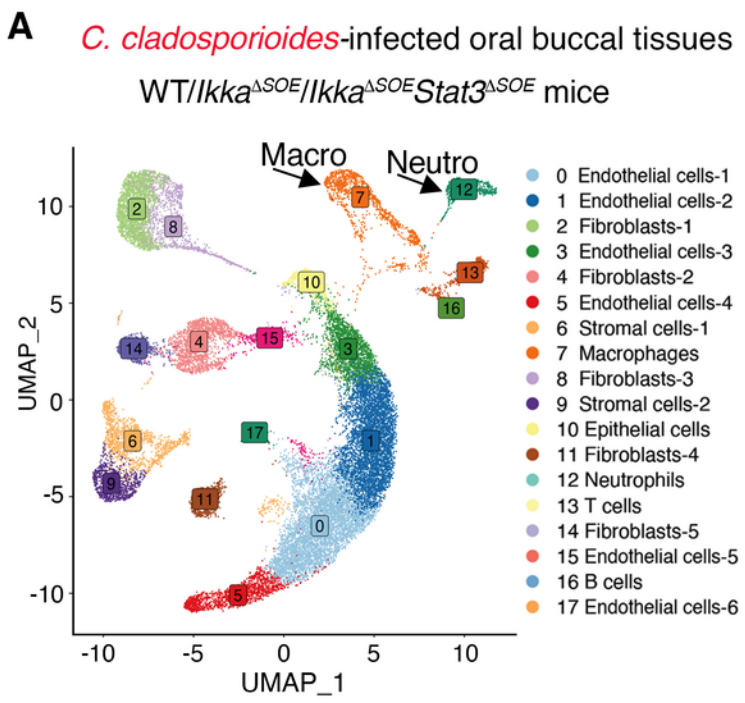

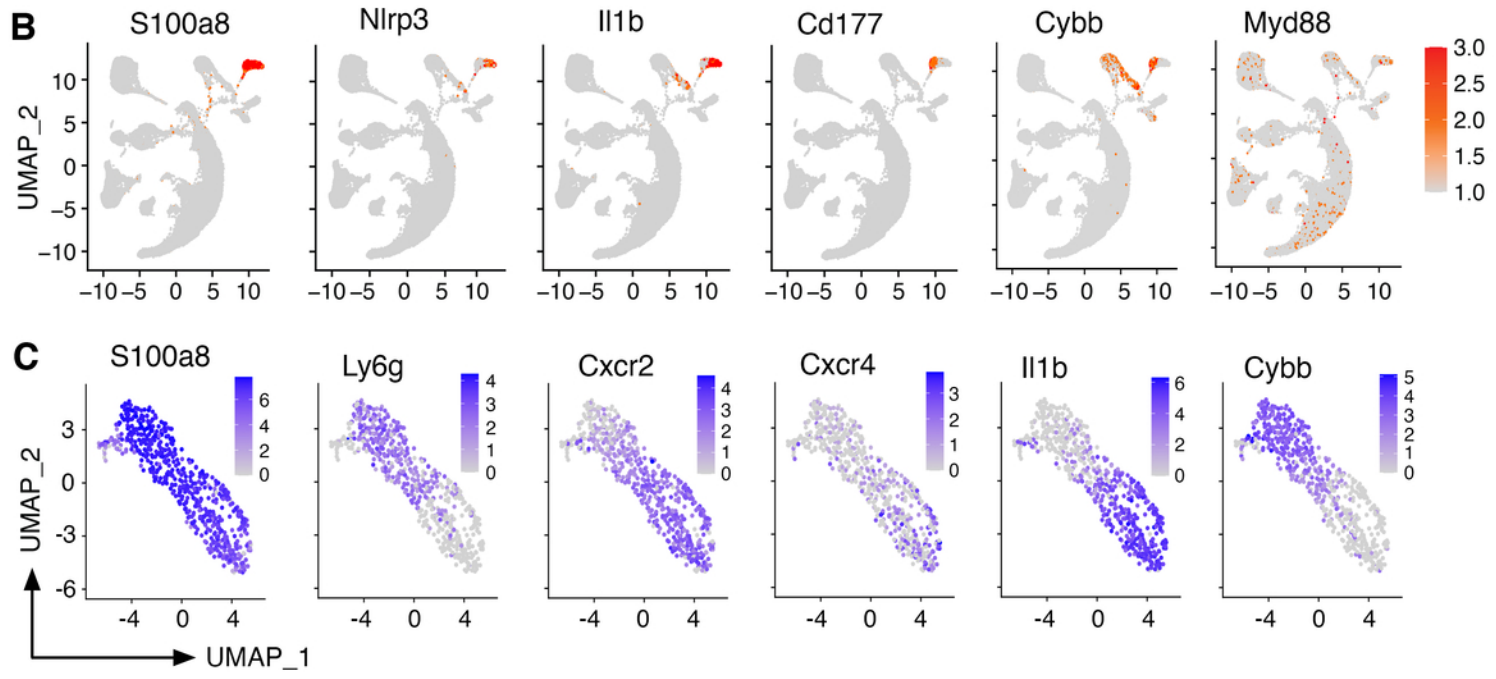

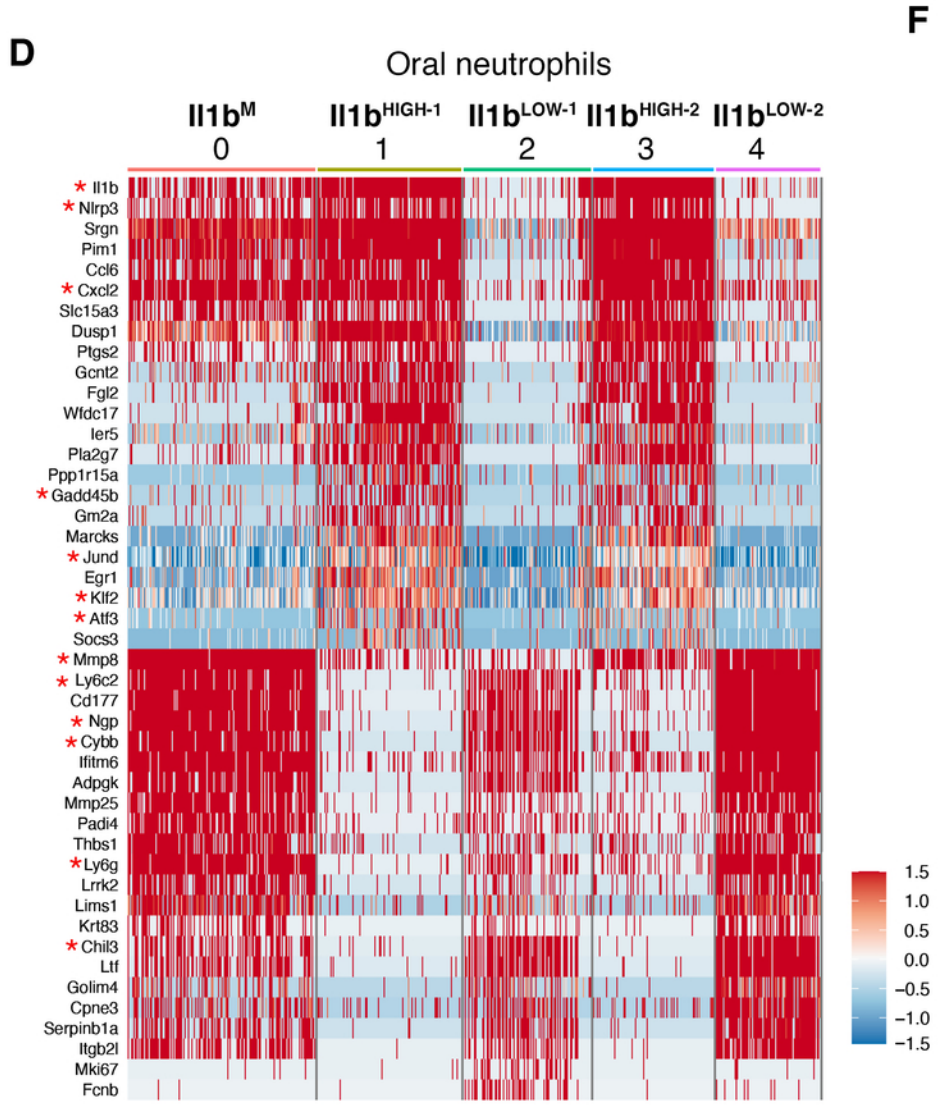

F

Extended differential/increased expression of genes in Il1b^LOW and Il1b^HIGH neutrophil subsets

Il1b^LOW: Cybb, Ncf1, Ncf4, Cyba, Padi4 (Pad4), Ly6g, Cd177, Cd55 (DAF), Cd47, Cd24a, Mmp8, Mmp9, Mmp25, Adam8, Adam19, Tnfsf13b, Csf1, Thbs1, Itgb2l, Sperinb1a

Il1b^HIGH: Cxcr2, Cxcr4, Cxcr21, Cxcr44, Csf1r, Csf2rb, Il13ra1, Il4ra, Il1ra2, Il6r, Sell, Il10rb, Ccr1, Tnfrsf1a, Cxcl2, Cxcl21, Ccl6, Ccl12, Nlrp2, Nlrp3, Nlrp12, Myd88, Nfe2l2, Cd44, Cd14, Cd53, Cd63, Cd84

Il1b^Low vs Il1b^HIGH or Il1b^HIGH vs Il1b^LOW
each comparision: P < 0.05

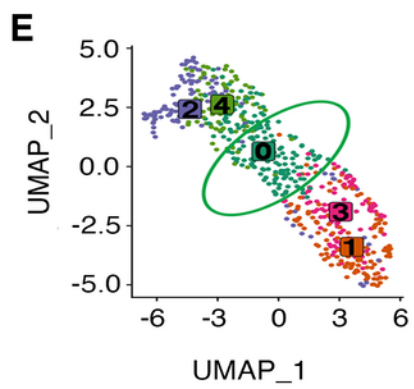

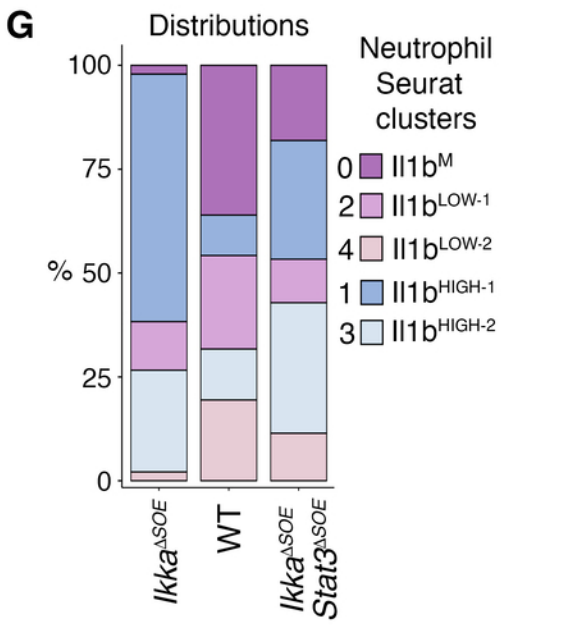

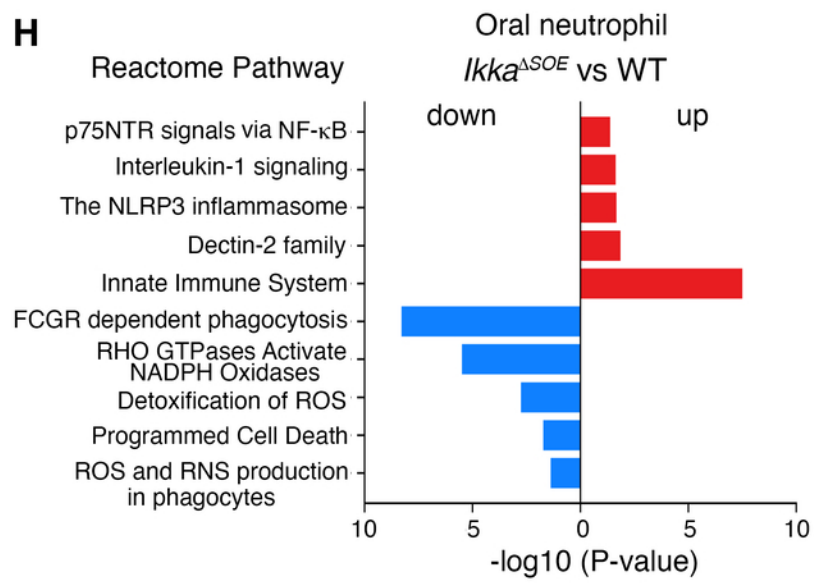

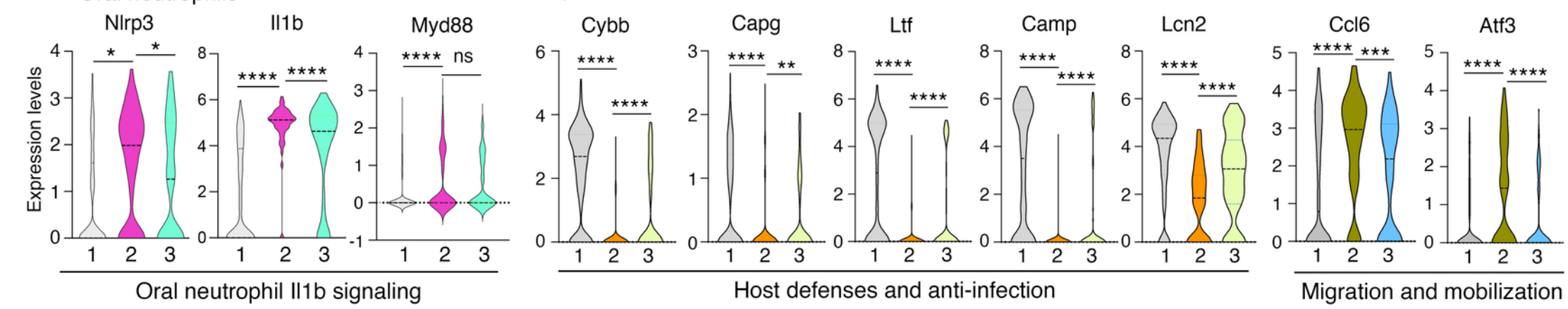

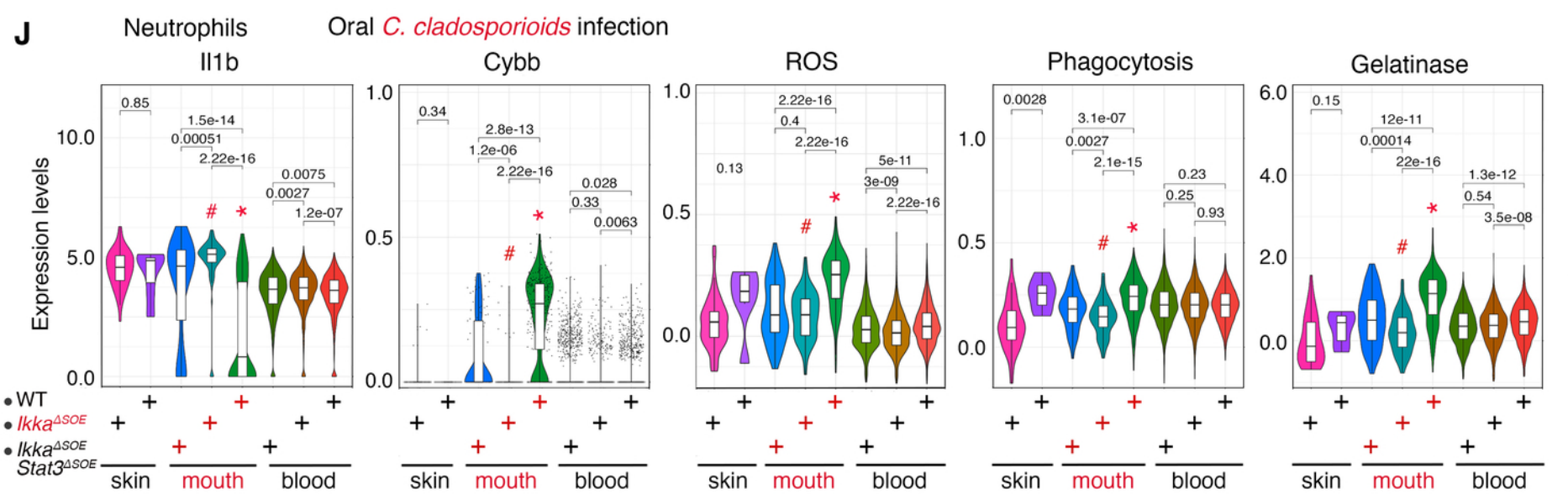

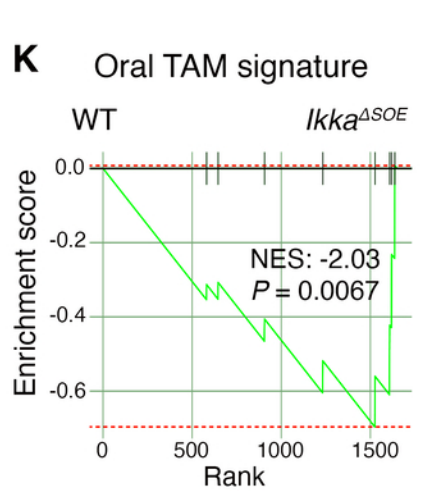

Downloaded from aacrjournals.org/cancerres/article-pdf/doi/10.1158/0008-5472.CAN-26-0070/3828896/can-26-0070.pdf by National Institutes of Health user on 15 September 2026

Figure 4

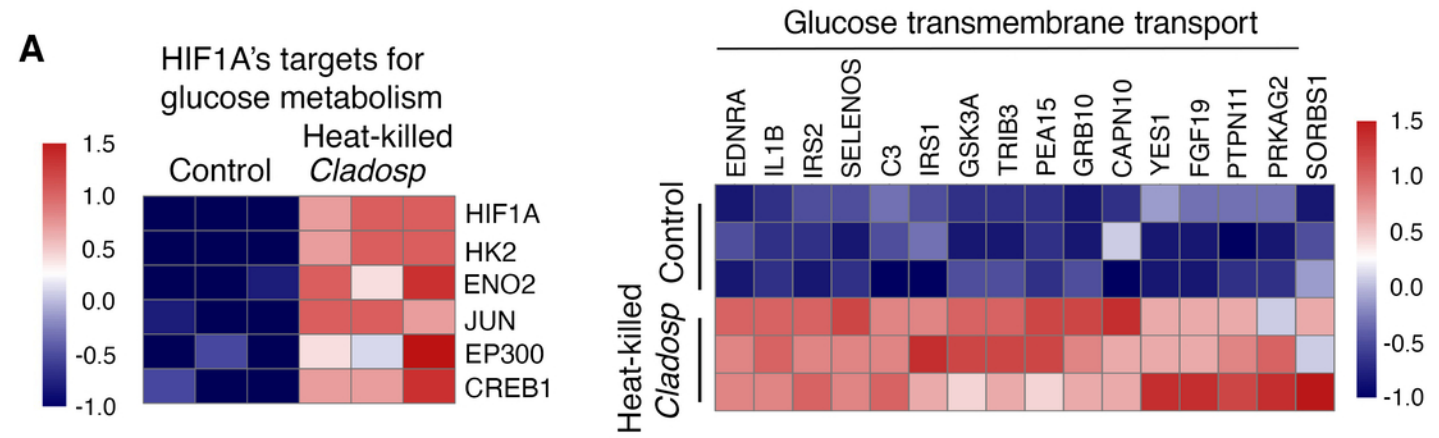

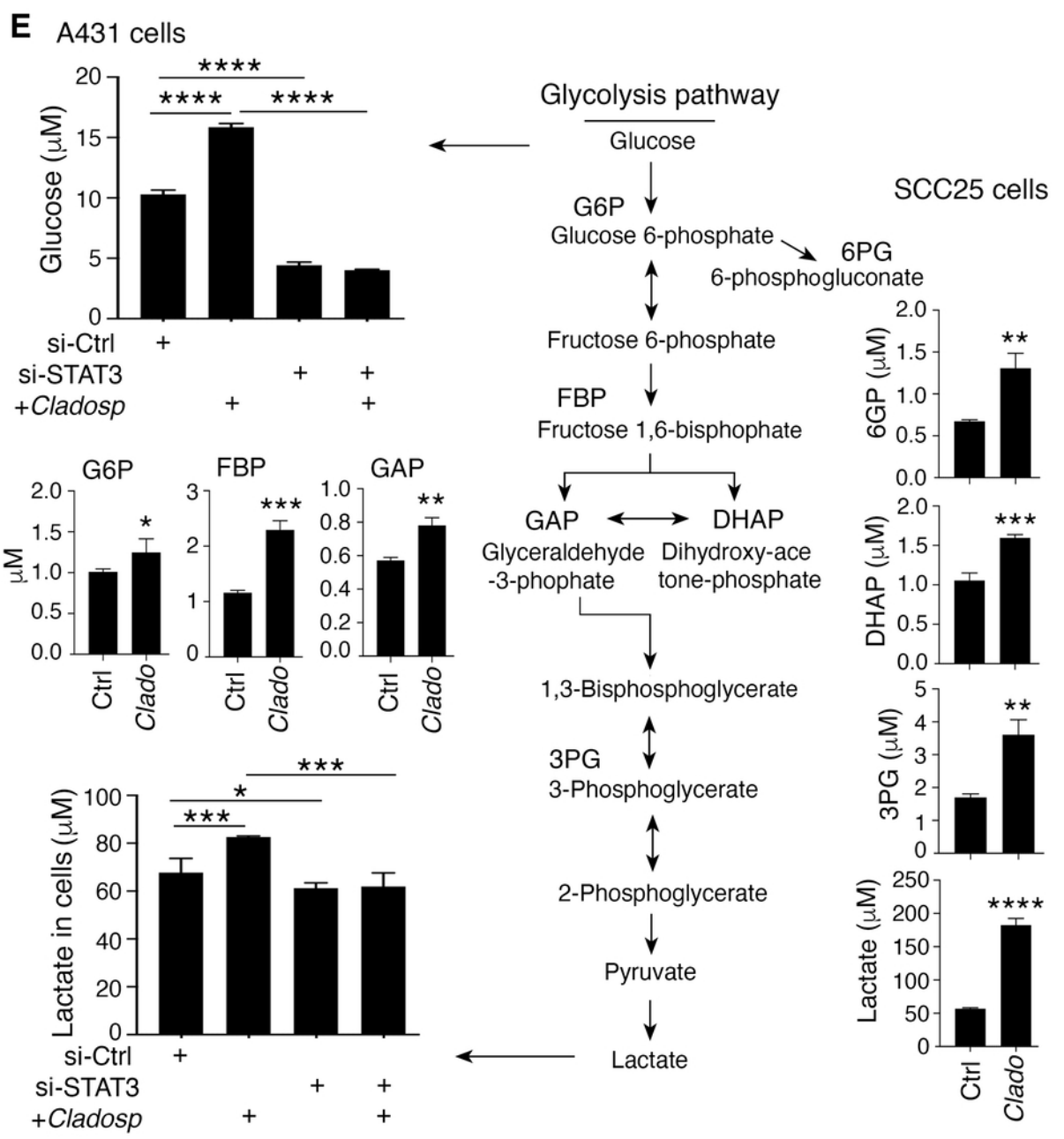

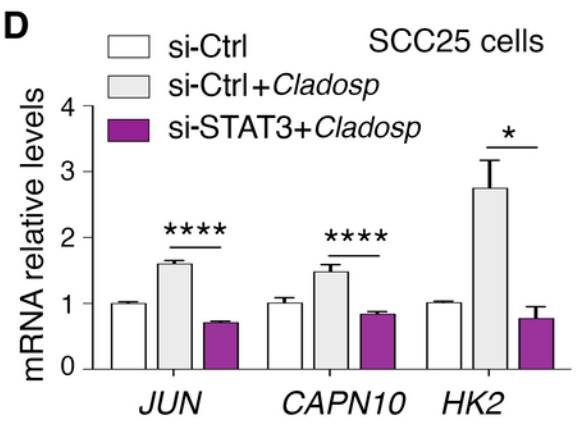

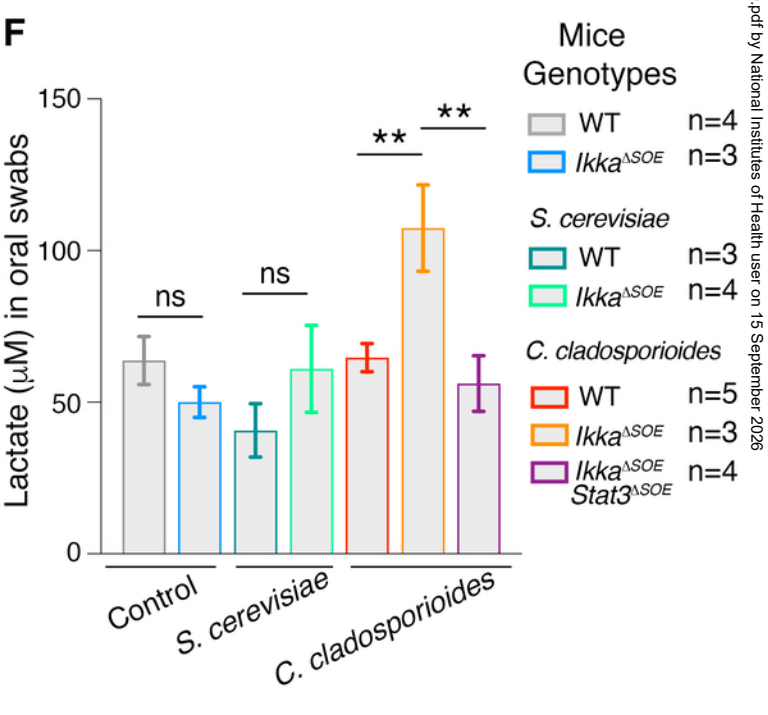

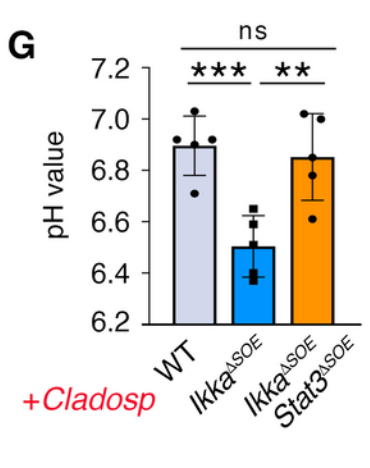

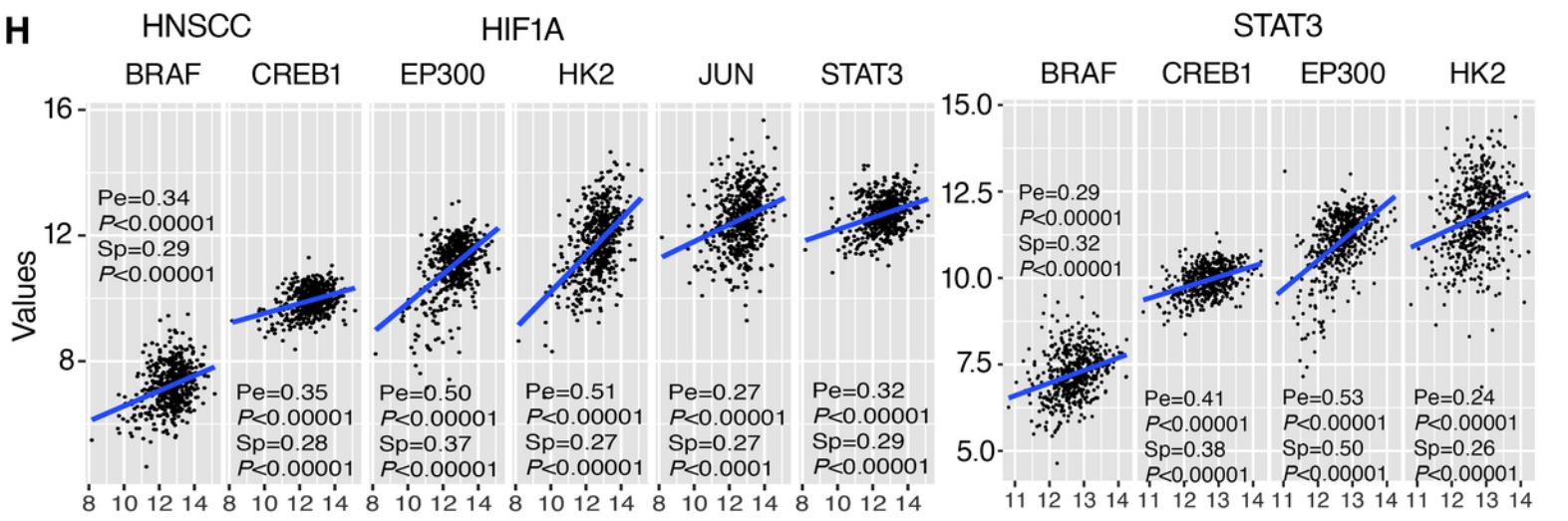

Downloaded from aacrjournals.org/cancerres/article-pdf/doi/10.1158/0008-5472.CAN-26-0070/3828896/can-26-0070.pdf by National Institutes of Health user on 15 September 2026

Figure 5

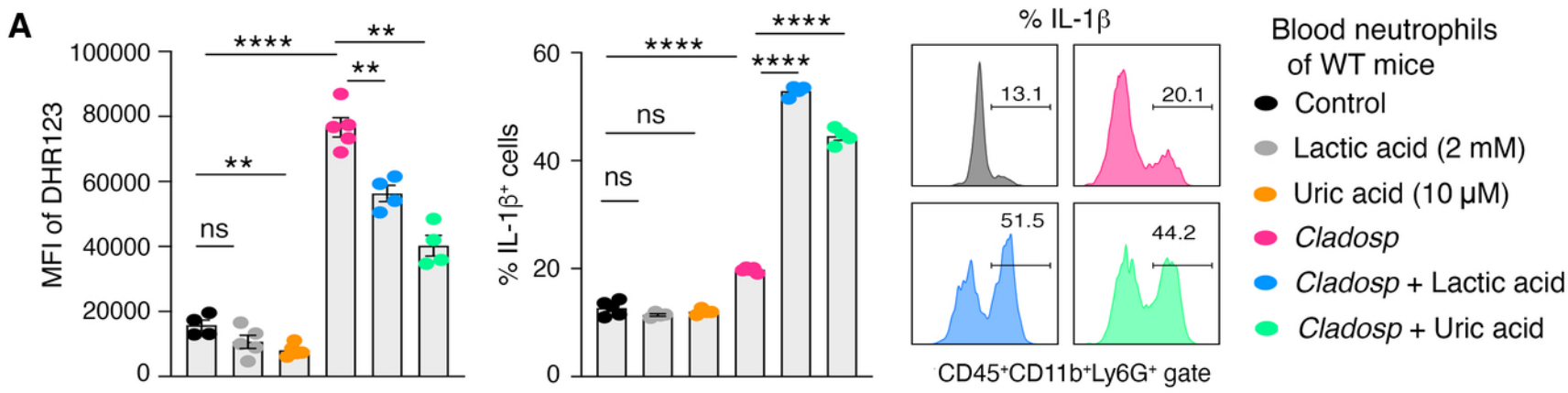

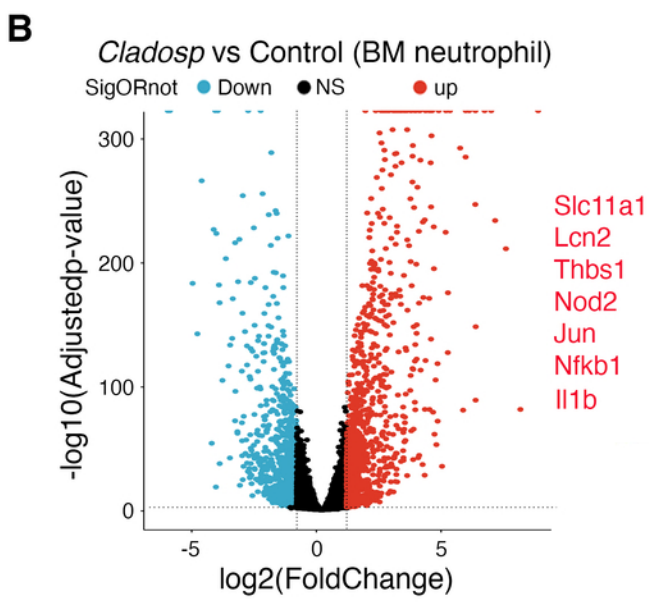

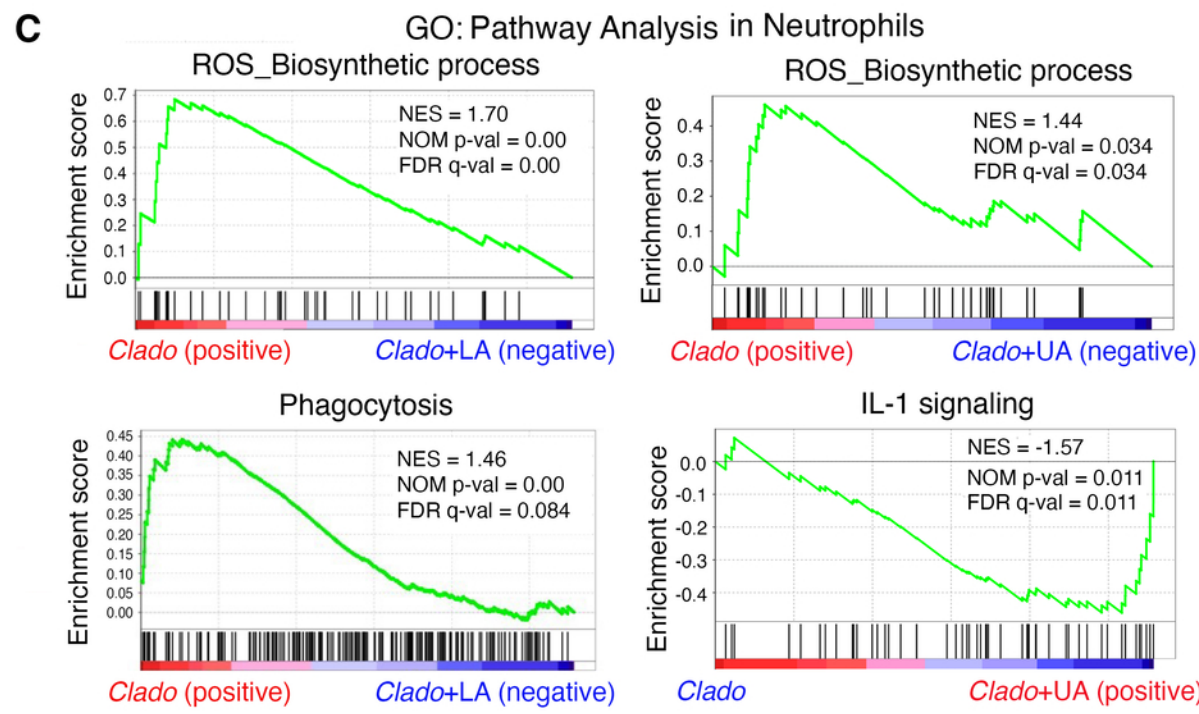

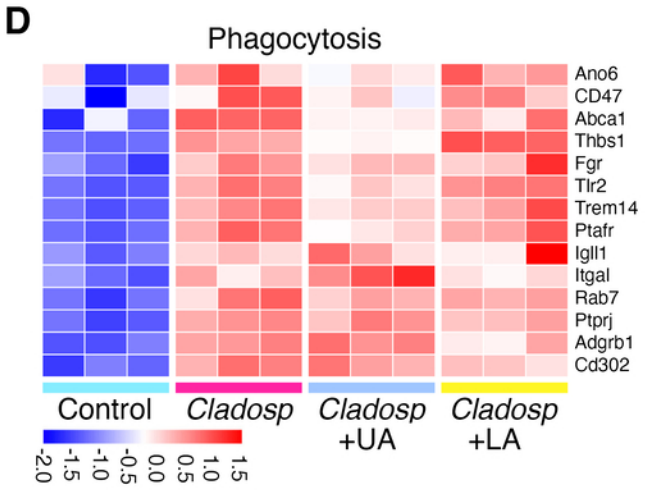

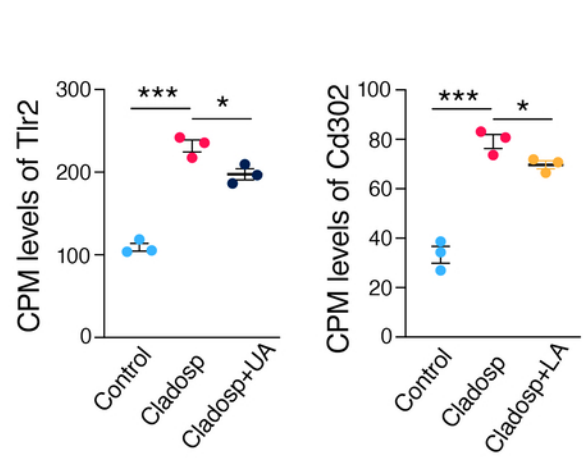

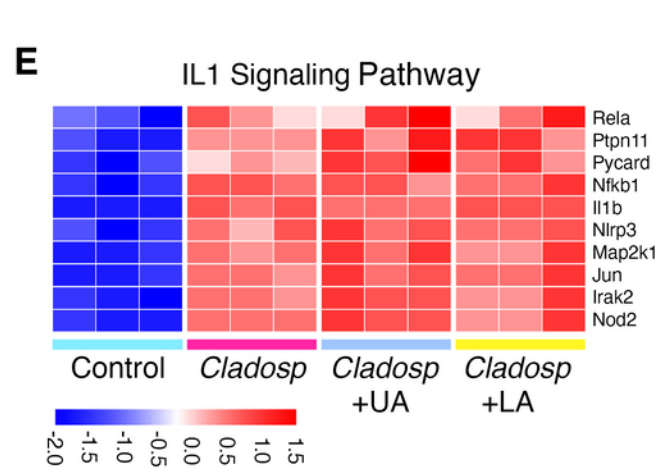

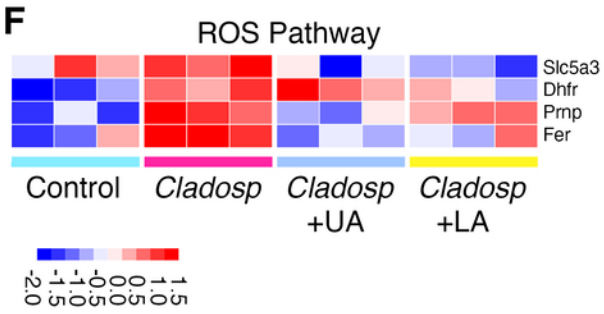

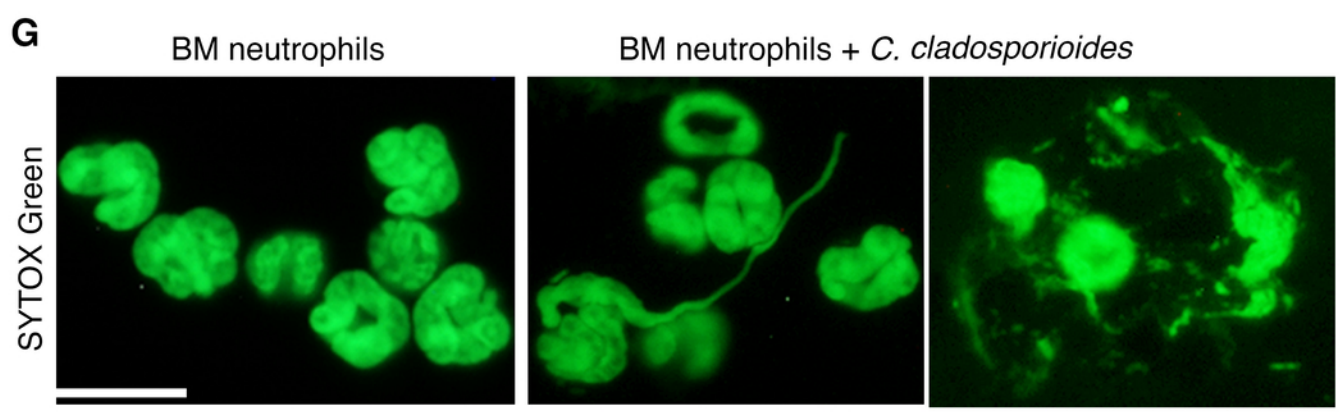

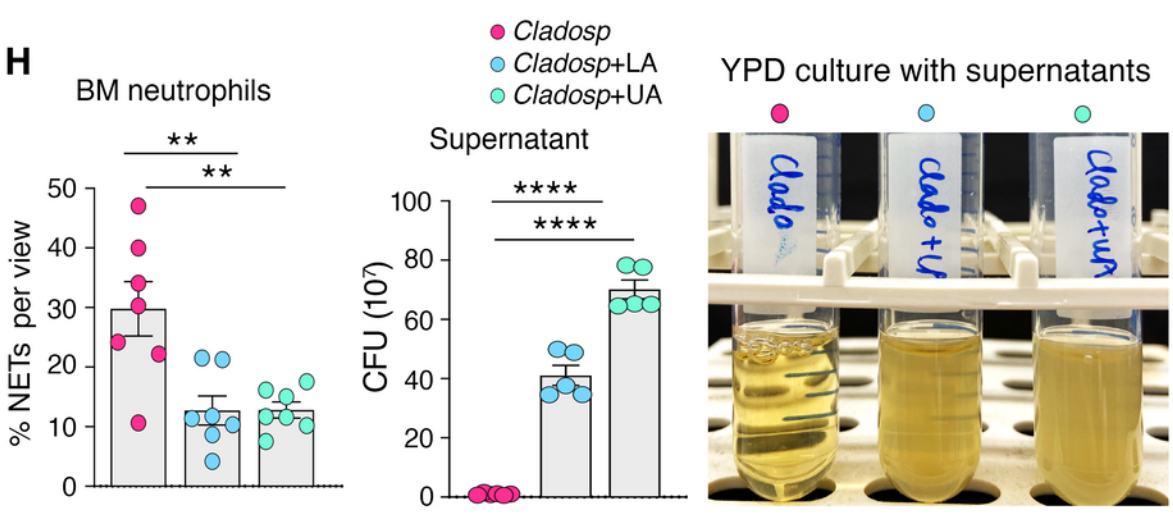

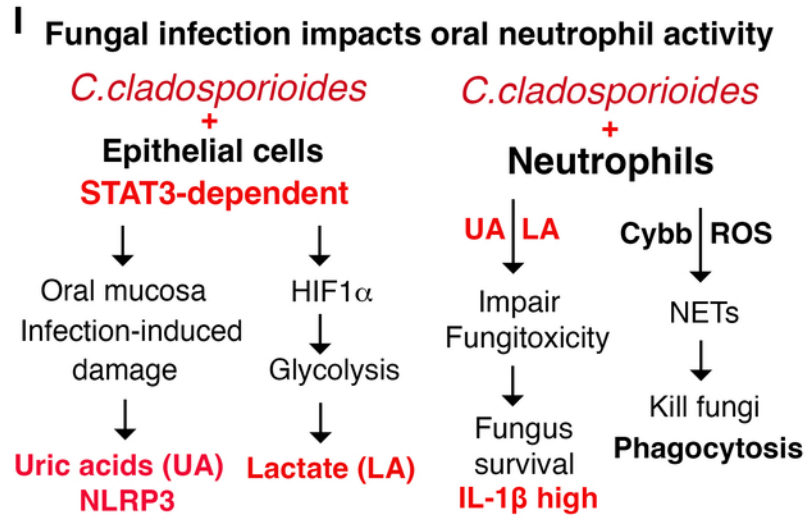

Downloaded from aacrjournals.org/cancerres/article-pdf/doi/10.1158/0008-5472.CAN-26-0070/3828896/can-26-0070.pdf by National Institutes of Health user on 15 September 2026

Figure 6

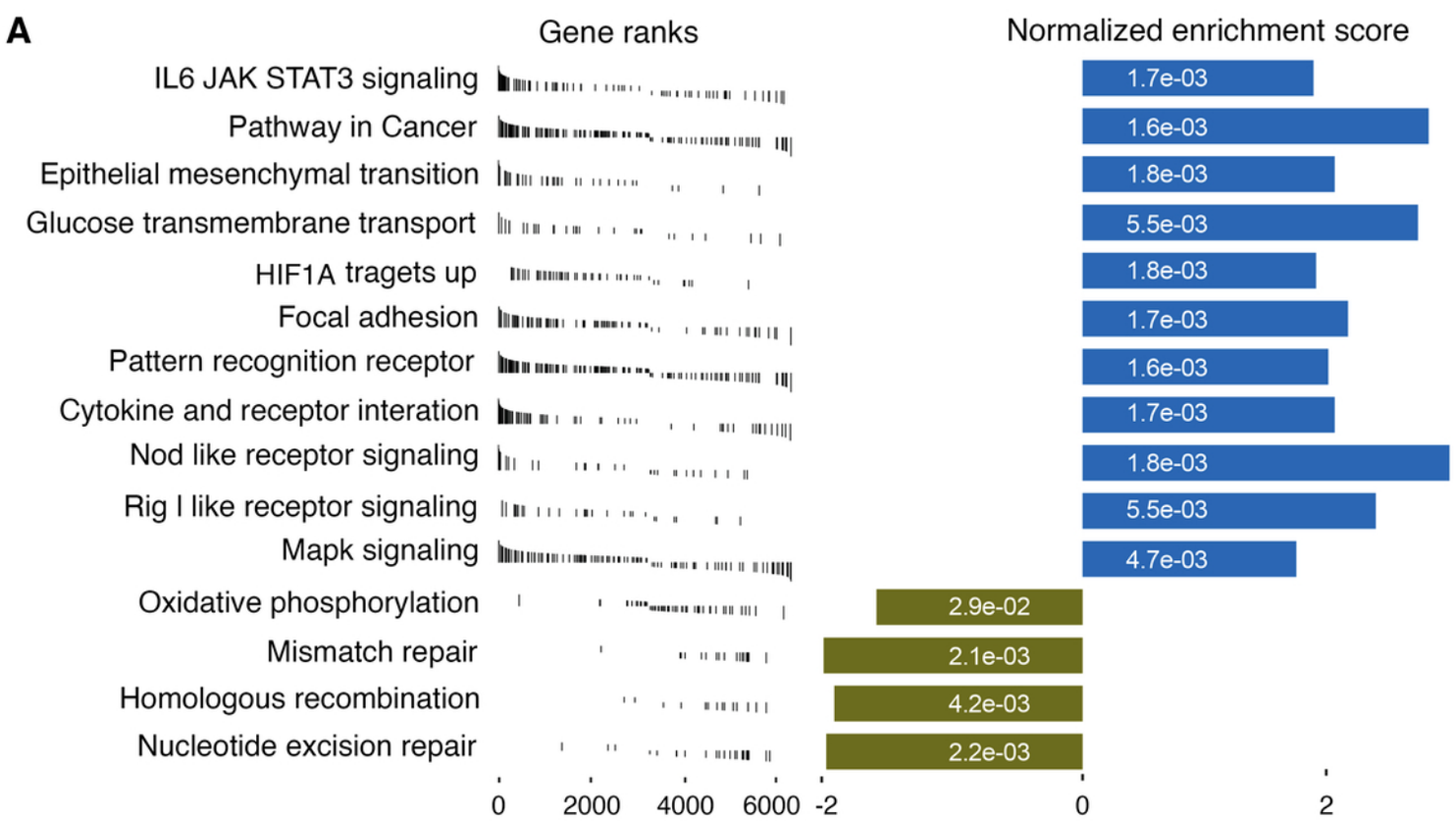

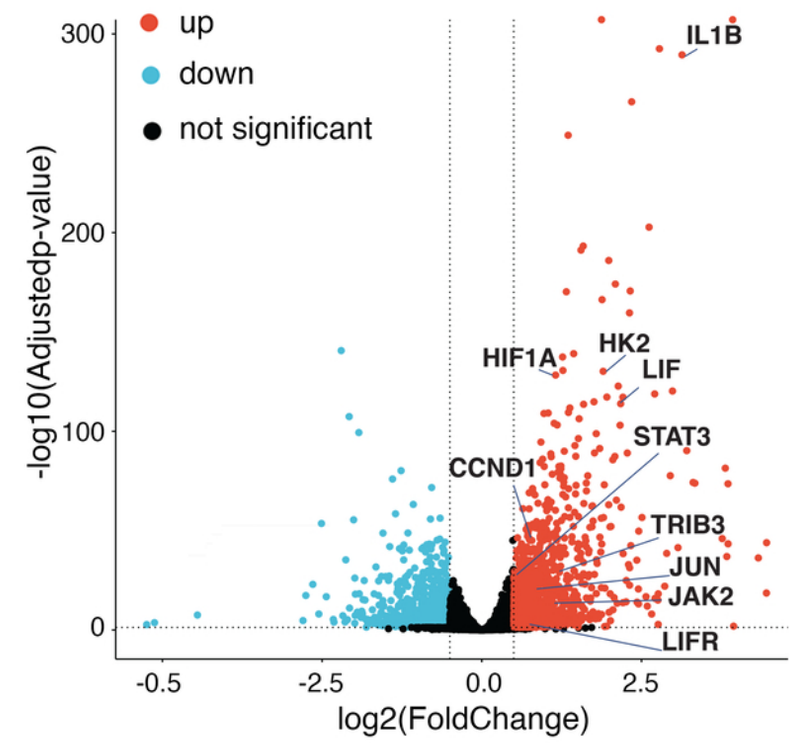

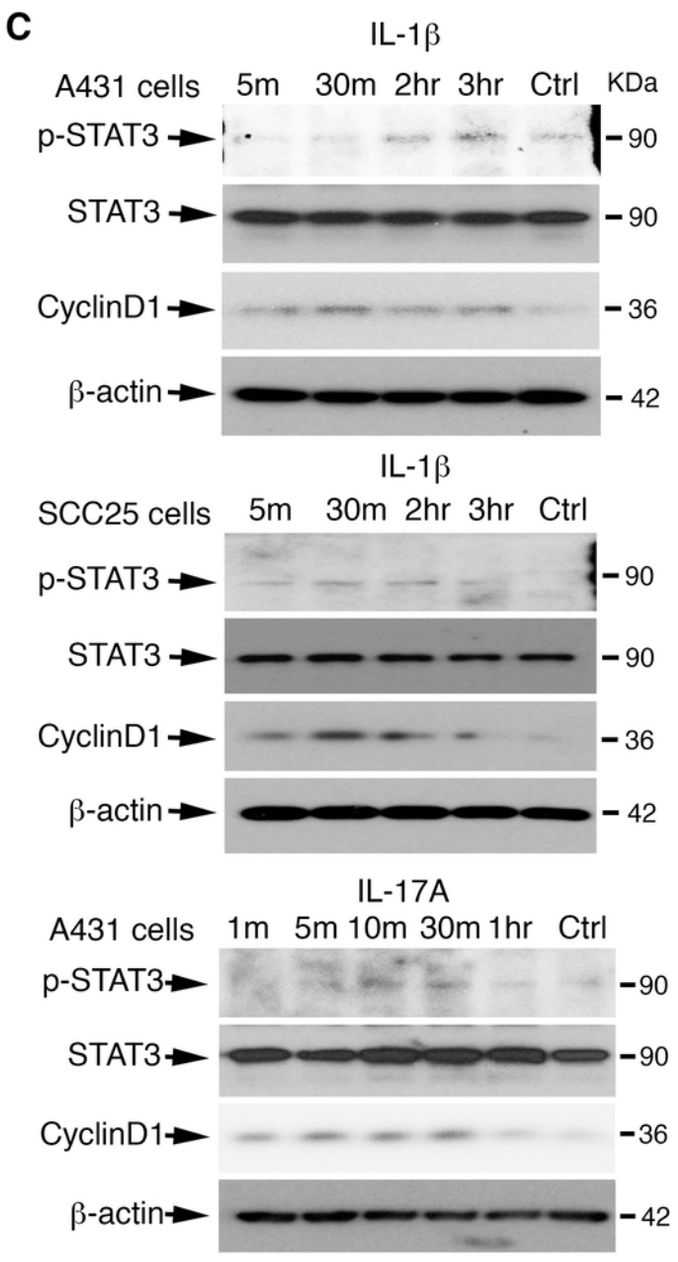

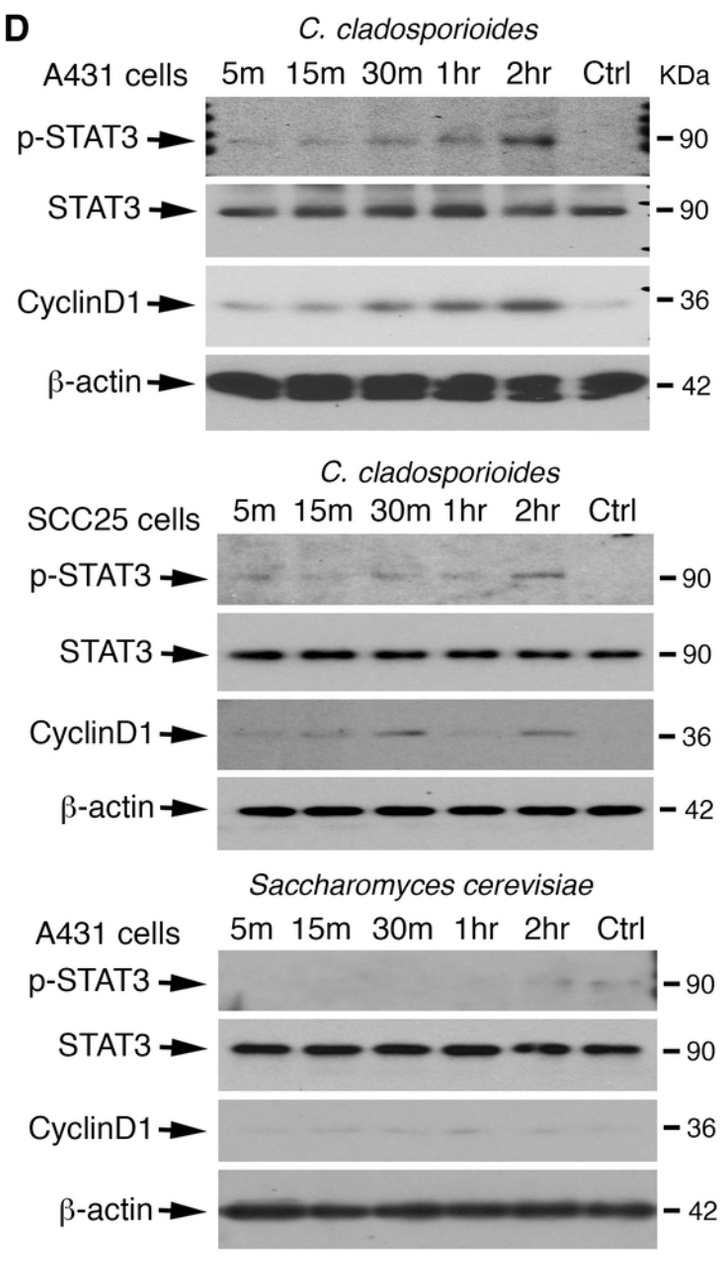

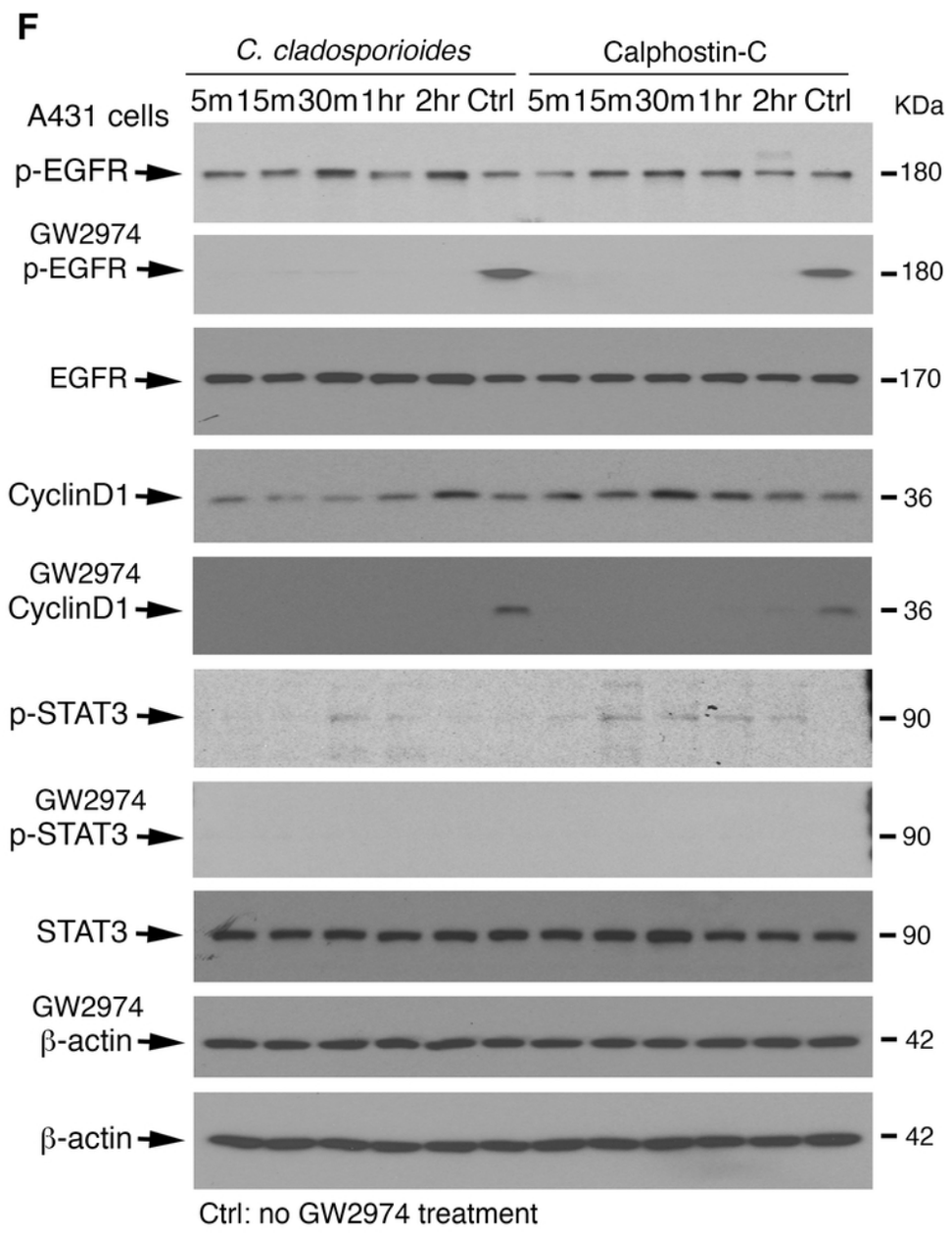

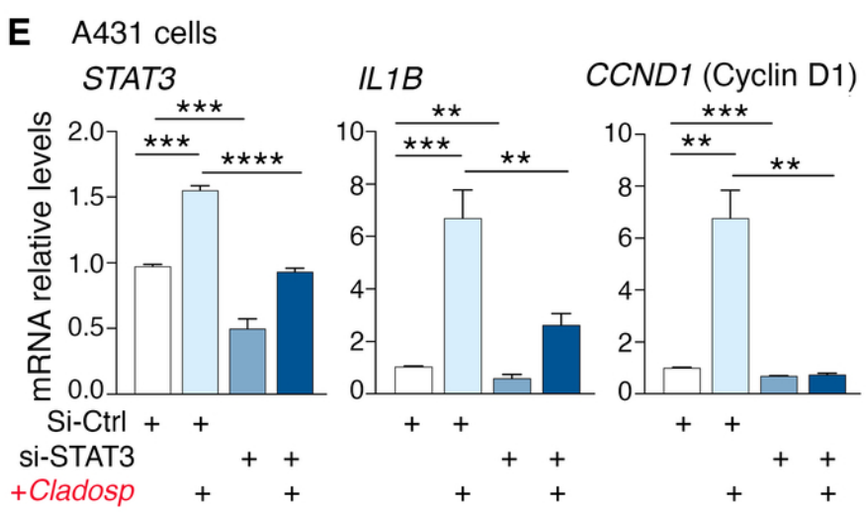

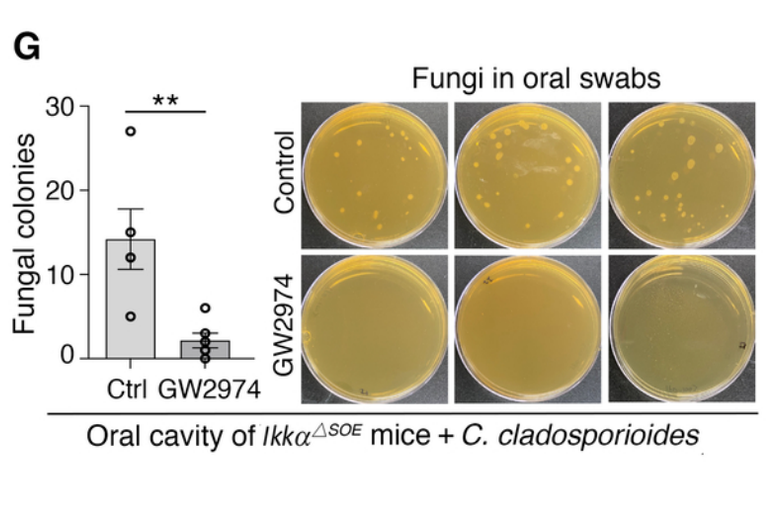

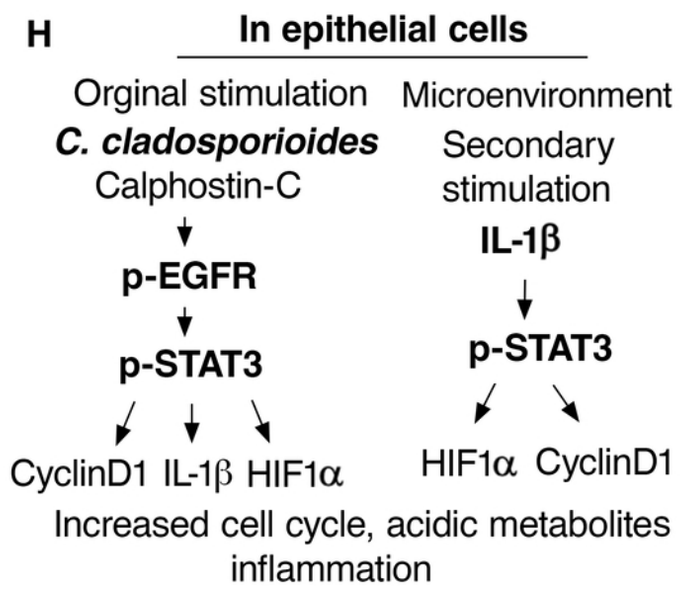

Downloaded from aacrjournals.org/cancerres/article-pdf/doi/10.1158/0008-5472.CAN-26-0070/3828896/can-26-0070.pdf by National Institutes of Health use r on 15 September 2026

Figure 7

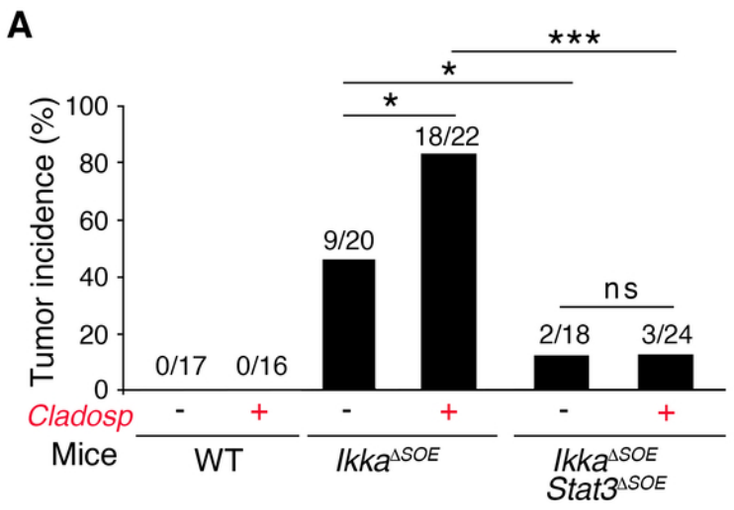

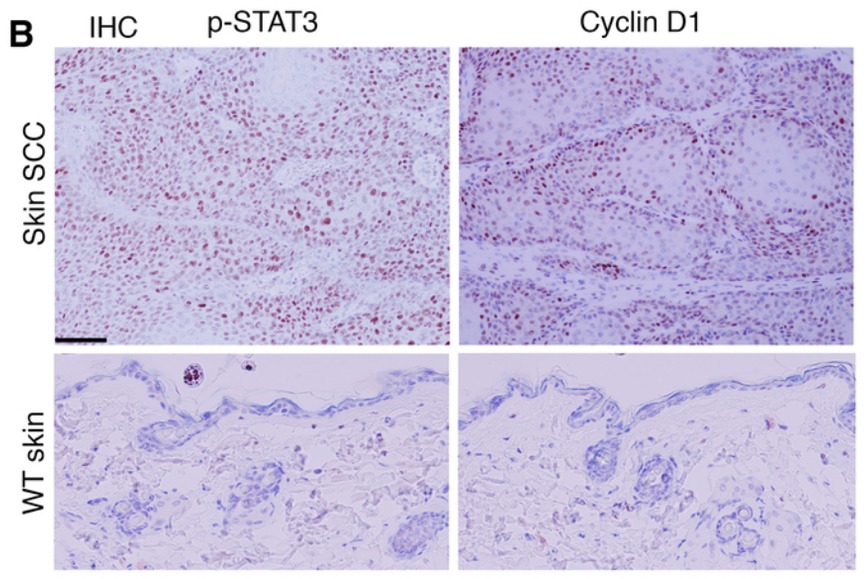

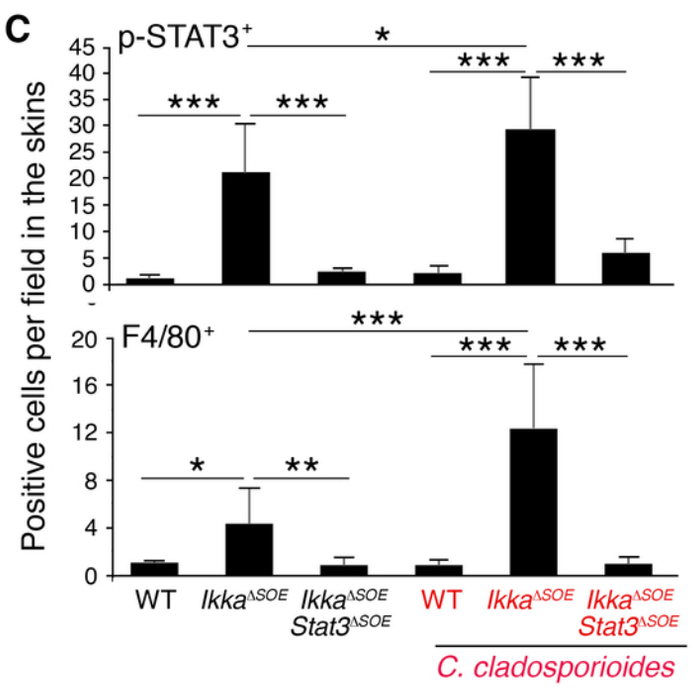

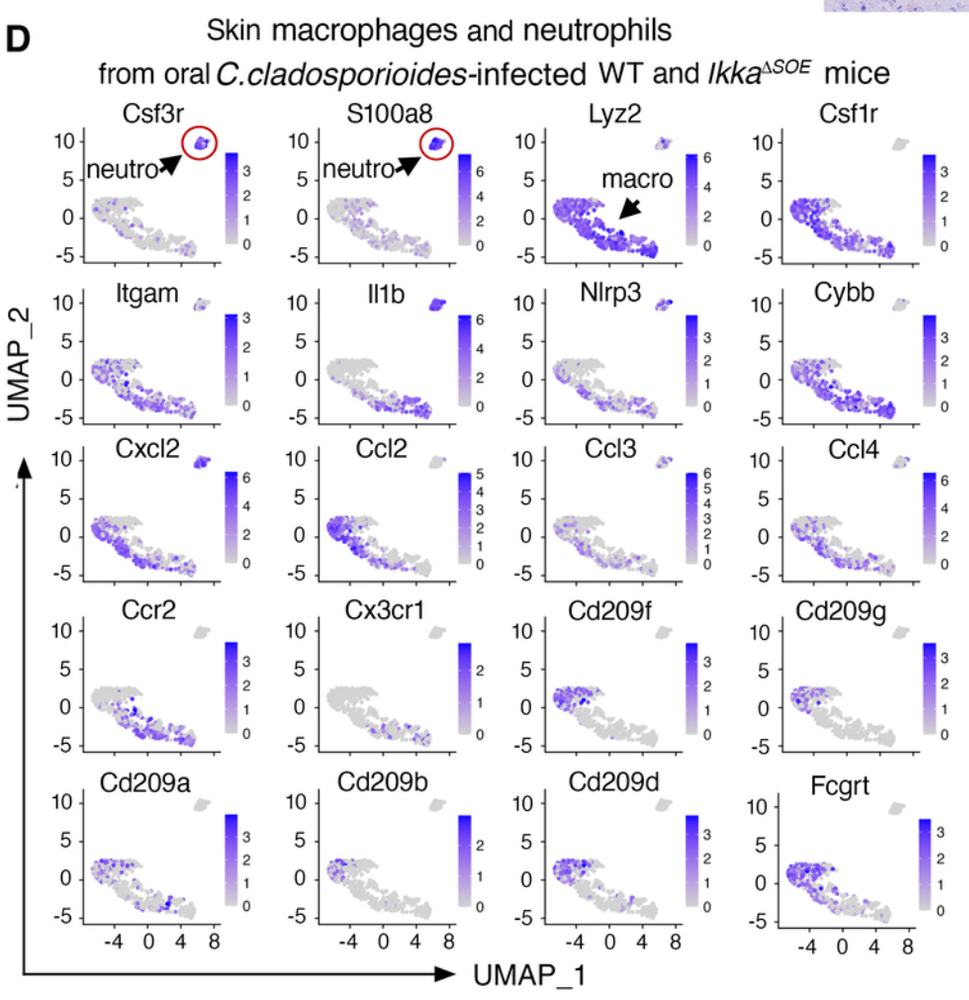

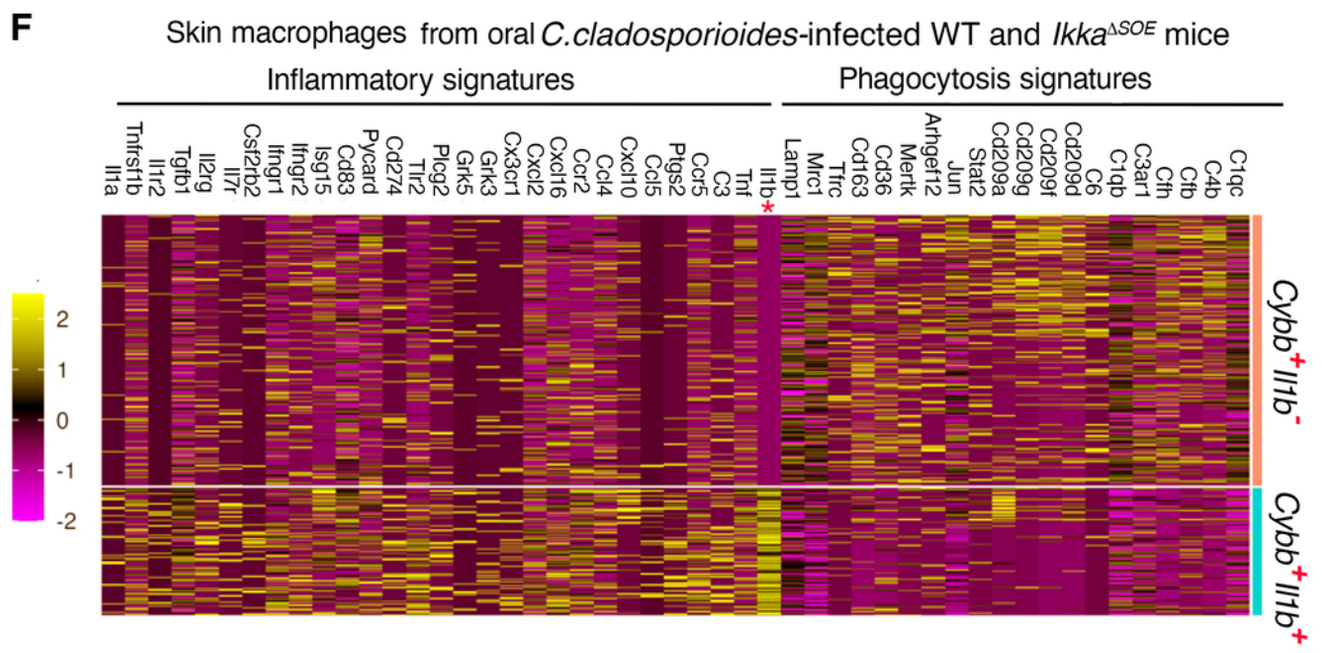

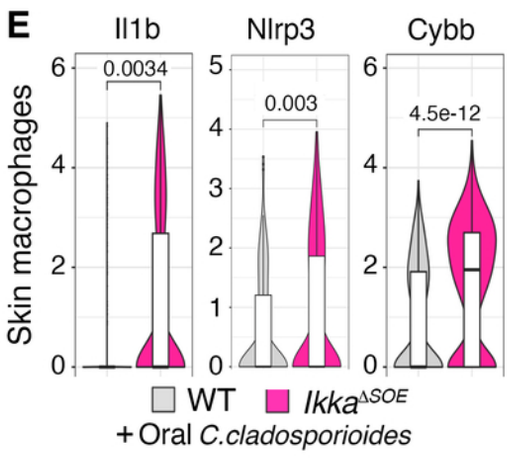

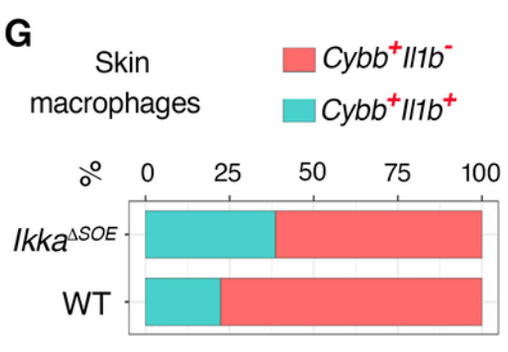

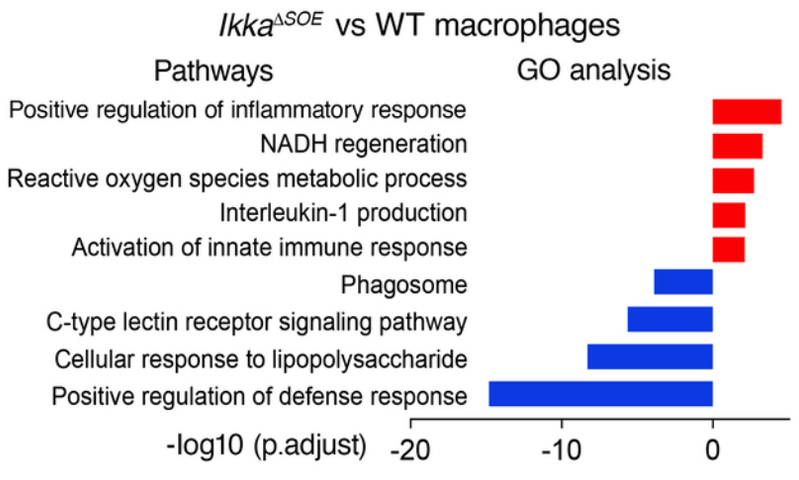

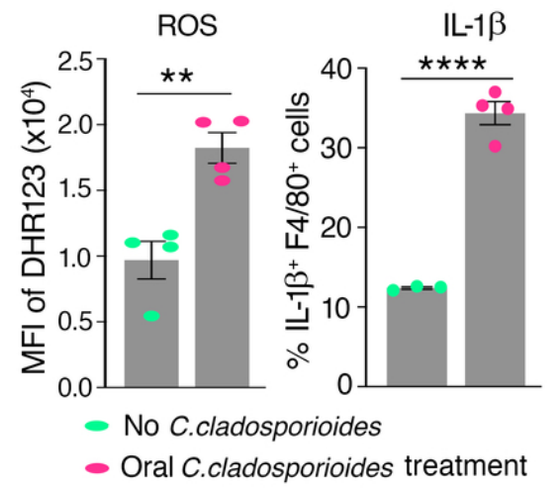

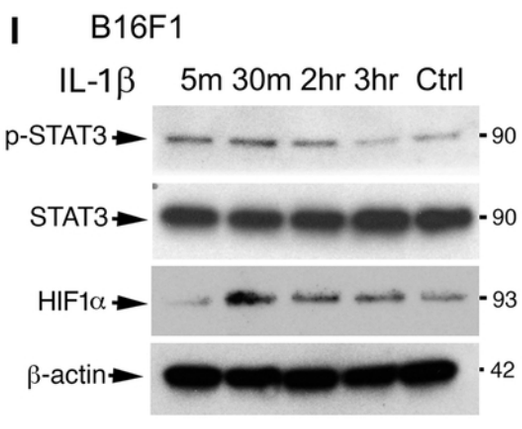

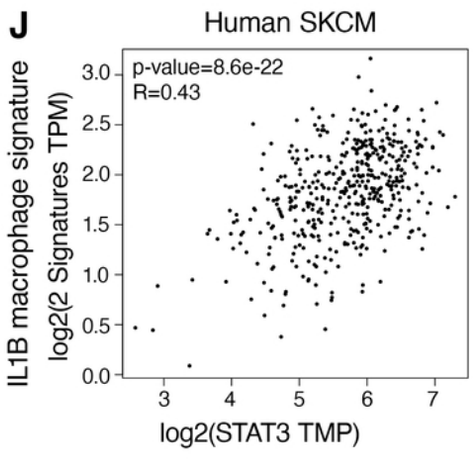

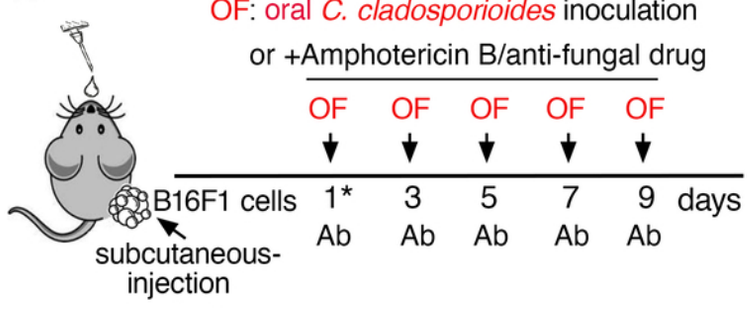

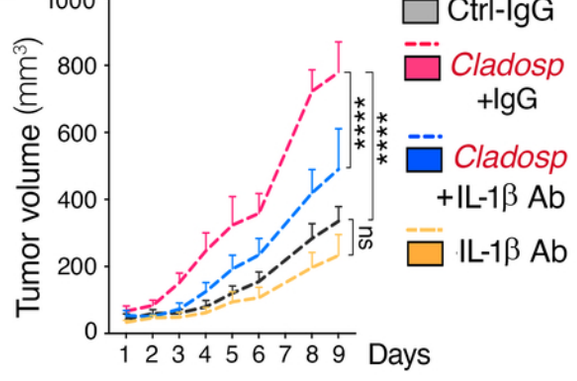

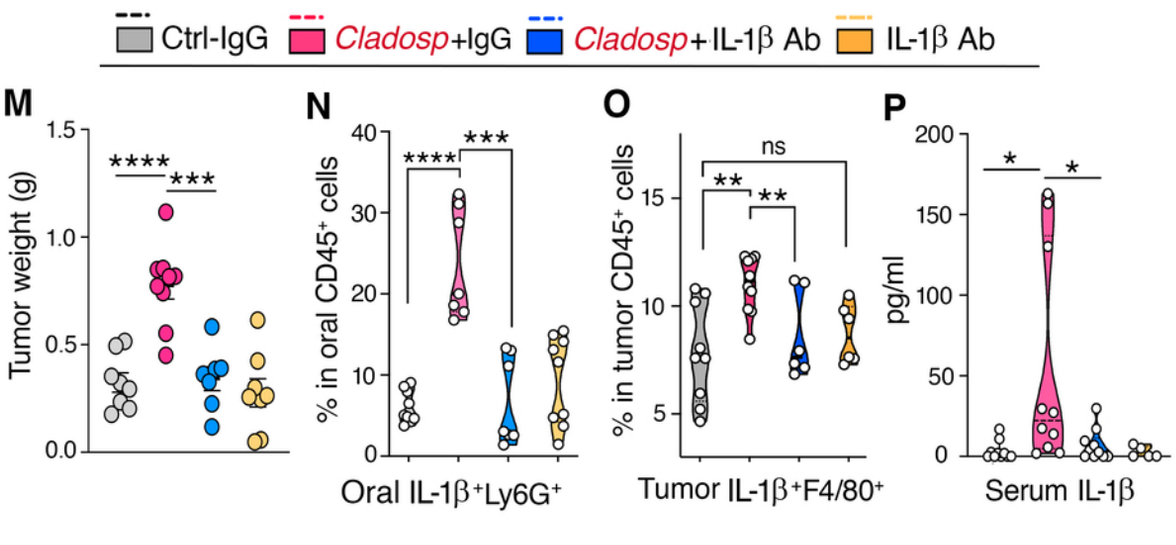

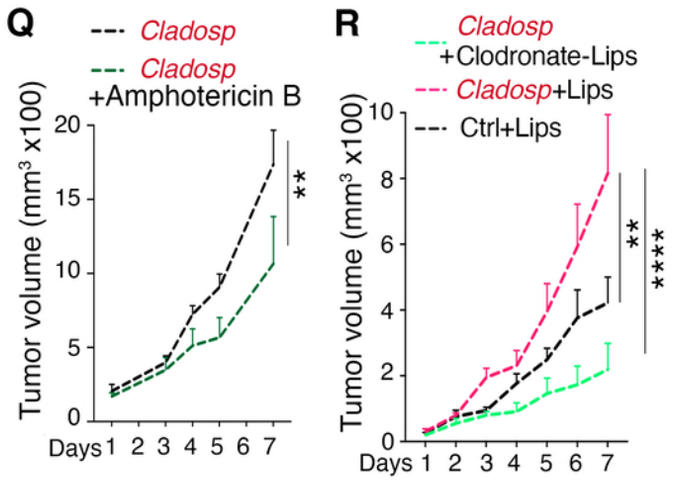

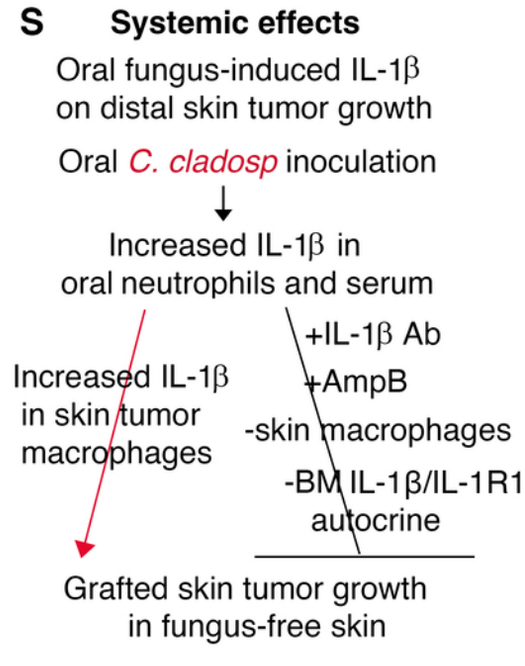

Downloaded from aacrjournals.org/cancerres/article-pdf/doi/10.1158/0008-5472.CAN-26-0070/3828896/can-26-0070.pdf by National Institutes of Health user on 15 September 2026